INSTITUTO SUPERIOR DE ENGENHARIA DO PORTO
MESTRADO EM ENGENHARIA MECÂNICA




# Optimization of the wing-fuselage interface of the UAS30-P2

**THOLKAPPIYAN DEENADAYALAN**
novembro de 2018

POLITÉCNICO
DO PORTO

Instituto Superior de Engenharia do Porto

# OPTIMIZATION OF THE WING-FUSELAGE INTERFACE OF UAS30-P2

Tholkappiyan Deenadayalan

**2018**

ISEP – School of Engineering, Polytechnic of Porto
Department of Mechanical Engineering

POLITÉCNICO
DO PORTO

Instituto Superior de Engenharia do Porto

# OPTIMIZATION OF THE WING-FUSELAGE INTERFACE OF UAS30-P2

Tholkappiyan Deenadayalan
1161618

Dissertation presented to ISEP – School of Engineering to fulfill the requirements necessary to obtain a Master's degree in Mechanical Engineering, carried out under the main guidance of Prof. Francisco José Gomes da Silva and co-supervision of Prof. Raul Duarte Salgueiral Gomes Campilho.

**2018**
ISEP – School of Engineering, Polytechnic of Porto
Department of Mechanical Engineering

POLITÉCNICO
DO PORTO

# JURY

**President**
Manuel Jorge Dores de Castro, PhD.
Adjunct Professor, Department of Mechanical Engineering
**Supervisor**
Francisco José Gomes da Silva, PhD.
Adjunct Professor, Department of Mechanical Engineering
**Co-Supervisor**
Raul Duarte Salgueiral Gomes Campilho, PhD.
Adjunct Professor, Department of Mechanical Engineering
**Examiner**
Ricardo José Alves de Sousa, PhD.
Auxiliar Professor, Department of Mechanical Engineering

# ACKNOWLEDGEMENTS

I would first like to thank my thesis supervisor Prof. Francisco José Gomes da Silva. The door to Prof. Francisco Silva's office was always open whenever I ran into a trouble spot or had a question about my research or writing. He consistently allowed this work to be my own work, but steered me in the right direction whenever he thought I needed it.

I also would like to thank my co-supervisor Prof. Raul Duarte Salgueiral Gomes Campilho for the support and constructive suggestions, which were determinant for the accomplishment of the work presented in this thesis.

A special thanks to my tutors from CEiiA for their guidelines in this research project:

Renato Machado, Team Leader-UAV Systems, CEiiA.

Miguel Sousa, Structural Engineer, CEiiA.

Without their passionate participation and input, this project work could not have been done successfully. I thank CEiiA for giving me this wonderful opportunity and support to do my Master's thesis in our company.

I also take this opportunity to thank the President of ISEP, Dr Maria João Viamonte, all the professors of ISEP for providing me such a wonderful platform of study environment and support for my Master's degree in our prestigious institution.

Finally, I must express my very profound gratitude to my family and friends for providing me with unfailing support and continuous encouragement throughout my years of study and through the process of researching and writing this thesis. This accomplishment would not have been possible without them, Thank you.

Tholkappiyan Deenadayalan.

**KEYWORDS**

Aircraft structures, Aircraft spar, Wing-fuselage attachment, Spar connector, Aerospace materials, Structure efficiency, Aluminium, Shape factors, Hyperworks, Optistruct, CATIA, Shape optimization.

# ABSTRACT

This thesis presents the optimization of the spar connector of the aircraft UAS30-P2.

The spar connector is the primary airframe structure of the aircraft. It connects the all flight surfaces of the aircraft with the fuselage. The structure is made up of extruded aluminium bars. The spar connector supports all aerodynamic loads and inertial loads of the aircraft. These loads are transmitted through the carbon fibre reinforced polymer (CFRP) spar of the aircraft. Since the spar connector supports all the aerodynamic and inertial loads of the aircraft, it is the most crucial component in the entire Unmanned aerial vehicle (UAV). Thus, it needs to be strong and stiff enough to withstand the exceptional circumstances in which the aircraft must operate.

The thesis reviews both, the choice of materials and shape optimization of the spar connector, achieving a more efficient structure. The choice of material is reviewed by studies conducted on the available materials for this purpose. The optimization is carried out using the studies and the results of the Finite element analysis (FEA) of the component. Later the optimized Finite element (FE) model of wing interface structure is analyzed based on the Finite element method results. The results were then compared with the analysis results of the original FE model of wing interface structure of UAS30-P2.

As a result, it was observed an appreciable reduction accompanied by the improvement in the performance characteristics is of the metallic spar connector of UAS30-P2.

**PALAVRAS-CHAVE**
Estruturas de aeronaves, Longarina principal de aeronaves, Ligação asa-fuselagem, Conector da longarina principal, Materiais aeroespaciais, Eficiência de estrutura, Alumínio, Fatores de forma, Hyperworks, Optistruct, CATIA, Otimização de forma.

# RESUMO

Esta tese apresenta a otimização do conector da longarina principal da aeronave UAS30-P2.

O conector da longarina principal é a estrutura primária da aeronave. Conecta todas as superfícies de voo da aeronave com a fuselagem. A estrutura é composta por barras de alumínio extrudido. O conector da longarina principal suporta todas as cargas aerodinâmicas e cargas inerciais da aeronave. Essas cargas são transmitidas através da longarina principal de polímero reforçado com fibra de carbono (CFRP) da aeronave. Como o conector da longarina principal suporta todas as cargas aerodinâmicas e inerciais da aeronave, é o componente mais crucial em todo o veículo aéreo não tripulado (UAV). Sendo assim, ele precisa ser forte e rígido o suficiente para suportar as circunstâncias excecionais em que a aeronave deve operar.

A tese analisa tanto a escolha dos materiais quanto a otimização da forma do conector longarina principal, conseguindo uma estrutura mais eficiente. A escolha do material é revisada por estudos realizados sobre os materiais disponíveis para esse fim. A otimização é realizada utilizando os estudos e os resultados da análise FE do componente. Posteriormente, a estrutura otimizada é analisada com base nos resultados do método dos elementos finitos. Os resultados foram então comparados com os resultados da análise da estrutura original.

Como resultado, foi observado uma redução apreciável, acompanhada pela melhoria nas características de performance do conector metálico da longarina principal do UAS30-P2.

# LIST OF SYMBOLS AND ABBREVIATIONS

List of abbreviations

| | |
|---|---|
| BVID | Barely Visible Impact Damage |
| CFRP | Carbon Fiber Reinforced Polymer |
| CMPST | Composite |
| DoF | Degrees of Freedom |
| EW | Electronic Warfare |
| FAA | Federal Aviation Administration |
| FAR | Federal Aviation Regulation |
| FEA | Finite Element Analysis |
| FEM | Finite Element Model |
| GCS | Ground Control Station |
| ISEP | Instituto Superior de Engenharia do Porto |
| MMC | Metal Matrix Composite |
| NASA | National Aeronautics and Space Administration |
| PMC | Polymer Matrix Composite |
| RBE | Rigid Body Elements |
| RPM | Rotation Per Minute |
| SCC | Stress Corrosion Cracking |
| SE | Structural Efficiency |
| SIGINT | Signal Intelligence |
| UAS | Unmanned Aircraft System |
| UAV | Unmanned Aerial Vehicle |

List of units

| | |
|---|---|
| Angle | degrees, [$^{o}$] |
| Area | $mm^2$ |
| Density | $kg/mm^3$ |
| Displacement | mm |
| Force | N |
| Heat Capacity | $J/kg.^{o}C$ |
| Length | mm |
| Mass | kg |
| Moment | N.mm |
| Moment of Inertia | $mm^4$ |
| Stress | MPa |
| Young's Modulus | MPa |

List of symbols

| | |
|---|---|
| $A$ | Area |
| $\gamma_{12}$ | Shear Strain |
| $\rho_a$ | Density of aluminium alloy |
| $\rho_c$ | Density of Composites |
| $\rho_h$ | Density of material in hybrid section |
| $\sigma_1$ | Principal Stress 1 |
| $\sigma_2$ | Principal Stress 2 |
| $\sigma_3$ | Principal Stress 3 |
| $\sigma_{vM}$ | Von Mises Stress |
| $e_L$ | Longitudinal strain limit |
| $e_{LT}$ | Shear strain limit |
| $e_T$ | Transverse strain limit |
| $\nu_{12}$ | Equivalent laminate Poisson ratio. |
| $\nu_{xy}$ | Laminate Poisson ratio |
| $\tau_{max}$ | Maximum Shear stress |
| $\tau_{tresca}$ | Tresca's Stress |
| $\epsilon_1$ | Principal Strain 1 |
| $\epsilon_2$ | Principal Strain 2 |
| € | Euro |
| μ | Poisson's ratio |
| $C_d$ | Coefficient of drag of a finite wing |
| $C_G$ | Centre of Gravity |
| $C_l$ | Coefficient of lift of finite wing |
| $d$ | Inner Diameter |
| D | Outer Diameter |
| $E$ | Young's Modulus |
| e | Elongation in percent |
| e/D | Ratio of edge distance (center of the hole to edge of the sheet) to hole diameter (bearing strength) |
| $E_{11}$ | Equivalent laminate modulus in longitudinal direction |
| $E_{22}$ | Equivalent laminate modulus in transverse direction |
| $E_c$ | Modulus of elasticity in compression |
| $E_{xx}$ | Young Modulus of Laminate in longitudinal direction |
| $E_{yy}$ | Young Modulus of Laminate in transverse direction |
| $F_{bru}$ | Design ultimate bearing stress |
| $F_{bry}$ | Design bearing yield stress |
| $F_{cy}$ | Design compressive yield stress |
| $F_{su}$ | Design ultimate stress in pure shear |
| $F_{tu}$ | Design tensile ultimate stress |
| $F_{ty}$ | Design tensile yield stress |

| | |
|---|---|
| G | Modulus of rigidity (shear modulus) |
| $G_{xy}$ | Shear modulus of Laminate |
| I | Moment of Inertia |
| L | Longitudinal (grain direction) |
| LT | Long transverse (grain direction) |
| M | Moment |
| max | Subscript “maximum” |
| min | Subscript “minimum” |
| MS | Margin of Safety |
| $M_{TOW}$ | Maximum Take-Off Weight |
| S | Shear strength |
| $S_{sy}$ | Yield strength in shear |
| $S_y$ | Yield Strength |
| $S_{yc}$ | Yield strength in compression |
| $S_{yt}$ | Yield strength in tension |
| t | Thickness |
| $X_c$ | Laminate longitudinal compressive strength |
| $X_t$ | Laminate longitudinal tensile strength |
| $Y_c$ | Laminate transverse compressive strength |
| $Y_t$ | Laminate transverse tensile strength |
| μ | Poisson’s ratio |
| σ | Stress |
| $S$ | Failure shear strain |
| $X$ | Longitudinal failure strain |
| $Y$ | Transverse failure strain |
| $l$ | Length |
| $\tau$ | Shear stress |

# GLOSSARY OF TERMS

| | |
|---|---|
| Aircrew | Includes the persons who operate aircraft while in flight |
| Airframe | The body of an aircraft as distinct from its engine |
| Aspect ratio | The ratio of the square of wing span to wing area |
| Catapult | An external device used to launch aircraft |
| Constraint | Limits placed on the model to restrict motion during FEA |
| Cross wing landing | Landing condition during which a significant component of the prevailing wind is perpendicular to the runway centerline |
| Dihedral angle | The upward angle from horizontal of the wings of a fixed-wing aircraft |
| Flight Envelope | The envelope of the flight loading conditions with respect to airspeed |
| Lift | Component of aerodynamic force that is perpendicular to the oncoming flow direction |
| Longeron | Main longitudinal brace or support in an airplane |
| Main-plane | The principal wing which is the main lifting surface of the aircraft |
| Maximum takeoff weight | Maximum weight at which the aircraft can attempt to take off |
| Miniature UAV | UAV with $M_{TOW}$ less than 25 kg |
| Operating weight | The weight of the aircraft, includes the weight of the structure, power plant, furnishings, installations, systems and fuel |
| Payload | The weight of occupants, cargo, baggage or any other load, which are not flight useful load |
| Pitch | Rotational motion about a lateral axis which causes nose up and nose down actions of aircraft |
| Portside | The left side of the aircraft from the pilot's perspective |
| Primary aircraft structures | The structure that carries flight, ground, loads, and whose failure would reduce the structural integrity of the airplane |
| Roll | Rotational motion about the longitudinal axis of the aircraft |
| Ruddervator | A control surface designed to perform the functions of both a rudder and an elevator |
| Secondary aircraft structures | Structures that are not primary load carrying members and their failure would not reduce the structural integrity of the airframe |
| Starboard | The right side of the aircraft from the pilot's perspective |
| Structural efficiency | The ratio of material's ultimate stress by density |
| Tail-plane | Lifting surface located on the aircraft tail to provide stability and control |
| Wingspan | The distance between one wing tip to the other |

| | |
|---|---|
| Yaw | Rotational motion about the normal axis of the aircraft |

# FIGURES INDEX

# TABLES INDEX

# INDEX

# INTRODUCTION

# 1 INTRODUCTION

## 1.1 Unmanned aircraft system (UAS)

UAS is a system of unmanned aircraft, its associated communication links and control components which are required for the safe and efficient operation of the unmanned aircraft. It comprises many sub-systems, which include the aircraft (often referred to as a UAV), its payloads, the control station(s) (and other remote stations), aircraft launch and recovery sub-systems, support sub-systems, communication sub-systems, transport sub-systems, etc., as shown in Figure 1. UAS usually have the same elements as systems based upon manned aircraft, but with the airborne element, i.e. the aircraft being designed from its conception to be operated without an aircrew aboard. The aircrew (as a sub-system), with its interfaces, aircraft controls and habitation is replaced by an electronic intelligence and control subsystem. The functional structure of a UAS is shown in Figure 2 [1].

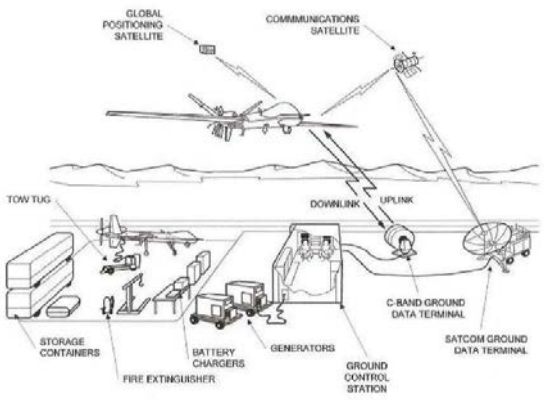


Figure 1- UAS with Control System Overview [1].

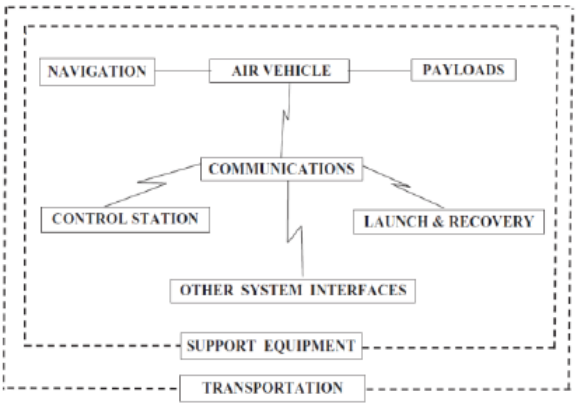


Figure 2 - UAS - functional structure [1].

### 1.1.1 Unmanned aerial vehicle (UAV)

The UAV is the airborne part of the system that includes the airframe, propulsion unit, flight controls, and electric power system, as shown in Figure 3. The air data terminal is mounted in the air vehicle, and it is the airborne portion of the communication data link. UAVs can be a remote-controlled aircraft or an aircraft that can fly autonomously based on pre-programmed flight plans or more complex dynamic automation systems [2]. The air vehicle can be a fixed-wing airplane, rotary wing, or a ducted fan. Lighter-

than-air vehicles are also eligible to be termed UAVs. In addition, a cruise missile can be a UAV, but is treated separately on the basis that the vehicle is the weapon [3].

Figure 3 - UAV General Atomics MQ-9 Reaper [4].

### 1.1.2 Launch and Recovery Equipment

Launch and recovery equipment can be accomplished by several techniques ranging from conventional takeoff and landing on prepared sites to vertical descent using rotary wing or fan systems. Catapults using either pyrotechnic (rocket) or a combination of pneumatic/hydraulic arrangements, as shown in Figure 4, are also popular methods for launching air vehicles. Some small UAVs are launched by hand, essentially thrown into the air like a toy glider. Nets and arresting gear are used to capture fixed-wing air vehicles in small spaces, as shown in Figure 5. Parachutes and parafoils are used for landing in small areas for point recoveries. For a rotary-wing or fan-powered vehicle the launch and recovery equipment usually is not necessary. However, operations from the deck of a pitching ship, even with a rotary-wing vehicle, will require hold-down equipment unless the ship motion is minimal [3].

Figure 4 - Boeing Insitu ScanEagle in its catapult launcher [5].

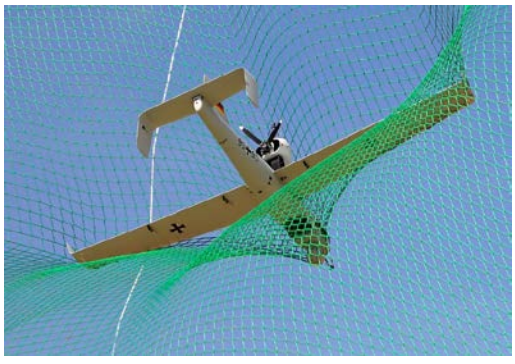

Figure 5 - UAV LUNA Landing in Nets [6].

## 1.2 Motivation

To many, the airplane is a structure of appalling flimsiness, yet the principle which it exemplifies, that of obtaining the maximum strength for a minimum of weight, constitutes a problem of which the solving is not only an unceasing labour, but one demanding the observance of the best engineering procedures. The whole future of aviation, commercially or otherwise, may be said to be indissolubly bound up with the development of efficiency; and whether this is to be attained in improvements in aerodynamical qualities, by the discovery of a material giving a greatly enhanced strength to weight ratio, or by progress in the arrangement of the various members of the complete structure of the airplane, is a matter upon which some diversity of opinion exists. However, it is certain that the very great developments of the last few years are due more to refinements in design rather than construction; and it is questionable whether the constructional work of the modern airplane has developed equally with design, so that, even taking for granted the oft-repeated, but very doubtful, statement that we are approaching the limitations of design, there is certainly plenty of scope for experiment and improvement in the constructional principles of the modern airplane [7].

> *"Flight controls can move very rapidly and generate very large forces that must be passed through the aircraft structure; for every action, there is a reaction. Therefore, we need to know exactly how the aircraft structure reacts to a given dynamic flight-control input".*
>
> *-Doug Pearson,*
>
> *Vice President, F-35 Integrated Test Force,*
>
> *Lockheed Martin.*

# BACKGROUND

### 1.2.1 Payloads

Carrying a payload is the ultimate reason for having a UAV system, and the payload usually is the most expensive subsystem of the UAV. Payloads often include video cameras, either daylight or night, for reconnaissance and surveillance missions, as shown in Figure 6. Armed UAVs carry weapons to be fired, dropped, or launched. “Lethal” UAVs carry explosive or other types of warheads and may be deliberately crashed into targets. Another major category of payloads is electronic warfare (EW) systems. They include the full spectrum of signal intelligence (SIGINT) and jammer equipment. Other sensors such as meteorological and chemical sensing devices have been proposed as UAV payloads [3].

Figure 6 - The Epsilon 135 gyro-stabilized gimbal [8].

### 1.2.2 Ground Control Stations (GCS)

The GCS of UAV is the nerve centre of activity during the planning, and execution of UAV missions. This system incorporates many technologies, such as communication, computer hardware, software, system engineering and human factor engineering. Each of these technologies is critical to the overall success of the GCS development and operation. Burgeoning power of open architecture computer hardware with industry standard operating systems and software, versatile display devices, fault-tolerant, network capability and common data link compatibility would be the driving forces for the future high availability GCSs for UAVs [9] A typical GCS Cockpit is shown in Figure 7.

Figure 7 - Advanced Cockpit GCS [4].

## 1.3 Objectives

The aim of the project is to optimize the aluminium spar connector of the unmanned aerial vehicle UAS30-P2, to a more efficient structure. Firstly, a detailed study and understanding of current spar connector of the aircraft will be made. Secondly, a possibility for change of material shall be analyzed, followed by optimization of the structure. It is expected, at the end of this project, that the aim will be achieved by a solution which also gives a balanced structural property and reduces the weight of the component.

# 2 BACKGROUND

## 2.1 Aircraft Spar

Spars are the principal structural members of the wing; a simple wing structure is shown in Figure 8. Spars correspond to the longerons of the fuselage. They run parallel to the lateral axis of the aircraft, from the fuselage toward the tip of the wing, and are usually attached to the fuselage by wing fittings, plain beams, or a truss. Classification of spars based on wing construction is shown in Table 1. The spar carries and transmits flight load during the flight and weight of the wing while on ground. The typical classification of spar based on its material is shown in
Table 2 [10].

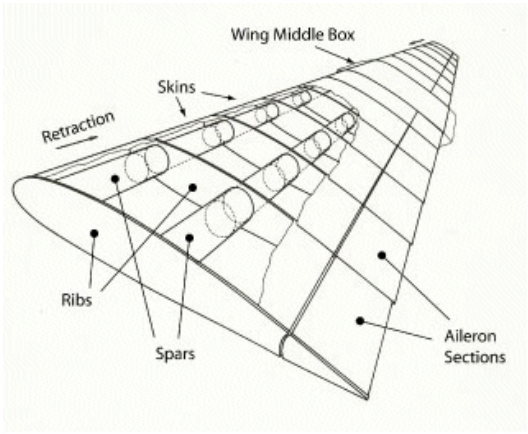


Figure 8 - Simple Wing Structure [11].

Table 1 - Classifications of wing based on spar and its construction [10], [12] and [13].

| | Classification | Description | Images |
|---|---|---|---|
| **Classification of wing based on spar and its construction.** | Mono-spar | The mono-spar wings are the light-weight configuration that incorporates only one main longitudinal member in its construction. | 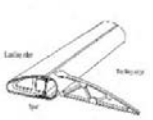 |
| | Multi-Spar | The multi-spar wing incorporates more than one main longitudinal member in its construction. | 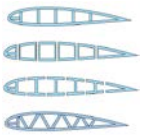 |
| | Box Beam | The box beam type of wing construction uses two main longitudinal members with connecting bulkheads to furnish additional strength and to give contour to the wing. |  |

| | Classification | Description | Images |
|---|---|---|---|
| **Classification of Spar based on its materials.** | Wooden construction | Wood was among the first materials used to construct aircraft Spars. Most of the airplanes built during World War-I were constructed of wood frames with fabric coverings. |  |
| | Metallic Spars | Metal allow engineers to extend performance parameters afforded by innovative structural designs. Currently, most manufactured aircraft have wing spars made of solid extruded aluminum or aluminum extrusions riveted together to form the spar. |  |
| | Composite Spar | Aircraft parts made from composite materials were developed during the 1960s for their weight savings over aluminum parts. New generation large aircraft are designed with all composite fuselage and wing structures. | 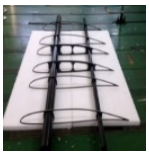 |

Table 2 – Classification of Spar based on its Material [10] and [14].

## 2.2 Airframe Materials

The airframe of a fixed-wing aircraft consists of the following five major units:

- Fuselage,
- Wings,
- Stabilizers,
- Flight controls surfaces,
- Landing gear.

The most commonly used commercial airframe structural materials are aluminium alloys, titanium alloys, high strength steels and composites, generally accounting for over 90% of the weight of airframes [15], as shown in Figure 9.

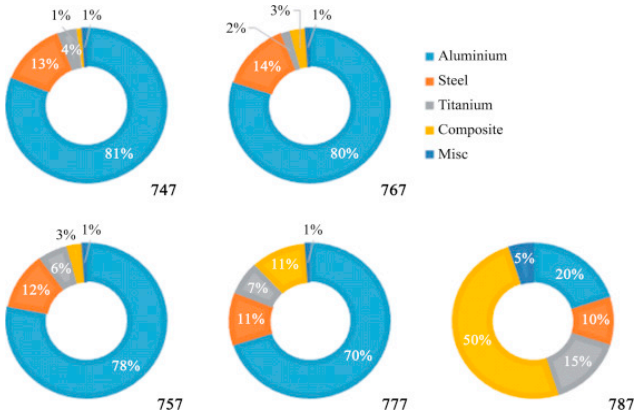


Figure 9 - Material distribution for a selection of Boeing aircraft series [16].

Some of the airframe materials are studied elaborately studied in the following sub-chapters.

### 2.2.1 Wood

Wood is the classical material for the Aircraft structure. But, as the aircraft design and manufacturing evolved, the development of lightweight metals and the demand for increased production moved the industry away from aircraft constructed entirely of wood. Some general aviation aircraft were produced with wood spars and wings, but today only a limited number of wood aircraft are produced. Wooden spar can be generally classified into four different types. By their cross-sectional configuration, they may be solid, box shaped, partly hollow, or in the form of an I-beam [10].

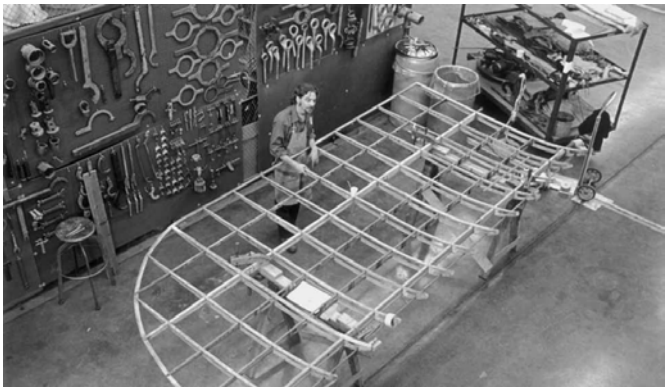

Figure 10 - Standard Spar and Rib Wing of Wooden Airplanes [14].

Table 3 - Wood Species in Aircraft [10] and [7].

| Species of Wood | Remarks | Strength Properties (as compared to spruce) |
|---|---|---|
| Spruce | Excellent for all uses. It works well with most tools. It glues and finishes well. Considered standard. | 100% |
| Douglas Fir | Difficult to work with hand tools. Some tendency to split and splinter during | Exceeds spruce. |

| | | |
|---|---|---|
| | fabrication and much greater care in manufacture is necessary. Satisfactory for gluing. | |
| Noble Fir | Satisfactory characteristics of workability, warping, and splitting. Hardness somewhat less than spruce. Satisfactory for gluing. | Slightly exceeds spruce except deficient in shear. |
| Western Hemlock | Less uniform in texture than spruce. Satisfactory for gluing. | Slightly exceeds spruce. |
| Northern White Pine | Excellent working qualities and uniform in properties, but somewhat low in hardness and shock-resistance. Satisfactory for gluing. | Properties between 85% and 96% those of spruce. |
| Port Orford White Cedar | Easy to work with hand tools. Gluing is difficult, but satisfactory joints can be obtained if suitable precautions are taken. | Exceeds spruce. |
| Yellow Poplar | Excellent working qualities. Somewhat low in shock-resistance. Satisfactory for gluing. | Slightly less than spruce except in compression and shear. |

Wood constitutes the material for the greater part of the structure of the airplane. However, the usage of wood is complicated by the very great variation found in the strength and characteristics of trees of the same species, and of different portions cut from the same tree. Thus, there is an unreliability of tabulated tests that exist indicating the strength, weight and other characteristics of various woods. Another point is shrinkage, which affects all timber in varying degrees [7]. Because of this the so-called structural revolution of the mid-1930s, the aircraft manufacturers started replacing wood with metal which allowed engineers to extend performance parameters afforded by innovative structural designs. Metal also played an important role in simplifying manufacturing techniques [14].

### 2.2.2 Aerospace Metals

From the 1920s to until the end of the 20$^{th}$ century, metal owing to its high strength and stiffness had replaced the usage of wood in airframes [15]. Metals used in airframes are listed in the next sub-chapters.

#### *2.2.2.1 Aluminium Alloys*

Aluminium (Al) alloys has a Structural Efficiency (SE) of 75.56 N·mm/kg. It is the most widely used materials in airframe structures. It is less expensive, could be easily formed and machined [17]. Lightweight aluminium alloys were the leading aviation structural materials (accounting for 70%–80% of the weight of the most airframe of civil aircrafts [15]. Currently, most manufactured aircraft have wing spars made of solid extruded aluminum or aluminum extrusions riveted together to form the spar [10]. The current spar connector in UAS30-P2 is made of aluminium (AA7075-T7351).

Table 4 - Salient Features of Aluminium [18], [19], [18] and [20].

| Salient Features of Aluminium | |
|---|---|
| High strength-to- | Aluminium is the lightest metal (density = 2795.67 kg/m$^3$) apart from magnesium. Its density is about one-third that of steel. The strength of aluminium alloys, however, |

| | |
|---|---|
| weight ratio | rivals that of mild carbon steel and can approach 100 ksi (700 MPa). |
| Ready fabrication | Aluminium is one of the easiest metals to form and fabricate, including operations such as extruding, bending, roll-forming, drawing, forging, casting, spinning and machining. Aluminium is the metal most suited to extruding. |
| Corrosion resistance | The aluminium cap placed at the top of the Washington Monument in 1884 is still there today. Aluminium reacts with oxygen very rapidly, but the formation of this tough oxide skin prevents further oxidation of the metal. |
| Aluminium in the Aerospace Industry | Even though the role of aluminium in future commercial aircraft will probably be threatened by the increasing use of composite materials, the high-strength aluminium alloys are, and will remain, important airframe materials. The attractiveness of aluminium is that it is a relatively low cost, lightweight metal that can be heat treated to high-strength levels and its relatively low manufacturing costs. |

Table 5 - Aluminium Series [21] and [20].

| Aluminium Alloys | |
|---|---|
| 1xxx Series | These alloys are aluminum of 99.00% or higher purity. They are characterized by excellent corrosion resistance, high thermal and electrical conductivities, low mechanical properties, and excellent workability. |
| 2xxx Series | Copper is the principal alloying element, often with magnesium as a secondary addition. In the solution heat-treated condition the mechanical properties sometimes exceed those of low-carbon steel. The precipitation heat treatment increase the yield strength of these alloys. They possess poor resistance to corrosion and may suffer from intergranular corrosion. |
| 3xxx Series | Manganese is the major alloying element of 3xxx series alloys. These alloys generally are non-heat-treatable but have about 20% more strength than 1xxx series alloys. |
| 4xxx Series | The major alloying element in 4xxx series alloys is silicon, which can be added in sufficient quantities (up to 12%) to cause substantial lowering of the melting range without producing brittleness. |
| 5xxx Series | The major alloying element in 5xxx series alloys is magnesium. It is a moderate-to-high-strength work-hardenable alloy. Alloys in this series possess good welding characteristics and good resistance to corrosion in marine atmospheres. However, operating temperatures above 65 °C may result in stress-corrosion cracking. |
| 6xxx Series | Alloys in the 6xxx series contain silicon and magnesium. They are heat treatable. 6xxx series alloys have good formability, weldability, machinability, and corrosion resistance, with medium strength. |
| 7xxx Series | Zinc, in amounts of 1 to 8%, is the major alloying element in 7xxx series alloys, and when coupled with a smaller percentage of magnesium results in heat-treatable alloys of moderate to very high strength. Other elements, such as copper and chromium, are added in small quantities. Higher strength 7xxx alloys exhibit reduced resistance to stress corrosion cracking and are often utilized in a slightly overaged temper to provide better combinations of strength, corrosion resistance, and fracture toughness. |
| 8xxx Series | These alloys constitute a wide range of chemical compositions, for example, improved elevated-temperature performance is achieved using dispersion-strengthened Al-Fe-Ce alloys (e.g., 8019) or Al-Fe-V-Si alloys (e.g., 8009). Lower density and higher stiffness can be achieved in lithium- |

| | |
|---|---|
| | containing alloys (e.g., 8090) which has replaced medium-to-high strength 2xxx and 7xxx alloys in some aerospace applications. |
| 9xxx Series | These alloys are typically unused. |

The attractiveness of aluminium is that it is a relatively low cost, lightweight metal that can be heat treated to high-strength levels and it is one of the most easily fabricated of the high-performance materials, which usually correlates directly with lower costs. Disadvantages of aluminium alloys include a low modulus of elasticity, rather low elevated-temperature capability (130 °C) and, in high-strength alloys, the susceptibility to corrosion [21]. The broadly used aluminium alloys in aerospace industries are AA2014, AA2019, AA2024, AA6061, AA7050, AA7075 [22].

Table 6 - Actual and proposed uses of conventional aerospace aluminium alloys in airframe structures [23].

| Product | Strength levels | Alloy/Treatment | Applications |
|---|---|---|---|
| Sheet | Damage tolerant | 2024-T3 | Fuselage/pressure cabin skins. |
| Plate | Damage tolerant | 2024-T351 | Lower wing covers. |
| | Medium strength | 2024-T62 | Tactical aircraft fuselage panels. |
| | Medium strength | 7050-T7451 | Internal fuselage structures. |
| | Medium strength | 7050-T7451 | Spars, ribs, other internal Structures. |
| Forgings | High strength | 7050-T7452 | Wing/fuselage attachments. |
| Extrusions | Damage tolerant | 2024-T3511<br>2024-T4312 | Lower wing stringers, Fuselage/pressure cabin stringers. |
| | Medium/high strength | 7075-T73511<br>7075-T79511 | Wing attachments, Fuselage stringers and frames, upper wing stringers, floor beams, seat rails. |

### *2.2.2.2 Beryllium alloys*

Beryllium (Be) alloys has a SE of 115.76 N·mm/kg. It has a very high structural efficiency. It is an expensive material. It has very limited formability, difficult to join, drill and mill. This metal is notch sensitive and cannot be welded. Beryllium is termed as a “Young” metal and unlike other metals which have been known since early civilizations, beryllium was discovered in 1828 and its commercial value was recognized only in 1926. It was first used in fast growing telephone relay applications by the company Siemens [24]. The standard Be alloys for aerospace industries are

specified as AMS 7906 and AMS 7902. The AMS 7906 are in the form of thin sheets and plates. AMS 7092 are in the form of bar, rod and tube [25].

Table 7 - Salient Features of Beryllium [26].

| Salient features of Beryllium | |
|---|---|
| Miracle Metal | Beryllium is a metal with an unusual combination of physical and mechanical properties. The beryllium has a combination of low weight and high stiffness. The most attractive features of beryllium are its low density, high elastic modulus and high specific modulus. |
| Dimensional Stability | Beryllium can be milled to extremely close tolerances. This attribute, in combination with its excellent dimensional stability, allows beryllium to be used for the manufacture of extraordinarily precise and stable components. |
| High Temperature Material | Beryllium has a high melting point of 1283 $^{o}$C also it has the highest heat capacity (1820 J/kg.$^{o}$C) among metals. Its thermal conductivity is comparable to aluminium. Thus, it is an efficient substrate material for conducting waste heat away from active solid-state electronic components in aerospace industry. |
| Toxicity Hazard | The main concern associated with the handling of beryllium is that particles of beryllium and its compounds, such as beryllium oxide, are toxic. Beryllium may also cause allergic reactions to individuals and at present, there is no way of predetermining those who may be hypersensitive to beryllium. |
| Fabrication | The disadvantages of Beryllium are its high cost, some difficulties in fabrication and health hazards. When it comes to joining them, beryllium can be readily brazed. Because of its high cost and toxic potential, machining operations should be minimized. |
| Corrosion | The corrosion of Beryllium is not a major problem. Beryllium is referred to as being self-protective against atmospheric oxidation, resembling aluminium and titanium in this respect. |

#### *2.2.2.3 Nickel alloys*

Nickel (Ni)alloys have a SE of 51.954 N·mm/kg. They exhibit good properties from the cryogenic range to 980 – 1100 °C. They are corrosion-resistant and readily welded (solution-treated). Three nickel alloys are of special interest to the aircraft designer, such as Inconel, Monel and K Monel. Inconel is a nickel- chromium alloy with good corrosion resistance and strength at normal and elevated temperatures. These properties are ideal for airplane-engine exhaust collectors. Monel is a Nickel-copper alloy with high corrosion resistance, reasonably good strength, and good working properties. K Monel is a nickel-copper-aluminum alloy with high corrosion resistance, exceptionally good strength (inherent as well as developed by heat treatment), and the property of being nonmagnetic. This latter property creates a use for this material as structural members near compasses [27]. The manufacturing cost of nickel alloys are very high compared to aluminium because of their alloying elements and difficulties in machining [28].

#### *2.2.2.4 Magnesium alloys*

Magnesium (Mg) alloy is known for its low density (1771.51 kg/m$^3$), excellent damping and has a SE of 61.318 N·mm/kg [17]. This material is not used for aircraft primary

structures and is usually avoided on airframes. As Figure 11 shows, the Mg alloys being applied to components which doesn't have higher structural significance in the aircraft [20].

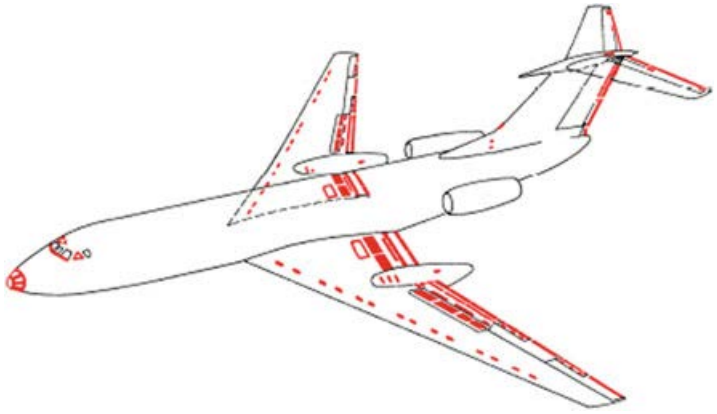

Figure 11 - Locations of Mg alloys in TU-134 Aircraft (marked in Red) [29].

Magnesium alloy has compatibility problems with other materials, especially in humid or salty atmospheres [30]. Magnesium alloy show good electromagnetic shielding, high recycling ability and machinability. The potential weight savings in using magnesium make it highly attractive for aerospace and automobile structural applications. Presently, most aerospace Mg alloy components are cast alloys for secondary structures. Some of the major aerospace Mg alloys are Elektron A8, AZ91C, AZ80A, ZM21, ZK 51A, 5Z/ML12, ZE41A, EZ33A and QE22A [20]. The use of Mg alloys in aerospace applications is rather limited due to the poor workability of the alloys. Further, corrosion resistance (notably galvanic corrosion), ductility, elevated temperature strength, fatigue and toughness properties of conventional Mg alloys are still of concern [31]. Adding to this, Mg has only a few optimized alloys, limited number of producers, no low and stable price [32]. Table 8 shows some salient features of Mg alloys.

Table 8 - : Salient features of Magnesium [20], [33], [34], [35] and [36].

| Salient Features of Magnesium | |
|---|---|
| Tensile Strength | Pure Mg has limited strength and is usually alloyed to improve the strength, as well as other properties. Mg alloys have the advantages of high strength to density ratios, high damping capacity and machinability compared to aluminium alloys, and the added ability to be cast into intricate shapes. |
| Fatigue Strength | Mg alloys do not have a well-defined endurance limit. Also, the fatigue properties are influenced by many factors, including micro-porosity, precipitate size and coherency, grain size and crystallographic texture. Micro-porosity in Mg alloys causes poor high cycle fatigue strength. |
| Corrosion resistance | The major disadvantages are poor corrosion resistance, cold formability and microstructural stability at elevated temperatures. Galvanic corrosion is an important problem. Mg oxidizes easily in normal air. However, the rate of oxidation is less than that of mild steel. Although Mg and its alloys form a thin oxide film in moist air, it leaves the surface unprotected because of its nonuniform, imperfect and porous structure. |
| Fracture toughness | The low fracture toughness of Mg alloys makes them generally unsuitable for primary load-bearing structures in aerospace applications. |

#### 2.2.2.5 *Titanium alloys*

Titanium alloys exhibit good SE of 98.58 N·mm/kg but, are heavier (with a density of 4428.78 kg/m$^3$) than other light-weight alloys [17]. These alloys have a good cryogenic temperature endurance and corrosion resistant. They are more expensive than aluminum alloys [37]. They can be formed, milled, and welded. They possess good toughness. Ti-6AI-4V alloys are widely used in annealed and heat-treated forms. Ti-SAI-2.5Sn alloy possess good weld joints. Titanium alloys are the principal replacements aluminium alloys when it comes to a need of better elevated temperature properties [27]. Titanium is expensive to produce, in part because the cost associated with refining, processing and fabrication are high compared with other metals [38]. The production cost of titanium is five times greater than that of aluminium and it is ten times costlier to fabricate it into finished products [39]. Figure 12 and Figure 13 show the use of titanium alloy in landing gear and bulkhead of aircraft, respectively.

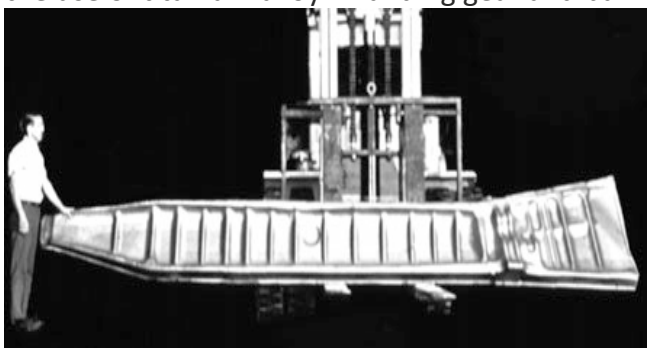

Figure 12 - Large Ti–6Al–4V forging for Boeing 747 landing gear [37].

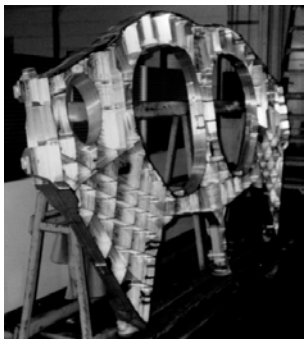

Figure 13 - Machined titanium bulkhead forging for a twin-engine aircraft [37].

#### 2.2.2.6 *Steel*

Steel have a SE of 88.83 N·mm/kg but it comes with a penalty of high density (7833.41 kg/m$^3$). Steel alloys are not widely used on airframe structures except for landing gear [17]. Currently, there are 20 main types of steels broadly used for fittings, propeller hubs, springs, landing gears and brace struts. But, because of its high-density, steels are predominantly avoided in airframes [27]. Despite of its abundant availability and low to moderate cost level, the use of steel in aircraft is often limited to just 5–8% of the total airframe weight. This is mainly because steel is 2.5 times heavier than aluminium. In addition to weight problems, most steels are susceptible to corrosion, which causes surface pitting, stress corrosion cracking and other damages. High-strength steels are prone to be damaged by hydrogen embrittlement [15].

### 2.2.3 Composite

Composite materials are becoming more important in the construction of aerospace structures. Aircraft parts made from composite materials, such as fairings, spoilers, and flight controls, were developed during the 1960s for their weight savings over aluminium parts, shown in Figure 14.


Figure 14 - Airframe materials distributions for the Airbus A380 [23].

The primary advantages of composite materials are their high strength, relatively low weight, and corrosion resistance. Composite materials consist of a combination of materials that are mixed together to achieve specific structural properties. The properties of the composite material are superior to the properties of the individual materials from which it is constructed [10]. The most relevant composite materials used in primary structures of aircraft are shown in Table 9.

Table 9 - Composites used in primary aircraft structures [10] and [15].

| Composites used in primary aircraft structures | |
|---|---|
| **Polymer matrix composites (PMC)** | The composites used in aircraft are almost exclusively polymer matrix materials. CFRP are the most widely used fibre-polymer matrix composites in aircraft structures. Table 10 gives some of the features of CFRP. Carbon-fibre composites are used in many major structural components including the vertical and horizontal tail planes, tail cone, centre wing box and wing ribs. |
| **Metal matrix composites (MMC)** | MMC are lightweight structural materials used in a small number of aircraft. MMC offer several advantages, including higher elastic modulus and strength, better fatigue performance, superior elevated temperature properties such as improved creep resistance. But MMC of aluminium and magnesium alloys, which have a lower or similar density to the ceramic reinforcement, may incur a weight penalty. |

Table 10 - Salient features of CFRP [20], [15] and [40].

| Salient features of CFRP | |
|---|---|
| Specific strength | 100% aligned-fibre CFRP laminates have intrinsically very high specific strengths, well beyond the capabilities of aluminium alloys. However, the dependence of CFRP strengths on the degree of fibre alignment is considered as the reduction factor that can eliminate the CFRP-specific strength advantages compared to aluminium alloys, as shown in Figure 15. |
| Specific stiffness | The overall advantages of CFRPs are much less than in the case of specific strengths. Even so, the aluminium alloys match only the 25 % aligned-fibre composites in terms of specific stiffness E/ρ, as shown in Figure 16. |
| Practical weight | Actual CFRP components are assembled from layers with different fibre orientations. Also, most aircraft structures are subjected to multidirectional loads, and this means that mechanical property |

| | |
|---|---|
| saving | isotropy will often be important. For CFRP components a requirement of mechanical isotropy means that the amount of fibres aligned in the principal loading direction will be about 25 %, which results in the final component to be bulkier. Thus, a direct translation to high weight savings in actual components is not possible. Only 10–20 % weight savings from using CFRPs instead of aluminium alloys is advisable. Thus, despite the increasing use of CFRPs in aircraft structures, there is still potential competition from aluminium alloys. |
| Impact Damage | CFRPs have high fatigue strengths compared to aluminium alloys. However, CFRPs are highly susceptible to impact damage, which can grow during service, but not necessarily or at all by fatigue. In fact, CFRPs have the least impact resistance of any composites, shown in Figure 17 |

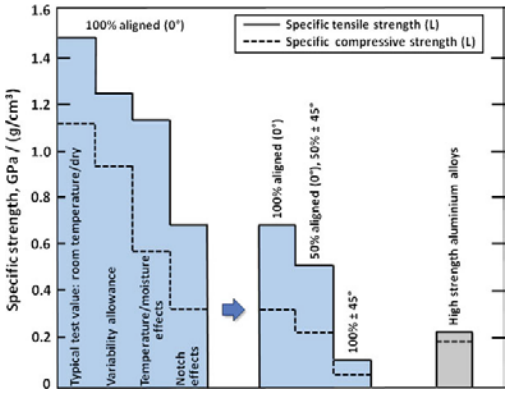


Figure 15 - Reduction factor effects on CFRP specific strengths, and comparison with high strength [20].

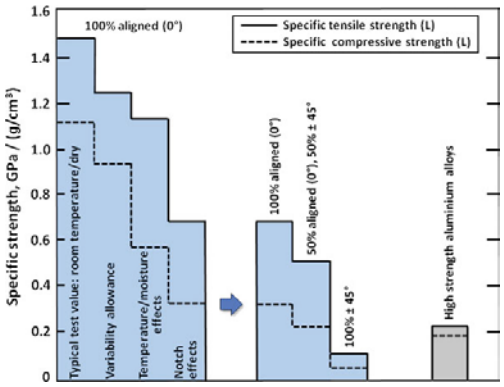


Figure 16 - Specific stiffness (average values) for CFRP composites, conventional aerospace aluminium and Al-Li alloys [20].

Note: In Figure 16, 60 % volume fibre-density CFRP composites tested in the aligned-fibre direction.

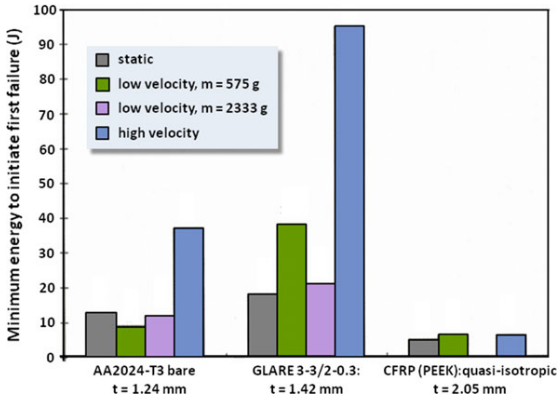


Figure 17 - Impact properties for a quasi-isotropic thermoplastic (PEEK) CFRP, aluminium alloy [20].

Note: In Figure 17, “m” represents the mass of the impactor (unspecified for the high velocity impacts).

Table 11 - Relative advantages and disadvantages of FMC compared to aluminium alloys [15] and [41].

| Advantages | Disadvantages |
|---|---|

| | |
|---|---|
| Higher and much higher specific stiffness, depending on percentages of aligned fibres. | Intrinsically anisotropic: complex components difficult to analyze, sometimes resulting in poor predictions; complex failure modes make it difficult to develop failure criteria, especially for compression loading. |
| Greater flexibility in designing structurally efficient components (tailored directional properties). | Possible delamination and other flaws during fabrication, e.g. from drilling fastener holes. |
| 10–20 % weight savings in actual components. | Higher notch sensitivity under static loading. |
| Dimensional stability. | Difficult validation and certification of repairs. |
| High fatigue strength. | High susceptibility to impact damage. The growth of damage in composite materials is difficult to control and predict. Thus, PMC are generally avoided in aircraft primary structures. |
| Corrosion resistant and reduced maintenance costs. | High material, labour and manufacturing costs. Slow production rates. |

The combination of high material, labour and manufacturing costs of composites makes aircraft components made of composites to be more expensive than the other classes of materials, as shown in Table 12.

Table 12 - Comparison of cost of different classes of aerospace material [42].

| Material class | Material | Specific strength (kN·m/kg) | Relative Price |
|---|---|---|---|
| Aluminium alloys | AA7075-T6 | 203.6 | €€ |
| Titanium alloys | Ti-6Al-4V | 264.1 | €€€ |
| Steels | AISI 4130 | 89.4 | € |
| Composites | CFRP | 937.5 | €€€€ |

CFRP is carbon fibre reinforced epoxy resin (120 °C cure) reinforced by standard CF (carbon fibre) UD (0°).

## 2.3 Spars and wing attachments

### 2.3.1 Study of spars designs

A mono-spar wing construction, shown in Figure 18, has a spar which is to the leading edge of the wing profile. This type of wing construction provides all advantages of the known wings having plywood leading edges, namely, a smooth non-buckling spar resisting to torsion. In addition, the weight is slightly reduced as it is a mono-spar configuration. Besides, the decisive advantage obtained is that all wing oscillations, which are practically bending stresses, have been eliminated. Thus, a fundamental increase in flying safety is achieved [12].

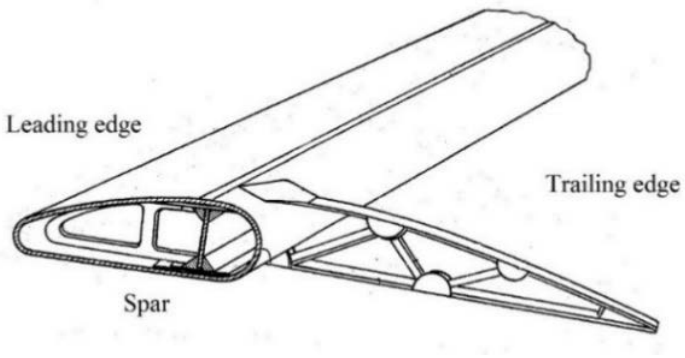


Figure 18 - Mono-spar wing construction [12].

A strong, lightweight blade provided for use on wind turbines utilizes an interior reinforcing strut, which extends part-way out the blade and consists of telescoped steel pipes welded to one another and mounted at their root ends to a steel cuff. A carbon graphite spar slips over the telescoped tubes and inside the cuff and extends radially outward, substantially to the end of the blade. A rigid skin which is airfoil-shaped in all its cross-sections attaches to the spar and spans from the root of the spar to the distal tip of the blade, defining the wind-driven surfaces of the blade, as shown in Figure 19. The blade construction maximizes the strength versus the weight of the blade. The blade is designed to enable the entire length of the blade to be externally configured to define an airfoil in cross-section and every point along its length, particularly at its tip where, the internal reinforcement structure should be sufficiently narrow in diameter so that the airfoil cross-section at that region need not be oversized. As, the oversized internal reinforcement may destroy the airfoil shape. Thus, reducing the efficiency of the rotor. The spar as described is a single spar, but with multiple sections with different diameters, or a "composite" spar composed of several sections bonded together, shown in Figure 20. The practical advantage of such spars are weight reduction and better structural integrity [43].

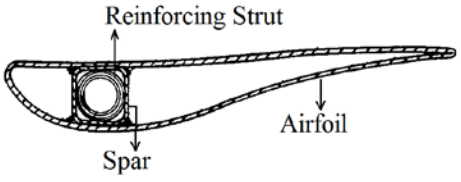


Figure 19 - Wind turbine blade construction airfoil cross section view [43].

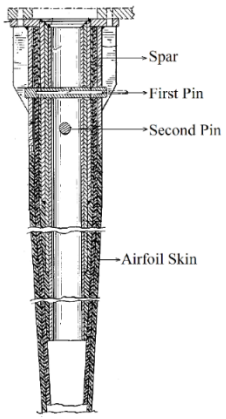


Figure 20 - Wind turbine blade construction [43]

A propeller blade includes a foam core, a structural layer formed of multiple layers that surrounds at least a portion of the foam core and at least one section of fibers formed separately from the structural layer located between two of the multiple layers, shown

in Figure 21. The blade is constructed by first forming its spar. The core is typically formed of a foam material that is injected into a mold. The mold can include a layer of fiberglass on the walls thereof that to which the foam of the core adheres. As such, the core can be surrounded by a layer of fiberglass. The structural layer is typically formed of a dry braided carbon fiber, which is subsequently resin injected, or a resin-impregnated fabric material (e.g. resin impregnated carbon fabric) and disposed such that it surrounds the core (and the fiberglass layer if it is included). The structural layer is typically braided onto the core. In some cases, the spar is heated to set the resin in the structural layer. The resultant structure gives high stiffness and stability [44].

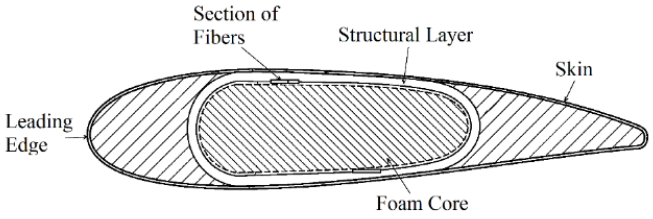


Figure 21 - Propeller blade with modified spar stiffness [44].

### 2.3.2 Study of removable wing attachments

The airplane's parts were made in such a manner that they may be easily assembled to simulate many different military, naval, commercial and pleasure flying airplanes. The idea is about a completely integrated airplane with each component being attached using different connection setup and the wing is attached by two hollow circular tubes which also serve as its spars, as shown in Figure 22. By this way, the aircraft can be quickly assembled for its flight and could by easily dismantled for the ease of transportation [45].

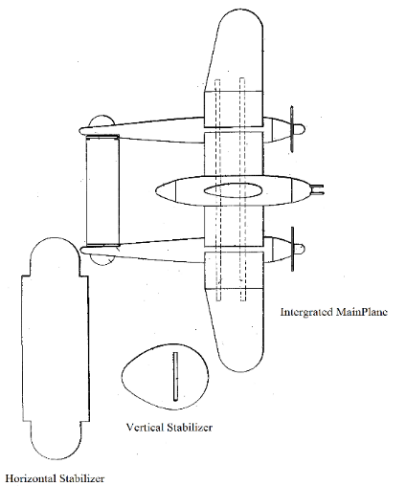


Figure 22 - Layout of Integrated Airplane [45].

A connector arrangement was created for the detachable attachment of airplane wings to the fuselages of airplanes. The arrangement utilizes generally tongue and groove-like T-shaped connector elements, which are connected to each other within the fuselage, or to a constructional element located therein, by a rubber band under pretension. These tongue and groove-like connector elements are adapted to be

swiveled or rotated in their extended positions, and may then meet an intermediate member or the outer surface of the fuselage, and are maintained in their rotated positions. In this position, the tongue and groove-like connector element, upon attachment of the airplane wing, may be positioned in a cutout formed in the end surface of the wing [46], as shown in Figure 23.

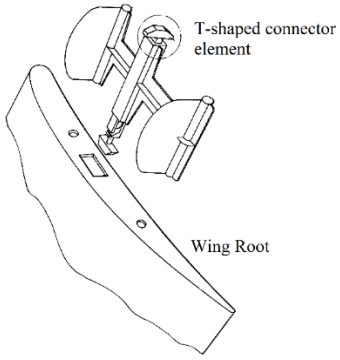


Figure 23 - Connector Arrangement for Aircraft [46].

A fixed-wing four-seat light aircraft is designed in such a way that it can be easily converted to a roadway vehicle, comprising a one-piece wing center panel with foldable wing tips on each side. The aircraft has a high wing configuration with the whole wing unit rotatable which is mounted on top of the fuselage. During the roadable position of the aircraft, the whole wing is rotated in such a way that the wing span is approximately parallel to the longitudinal axis and the two foldable tips are folded to overlap on top of the center panel of the aircraft [47], as shown (step:1 and step:2) in Figure 24.

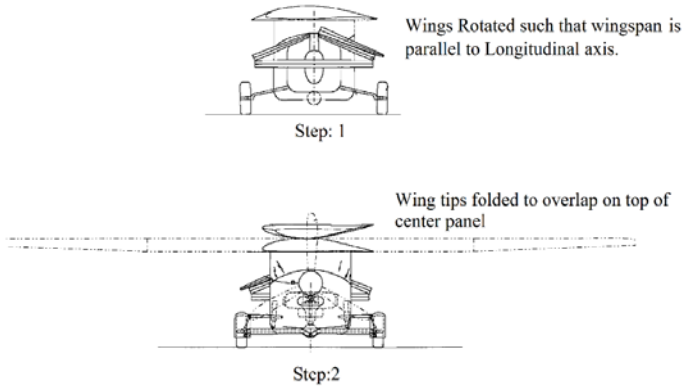


Figure 24 - Convertible Fixed Wing Aircraft [47]

The damage of complex and expensive airframe component due to harsh flight loads resulted in a failsafe method of wing attachment, termed as impact absorbing wing connection system. In this, the wings are oriented into their proper flying positions by their exact fit with the fuselage, as shown in Figure 25, and they are kept in these positions during normal flight by a set of non-elastic break-away links which are attached to the wings and to the fuselage through a corresponding set of wing and fuselage connecting members, respectively. In case of a crash, the inertia forces of the wings are conveyed to the break-away links by the connecting members. The break-

away links are calibrated so that they are strong enough to prevent any lateral movement of the wings under reasonable flying conditions, but they break open under higher forces as shown in Figure 26, releasing the wings. The detachment of the wings absorbs most of the impact forces, protecting the aircraft from breaking. However, this wing attachment system could be applicable only to very smaller UAV since detachment of wing structure of an aircraft during flight is a catastrophic failure [48].

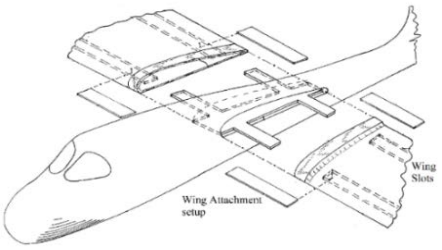


Figure 25 - Impact absorbing wing connection system [48].

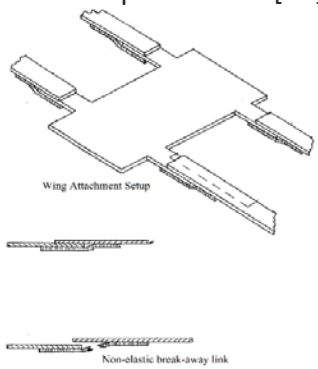


Figure 26 - Breakaway links [48].

The mating faces of the starboard and port side wings are disposed with complementary engaging the seat and the engaging block, which are mated with each other and tightened by a conic screw, as shown in Figure 27. Therefore, both the wings can be quickly firmly assembled to form the main wing and easily disassembled for the ease of transportation of the aircraft [49].

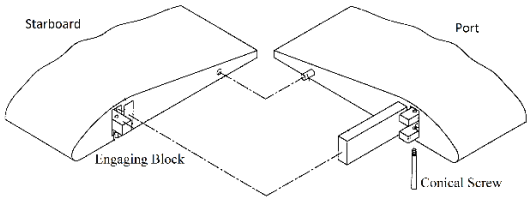


Figure 27 - Wing assembly structure [50] .

The wing is attached to the fuselage of the aircraft with a mechanism which includes a mounting base, a wing bolt, a retaining device (threaded washer) that holds the wing bolt in the mounting base, and a flexible support member positioned between the retaining device and the mounting base. Upon installation of the wing, a threaded bolt or screw is used to attach the wing to the wing-attachment surface, as shown in Figure 28. It is also claimed that a breakaway link could be achieved by this way so that it prevents critical damage of airframe when the wingtip strikes the ground during landing [50].

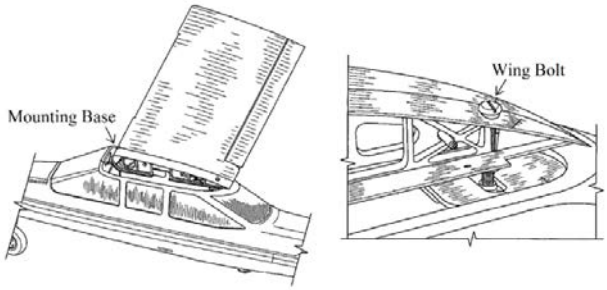


Figure 28 - Wing-attachment mechanism for Airplane [50].

An extended connecting member with a ferromagnetic tip connects the wing with the fuselage, as shown in Figure 29. The joint is created by the ferromagnetic attraction of two magnets, each placed in wing and the ends of connecting member respectively, as shown in Figure 30 [51].

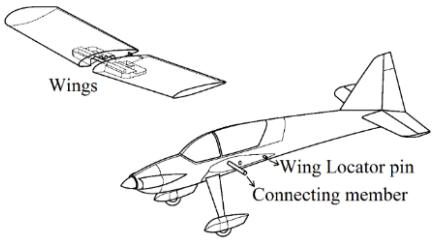


Figure 29 - Wing attachment in the airplane [51].

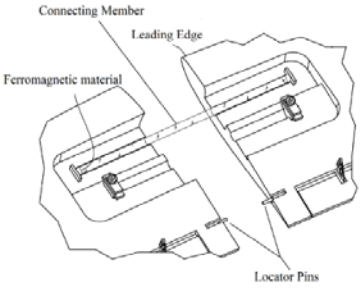


Figure 30 - Wing attachment in the airplane [51].

## 2.4 Materials and Shape selection

### 2.4.1 Material selection

Airframe materials have seen remarkable evolution from the Wright brothers first powered-flight airplane, which was made primarily of wood and fabric, to modern engineered alloys, primarily aluminum and CFRP composites. Since, the aircraft itself is a very complex system of machine, the structural design of an aircraft including its choice of materials are governed by the requirements defined by government agencies, industry, and their customers, such as the Federal aviation administration (FAA), National aeronautics and space administration (NASA) and other military agencies. Most of the requirements are interdependent, and many are readily quantifiable, but some are less tangible [52].

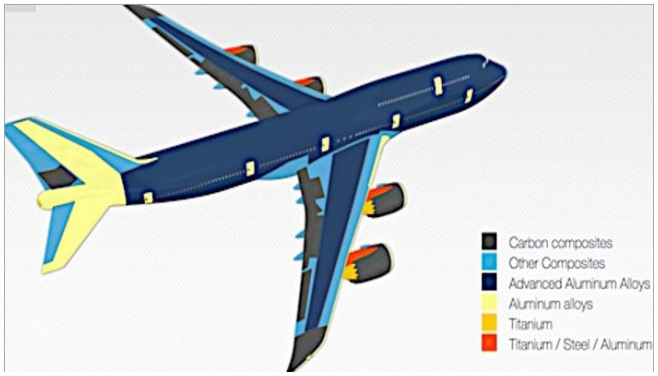


Figure 31 – Construction materials of Boeing 747-800 [53].

The process of selecting materials to be used in the airframe is an important event in the design of aircraft. The key objective of materials selection is to identify the materials that are best suited to meet the design and structural requirements of an aircraft component [27]. Materials selection in aerospace involves one of two situations, the selection of either so-called revolutionary or evolutionary materials (Figure 31). Revolutionary materials selection involves selecting a material that has not been used previously in aircraft and the other is evolutionary material which involves selecting an existing material for an application where it has been used before. Regardless of whether new or existing materials are chosen, the process by which the best material is selected is the same. The weight, strength, and reliability of materials used in aircraft construction are extremely important. The materials used must have a good strength/ weight ratio in the form used, and must be thoroughly reliable to eliminate any possibility of dangerous, unexpected failures. In addition to these general properties, the material selected for a definite application must have specific properties that make it suitable for the purpose. No single material is adaptable for all purposes. A part, member or assembly is studied from many viewpoints before the best material that can be used in its construction is detainable [27]. Aerospace structural material critical requirements include mechanical, physical and chemical properties, such as high strength, stiffness, fatigue durability, damage tolerance, low density, high thermal stability, high corrosion and oxidation resistance, as well as commercial criteria such as cost, servicing and manufacturability [54]. Thus, materials are selected based on their ability to meet these requirements [15]. These requirement gives rise to a huge number of factors to be considered during the process of material select and making it very difficult to carry out. Thus, based on these requirements, the points to be considered in materials selection are summarized and are arbitrability divided into economic and engineering considerations, as tabulated in Table 13.

Table 13 - Considerations in Material Selection [27] [15], [55] [42] and [54].

| Considerations | |
|---|---|
| **Economic Considerations** | |
| Availability | It is extremely important that the material selected for use in the construction of aircraft should be |

| | |
|---|---|
| | available in sufficient quantities to satisfy normal and emergency requirements. The material should also be purchasable from a reputable manufacturer who can guarantee a reasonable delivery date. |
| Cost | The cost per unit weight airframe material should be compared with the cost of other available materials. In making this comparison the savings resulting from a higher strength/weight ratio or better working properties must be considered. |
| Shop Equipment Required | The initial and maintenance cost of shop equipment required for the working of the material selected must be considered. |
| Standardization of materials | It is advantageous to stock as few materials as possible. In selecting a material for an application, the possibility of using one already on hand for other purposes should be considered. |
| Reliability | It is essential that the material selected be of consistent high quality. The selection of a standard material manufactured by a reputable manufacturer will minimize the likelihood of obtaining a sour lot of material. |
| Supplementary operations required | In selecting a material, the cost and time necessary for such operations as machining, heat treatment, cleaning, plating and so on, should be considered. |
| **Engineering Considerations** | |
| Strength | The material must develop the required strength within the limitations imposed by dimensions and weight. Dimensional limitations are particularly important for external members and for wing beams in shallow wings. |
| Weight | An effective way to increase energy efficiency and reduce fuel consumption is reducing the mass of aircraft. Lightweight design and materials enables, longer flight duration and other improved performance parameters. |
| Corrosion | Due to the thin sections and small safety factors used in the design of aircraft, it would be dangerous to select a material that is subject to severe corrosion under the conditions in which it is to be used. |
| Working Properties | The ability to form, bend, or machine the material selected to the required shape is important. |
| Joining Properties | The ability to make a structural joint oy means of welding or soldering, as well as by mechanical means such as riveting or bolting, is a big help in design and fabrication. |
| Shock and Fatigue Strength | Aircraft are subject to both shock loads and vibrational stresses. It is essential that materials used for critical parts should be resistant to these loads. |

### 2.4.2 Shape selection

Apart from meeting the basic service requirements, the improvement of structural efficiency in aerospace structural design becomes increasingly critical because the application of lightweight structures brings benefits to aircraft performance such as increased energy efficiency, acceleration performance, payload, flight endurance, and reduced life cycle cost and greenhouse gas emissions [42]. There are many different types of structures in aircraft, each of which has a specific purpose or function. However, the structure which is more suitable for a purpose is more efficient than the others in the same purpose (Figure 32). By “efficient” it means that, for given loading conditions, the section uses as little material, and is therefore as light, as possible.

Figure 33, shows the comparison of bending stiffness factors of a solid rectangular bar and an “I” section, where “I” section possess identical bending stiffness with a comparatively lower cross section, thus, it is more efficient in terms of bending stiffness than the solid rectangular bar.

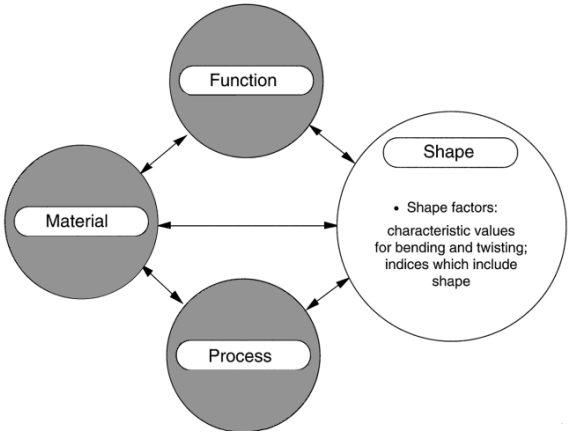


Figure 32 – Importance of shape selection in product development [56].

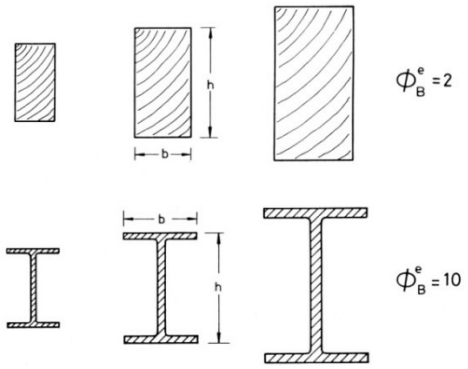


Figure 33 - Comparison of size and shape [56].

The principle of lightweight design is to use less material or materials with lower density but ensure the same or enhanced technical performance. A typical approach to achieve lightweight design for aerospace components and systems is to apply advanced lightweight materials on numerically optimized structures, which can be fabricated with appropriate manufacturing methods. As such, the application of advanced lightweight materials can effectively achieve both weight reduction and performance improvement. Structural optimization is another effective way to achieve light-weighting, by distributing materials to reduce resources use, and enhance the structural performance such as higher strength and stiffness. Advanced optimization approaches can be applied to optimize the layout of structural elements, as well as geometrical parameters to maximize structural stiffness, minimize mass and enable incorporation of energy storage features [42]. The conventional approach to optimization relies on the intuition and experience of the engineers based on experimental outcomes and, consequently, it could require extensive studies and time to achieve the desired results. In numerical structural optimization, an approximate

model is created and optimized at each design cycle. Afterwards, the design solution of the approximate optimization is used to update the finite element model to perform a full system analysis to create the next approximate model. The sequence of design iterations continues until the section properties of a given part are modified to meet a specified target, which could be stress or displacement [57] (Figure 34).

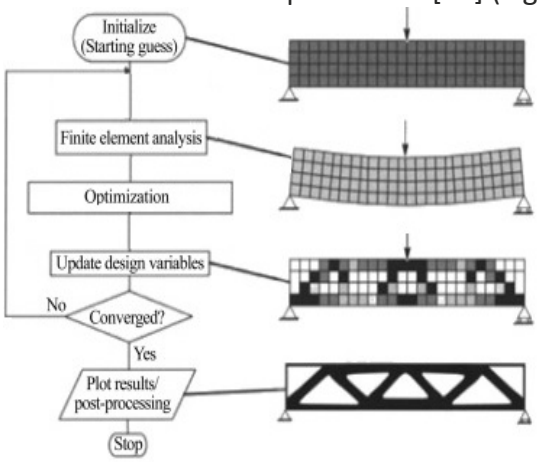


Figure 34 - Flowchart of a computational structural optimization process [42].

### 2.4.2.1 *Shape optimization*

It is commonly used to design the shape of the boundaries of the structure by modifying the location of grids, shown in Figure 35. However, the connectivity of the structure is not changed in the process of this type of optimization [58].

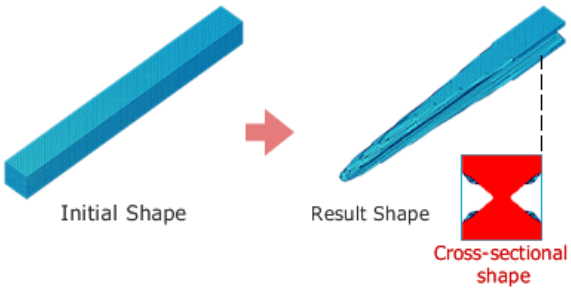


Figure 35 - Shape optimization.

### 2.4.2.2 *Shape Factors*

A material can be thought as having properties but no shape; a component or a structure is a material made into a shape. A shape factor is a geometrical parameter. It is a dimensionless number which characterizes the efficiency of the shape, regardless of its scale, in each mode of loading. Thus, there is a shape factor, $\phi_B^e$, for elastic bending of beams, and another, $\phi_T^e$ for elastic twisting of shafts. **Error! Reference source not found.** gives the moments and areas of sections for common shapes used in general applications. The shape factor is calculated from the formulas given in the table. The shape factors are more appropriate when design is based on stiffness, instead of being based on strength. Strength can be a material constraint.

Table 14 gives the formulas for the shape factors of common sections used in general applications.

Table 14 - Shape factors [56].

| Section Shape | Stiffness | | Failure/Strength | |
|---|---|---|---|---|
| | $\phi_B^e$ | $\phi_T^e$ | $\phi_B^f$ | $\phi_T^f$ |
|  | 1 | 1 | 1 | 1 |
|  | $\frac{\pi}{3}=1.05$ | 0.88 | $\frac{2\sqrt{\pi}}{3}=1.18$ | 0.74 |
| 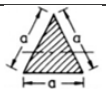 | $\frac{2\pi}{3\sqrt{3}}=1.21$ | $\frac{2\pi}{5\sqrt{3}}=0.73$ | 0.77 | 0.62 |
|  | $\frac{r}{t}$ | $\frac{r}{t}$ | $\left(\frac{2r}{t}\right)^{1/2}$ | $\left(\frac{2r}{t}\right)^{1/2}$ |
| 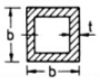 | $\frac{\pi b}{6t}$ | $\frac{\pi b}{8t}\left(1-\frac{t}{b}\right)^4$ | $\frac{2\sqrt{\pi}}{3}\left(\frac{b}{t}\right)^{1/2}$ | $\frac{\sqrt{\pi}}{2}\left(\frac{b}{t}\right)^{1/2}\left(1-\frac{t}{b}\right)^2$ |
|  | $\frac{\pi h(1+3b/h)}{6t(1+b/h)^2}$ | $\frac{\pi h(1+3b/h)}{6t(1+b/h)^2}$ | $\frac{\sqrt{2\pi}}{3}\left(\frac{h}{t}\right)^{1/2}\frac{(1+3b/h)}{(1+b/h)^{3/2}}$ | $\frac{\sqrt{2\pi}h}{(bt)^{1/2}(1+h/b)^{3/2}}$ |
|  | $\frac{a(1+3b/a)}{t(1+b/a)^2}$ | $\frac{8(ab)^{5/2}}{t(a^2+b^2)(a+b)^2}$ | $\left(\frac{a}{t}\right)^{1/2}\frac{(1+3b/a)}{(1+b/a)^{3/2}}$ | $\frac{4a^{1/2}}{t^{1/2}(1+a/b)^{3/2}}$ |

$\phi_B^e$, $\phi_T^e$ are, stiffness in bending and torsion, respectively; $\phi_B^f$, $\phi_T^f$ are failure/strength in bending and torsion, respectively.

The shape factors are defined in comparison with the solid circular section with cross section area as that of a shaped section. Thus, a solid circular section has a shape factor of 1. Sections which have shape factors more than 1 are considered of be more efficient that the solid circular section of same cross section area. The structure factor for bending is the ratio of the bending stiffness of the shaped beam to that of a solid circular section with the same cross-sectional area, thus [56]:

$$\phi_B^e = \frac{S_B}{S_{B_o}} = \frac{I}{I_o} \tag{2.1}$$

$S_{Bo}$ and $I_o$, are the bending stiffness and Second moment of Area of the solid circular section with the same cross-sectional area of that of shaped beam section, respectively.

The structure factor for torsion is the ratio of the torsional stiffness of the shaped shaft to that of a solid circular section with the same cross-sectional area, thus [56]:

$$\phi_T^e = \frac{S_T}{S_{T_o}} = \frac{K}{K_o} \tag{2.2}$$

$S_{To}$ and $K_o$, Torsional stiffness and Resistance to Twisting of circular section with the same cross-sectional area of that of shaped section respectively. (Equivalent to polar moment *J* of a circular section); $S_T$ and K, Torsional stiffness and resistance to twisting of shaped beam section respectively.

The most efficient shape for a given material is the one which, for a given load, uses the minimum material. Mechanical efficiency is obtained by combining material with shape. Thus, it is the material and the structure combined to make a structure more efficient. For spars, which functions like a beam, the best choice for the material-shape combination for a light stiff spar is with the greatest value of the index $M_1$ index for high efficiency.

$$M_1 = \frac{(E\phi_B^e)^{\frac{1}{2}}}{\rho} \tag{2.3}$$

$\phi_B^e$ = structure factor for bending; $E$ = Young's modulus of the material; $\rho$ = Density of the material.

From Equation 2.3, $E$ and $\rho$ are the material property and $\phi_B^e$ is the shape function [56]. The most effective way to improve structural efficiency is by using lightweight materials (low density), which can be more effective than increasing stiffness or strength of the structure [54].

## 2.5 Finite Element Analysis

Most engineers and scientists studying physical phenomena are involved with two major tasks;

- Mathematical formulation of the physical process;
- Numerical analysis of the mathematical model.

The mathematical formulation of a physical process requires background in related subjects such as physics and most often certain mathematical tools. The formulation results in mathematical statements, often differential equations, relating quantities of interest in the design of the physical process. Development of the mathematical model of a process is achieved through assumptions concerning how the process works. In a

numerical simulation, one must uses a numerical method through computers to evaluate the mathematical model and estimate the characteristics of the process [59].

### 2.5.1 Finite Element Method

The finite element method (FEM) is a numerical technique for solving mathematical problems which are described by partial differential equations or can be formulated as functional minimization. A domain of interest is represented as an assembly of finite elements. Approximating functions in finite elements are determined in terms of nodal values of a physical field which is sought. A continuous physical problem is transformed into a discretized finite element problem with unknown nodal values. For a linear problem, a system of linear algebraic equations should be solved using the approximating function. Values inside finite elements can be recovered using nodal values. Two features of the FEM are worth to be mentioned [60]:

- Piece-wise approximation of physical fields on finite elements provides good precision even with simple approximating functions (increasing the number of elements one can achieve any precision);
- Locality of approximation leads to sparse equation systems for a discretized problem. This helps to solve problems with very large number of nodal unknowns.

The steps involved in finite element method are summarized below [61]:

**Discretize the continuum:** The first step is to divide a solution region into finite elements.

**Select interpolation functions:** Interpolation functions are used to interpolate the field variables over the element.

**Find the element properties:** The matrix equation for the finite element should be established, which relates the nodal values of the unknown function to other parameters. For this task, different approaches can be used; the most convenient are: the variational approach and the Galerkin method.

**Assemble the element equations:** Combine local element equations for all elements used for discretization. Element connectivities are used for the assembly process. Before solution, boundary conditions should be imposed.

**Solve the global equation system:** Direct and iterative methods can be used for solution. Then the nodal displacements of the sought function are determined from the solution.

**Compute additional results:** In many cases, one needs to calculate additional parameters. In mechanical problems strains and stresses are of interest in addition to displacements, which are obtained after solution of the global equation system.

The routine aspects of structural analysis can be performed by digital computers after the assumptions as to material behavior, member properties, geometry and loading have been made. The direct stiffness method is the most widely used approach for the analysis of linear elastic structures and it is based on the matrix equilibrium equation. The structure is defined by several nodes connected by members. The members are

usually assumed straight between the nodes. Each of the nodes can displace and the displacements in directions defined by the coordinate system are the degrees of freedom (DoF) of the structure. The direct stiffness method is a displacement method because it aims to determine the displacements corresponding to the DoF of the structure.

$$KD = Q \tag{2.4}$$

K = stiffness matrix; D = vector of the nodal displacements corresponding to the degrees of freedom of the structure; Q = vector of applied loads corresponding to the degrees of freedom.

Thus, *K* is a matrix of stiffness-influence coefficients which is an inherent property of the structure. The stiffness matrix is symmetric and positive definite. It becomes non-positive definite if the structure is unstable. If there are *n* degrees of freedom, the stiffness matrix *K* is a n*n array, and *D* and *Q* are n*1 arrays. Equation 2.4 is then solved for *D*. Once the displacements are known, the member properties can be used to determine internal forces [62].

### 2.5.2 Elastic Failure Theories

Many aircraft components are subjected to several combinations of loads simultaneously. These components, subjected to combined loads, should be related to experimentally determined properties of material under "similar" conditions. However, it is not possible to conduct such tests for different possible combinations of loads and obtain mechanical properties. In practice, the mechanical properties are obtained from a simple tension test. They include yield strength, ultimate tensile strength and strain. In the tension test, the specimen is axially loaded in tension and not in any other combination of loads. Theories of elastic failure provide a relationship between the strength of isotropic components (metals) subjected to complex state of stresses with the mechanical properties obtained in the tension test. With the help of these theories, the data obtained in the tension test can be used to determine the dimensions of the component, irrespective of the nature of stresses induced in the component due to complex loads. Several theories have been proposed, each assuming a different hypothesis of failure:

- Maximum principal stress theory (Rankine's theory);
- Maximum shear stress theory (Coulomb, Tresca and Guest's theory);
- Distortion energy theory (Huber von Mises and Hencky's theory);
- Maximum strain theory (St. Venant's theory);
- Maximum total strain energy theory (Haigh's theory).

Ductile materials typically have the same tensile strength and compressive strength. Also, yielding is the criterion of failure in ductile materials. Therefore, maximum shear stress theory and distortion energy theory are used for ductile materials [63].

#### 2.5.2.1 Maximum shear stress theory

As per the maximum shear stress theory, the material yields when the maximum shear stress at a point equals the critical shear stress value for that material. Since this should be true for uniaxial stress state, one can use the results from uniaxial tension test to determine the maximum allowable shear stress. The maximum shear stress in an element loaded in pure tension is one-half the maximum tensile stress, the shear yield is taken to be $0.5S_{ys}$.

The yield criterion for the maximum shear stress theory is:

$$\tau_{max} = \tau_{Tresca} = \frac{(\sigma_1 - \sigma_3)}{2} \tag{2.5}$$

$\tau_{max}$ = Maximum shear stress; $\tau_{Tresca}$ = Tresca's Stress.

The condition for yielding is when the Tresca's stress is equal to half of the yield strength [64]:

$$2\tau_{Tresca} = S_{yt} \tag{2.6}$$

$\tau_{Tresca}$ = Stress Tresca's; $S_y$ = Yield Strength.

#### 2.5.2.2 Distortion energy theory

As per the distortion energy theory, a ductile solid will yield when the distortion energy density reaches a critical value for that material. Since this should be true for uniaxial stress state also, the critical value of the distortional energy can be estimated from the uniaxial test.
The von Mises criterion is given by the following equation:

$$\sigma_{vM} = \sqrt{0.5[(\sigma_1 - \sigma_2)^2 + (\sigma_2 - \sigma_3)^2 + (\sigma_3 - \sigma_1)^2]} \tag{2.7}$$

$\sigma_{vM}$ = von Mises Stress; $\sigma_1$, $\sigma_2$ $and$ $\sigma_3$ = Principal stresses.

The condition for yielding is when the equivalent von Mises stress equals the yield strength [64]:

$$\sigma_{vM} = S_{yt} \tag{2.8}$$

$\sigma_{vM}$ = von Mises Stress; $S_y$ = Yield Strength.

Figure 36 represents the two–dimensional failure envelope as per maximum shear stress theory and maximum distortion energy theory.

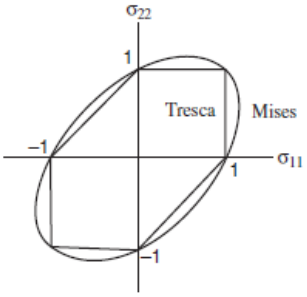


Figure 36 – Failure envelope of maximum distortion energy theory and maximum shear stress theory calibrated on $S_{yt}$ [64].

Both, maximum shear stress theory and distortion energy theory are one-parameter forms, specified by either the uniaxial tensile strength, $S_{yt}$ (with $S_{yc} = S_{yt}$), or the shear strength, $S_{ss}$. Shear stress involves only one parameter, and that does not naturally generalize to a two-parameter form, which is necessary for non-perfectly ductile materials. Thus, both maximum shear stress theory and distortion energy theories, are specified by $S_{yt}$ equal to $S_{yc}$. With calibration by $S_{yt}$, there is still the choice between the Mises and Tresca forms. Mises is smooth, while Tresca has corners [64]. The hexagonal diagram of maximum shear stress theory is inside the ellipse of distortion energy theory. Therefore, maximum shear stress theory gives results on the conservative side. On the other hand, distortion energy theory is slightly liberal [63]. At the crystal level (single grain) yielding is associated with dislocation movement on slip planes. This is caused by shear stress on the slip system (resolved shear stress). It would be tempting to say that this justifies and validates the Tresca criterion. But the condition of isotropy implies and applies to polycrystalline aggregates with the individual crystals taking all possible orientations. Dislocation-induced plastic flow occurs over many slip systems. Furthermore, dislocation pile-up occurs at the grain boundaries. The vastly more complex behavior at the aggregate level compared with the crystal level, must involve averaging over a wide variety of physical conditions and effects. This averaging has a smoothing effect that is much more supportive of the smooth Mises criterion than of the non-smooth Tresca form [64]. Thus, the Distortion energy theory is used when the factor of safety is to be held in close limits, supporting practical weight savings This theory predicts the failure most accurately [63].

### 2.5.3 Composite failure theories

The failure of composites has been investigated extensively from the micro-mechanical and macro-mechanical points of view. On the micro-mechanical scale, failure mechanism and the processes.to predict the failure, vary widely with type of loading and are intimately related to the properties of the constituent phases, i.e., matrix, reinforcement and interface-interphase. Failure predictions based on micromechanics, even when they are accurate about failure initiation at critical points, are only approximate about global failure of a lamina and failure progression to ultimate failure of a multi-directional laminate. For this reason, a macro-mechanical approach to failure analysis is preferred. The main properties that describe a composite material

are the engineering constants and the strength properties of a single unidirectional lamina that make the laminated structure. The experimental evaluation of these properties is quite costly and time consuming because they are functions of several variables such as the individual constituents of the composite, fiber volume fraction, packing geometry and fabrication processes. Hence, analytical models to predict these properties were developed to aid the design of composites. Numerous failure theories have been proposed and are available to the composite structures. They are classified into three groups [65]:

- Limit or noninteractive theories (maximum stress, maximum strain);
- Interactive theories (TsaiHill, Tsai-Wu);
- Partially interactive or failure mode based theories (Hashin-Rotem, Puck).

The validity and applicability of a given theory depend on the convenience of application and agreement with experimental results. The plethora of theories is accompanied by a dearth of suitable and reliable experimental data, which makes the selection of one theory over another rather difficult. These six failure theories were reviewed and comparisons of theoretical predictions with experimental results was analyzed using existing lamina and laminate strength data. For some laminates under certain loading conditions, all six criteria may predict similar results, and their performance cannot be ranked. Therefore, several laminates are identified for which the strength predictions as per these six criteria are substantially different. The maximum strain, maximum stress, Tsai-Hill and Tsai-Wu are the very widely used theories in about 80% of cases among which Maximum Strain is most commonly used at 30% [65], shown in Figure 37.

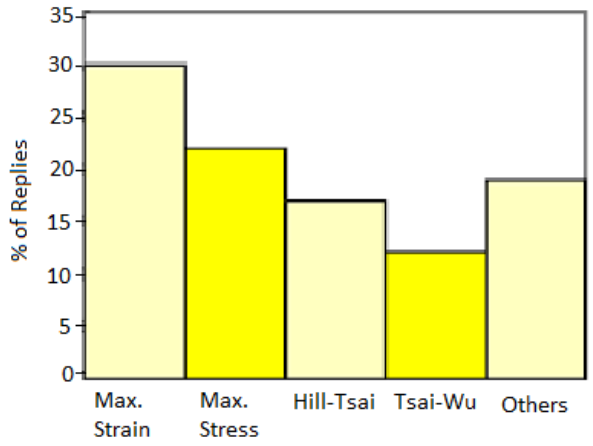


Figure 37 - Results of AIAA failure criteria survey [65].

### 2.5.3.1 *Maximum Strain Theory*

The maximum strain theory (Saint Venant's theory) predicts failure when any principal material axis strain component exceeds the corresponding ultimate strain. Three different conditions of failure are considered in correspondence with a maximum

strain in fibre direction, matrix or transversal direction and for shear strains. The criterion to avoid failure is given in the following equations [66]:

$$-e_L^- < \epsilon_1 < e_L^+ \tag{2.9}$$

$$-e_T^- < \epsilon_2 < e_T^+ \tag{2.10}$$

$$|\gamma_{12}| < e_{LT} \tag{2.11}$$

$e_L$= Longitudinal strain limit; $e_T$ = Transverse strain limit; $\gamma_{12}$= Shear Strain; $\epsilon_1$= Principal Strain 1; $\epsilon_2$= Principal Strain 2; $e_{LT}$= shear strain limit.

The failure index is calculated as the maximum ratio of ply strain to allowable strain [67]:

$$F_{index} = \max\left(\left|\frac{\epsilon_1}{X}\right|, \left|\frac{\epsilon_2}{Y}\right|, \left|\frac{\gamma_{12}}{S}\right|\right) \tag{2.12}$$

$\epsilon_1$= Principal Strain 1; $\epsilon_2$= Principal Strain 2; $X$= Longitudinal failure strain; $Y$= Longitudinal failure strain; $S$= Failure shear strain.

### 2.5.4 Safety factors

#### *2.5.4.1 Isotropic parts*

The ultimate aircraft structural factor of safety is defined as the ratio of design ultimate load to design limit (or actual applied) load on the structure and is usually equal to 1.5 [68]. In aeronautics, the margin of safety is calculated after applying the ultimate structural factor of safety. The metallic structure must carry the ultimate load without any failure. In the case of a margin of 0, the part is at exactly the required strength (the safety factor would equal the design factor). The margin of safety for isotropic parts is calculated using the following equation [69].

$$MS_{vM} = \frac{F_{tu}}{\sigma_{vM} * UF} - 1 \tag{2.13}$$

$MS_{vM}$= Margin of Safety (von Mises); $F_{tu}$= Ultimate tensile strength; $\sigma_{vM}$= von Mises stress; $UF$= Ultimate factor of safety.

#### *2.5.4.2 Composite parts*

To obtain the margin of safety for composite structural parts, the strain at limit Load condition is checked, considering the maximum allowable as barely visible impact damage (BVID) criteria [70]. BVID was introduced to satisfy conditions representative of the requirements in FAR. The requirement is that composite structure with damage, including BVID, shall demonstrate a reliable service life while retaining ultimate load capability [71]. The following equation shows the maximum strain allowable as BVID criteria [70]:

$$e_T = 5000\mu e;\ e_C = -2600\mu e;\ e_{LT} = \pm 5200\mu e \tag{2.14}$$

$e_L$= Longitudinal strain limit; $e_T$ = Transverse strain limit; $\gamma_{12}$= Shear Strain

Thus, the condition for the composite material to satisfy BVID criteria is;

$$\left(\left|\frac{\epsilon_1}{e_L}\right|, \left|\frac{\epsilon_2}{e_T}\right|, \left|\frac{\gamma_{12}}{e_{LT}}\right|\right) < 1 \tag{2.15}$$

$e_L$= Longitudinal strain limit; $e_T$ = Transverse strain limit; $\gamma_{12}$= Shear Strain; $\epsilon_1$= Principal Strain 1; $\epsilon_2$= Principal Strain 2; $e_{LT}$= shear strain limit.

# THESIS DEVELOPMENT

# 3 THESIS DEVELOPMENT

## 3.1 Study of UAS-30 P2

The UAS30-P2, shown in Figure 38 and Figure 39, is a medium sized UAV made by CEiiA. It is designed for stable flight with less maneuvering flight envelope. The aircraft is featured with a $M_{TOW}$ of 30 kg. The UAV is manufactured majorly with laminated composite materials and metallic (aluminium and steel) alloys. The CFRP is used for the construction of entire aircraft skins and contributes to most of the primary structural components as such as the spars, main landing gears, etc. The CFRP is used in large amount to meet the weight requirements of the aircraft, pushing it to a specification of Miniature UAV. The secondary structures such as ribs and longerons are CFRP-Airex sandwich structures. The operating weight of the aircraft is as low as 21.5 kg. In some cases, the aircraft is operated without the landing gear saving another 2.9 kg of weight. In this case the aircraft is launched using a catapult setup and landed safely using the net arrest operations, as studied in Section 1.1.2. The aircraft is designed with a removable wing configuration for ease of transportation.

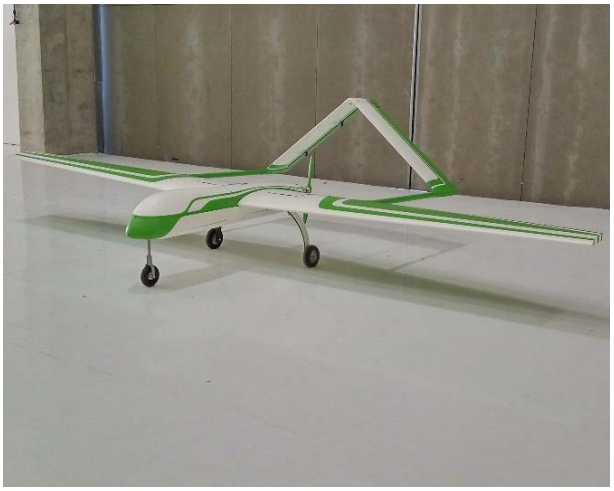

Figure 38 - UAS30 - P2 in hanger.

Figure 39 - UAS30 - P2 in air field.

As the aircraft is designed for more stable operations, the aerodynamic loads during cruise and maneuvering are not the most crucial loading cases. The studies made in the stress reports of the aircraft revealed that the catapult launch and the net arrest operations were the most crucial loading conditions for the aircraft. Considering the CFRP, which contributes to most of the structural components of the aircraft, those operations create even more impact on the aircraft structures.

### 3.1.1 UAS-30 P2 Spar Connector

Figure 40 reviews the entire wing and tail attachment setup of the aircraft UAS30-P2. Figure 41 shows the spar connector for the Aircraft UAS30- P2. It is a part made of single piece of solid extruded aluminium 7075-T7351, machined by CNC and then post processed by abrasive blasting.

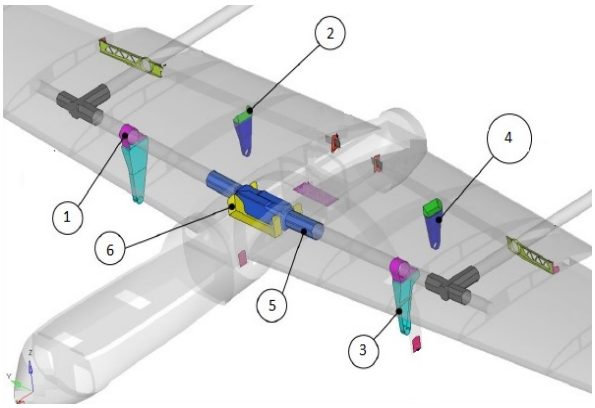


Figure 40 - UAS30-P2 Wing attachment setup.

Note: In Figure 40; 1,2,3 and 4 - Catapult arms; 5 - Spar connector; 6 - wing attachment frame; Spar connector.

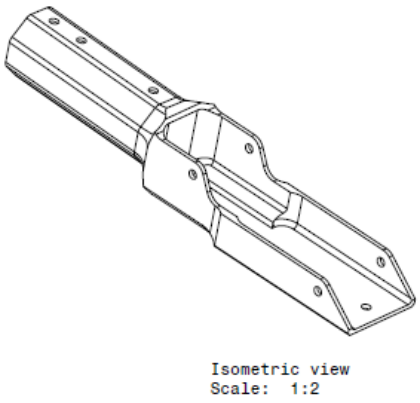


Figure 41 - UAS30-P2 Spar connector.

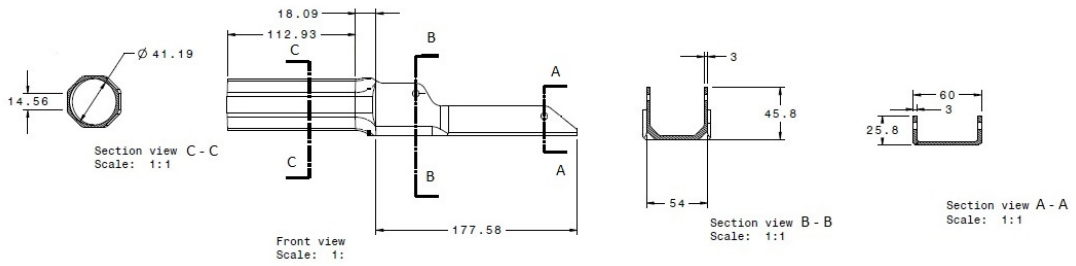


Figure 42 - Spar connector sections.

Figure 42, shows the sections of the spar connector, and the cross sections A-A and B-B houses inside the fuselage facilitating the spar connector to be attached to the aircraft along with its other pair of spar connectors. These sections are supported by a metallic frame, with which, they are fastened. The section C-C protrudes out of the fuselage, facilitating it to be attached to the main wing spar of the aircraft. From the studies carried out in the stress report of UAS30-P2, this section was identified to be the critical among the other two sections. Thus, the calculations made on spar connectors are preliminarily based on section C-C.

### 3.1.2 UAS-30 P2 Spar

Like most of UAS30-P2's primary structures, the main wing spar is made of composites (CFRP). The spar is currently being outsourced by CEiiA. Figure 43 shows the main wing

spar of the aircraft.

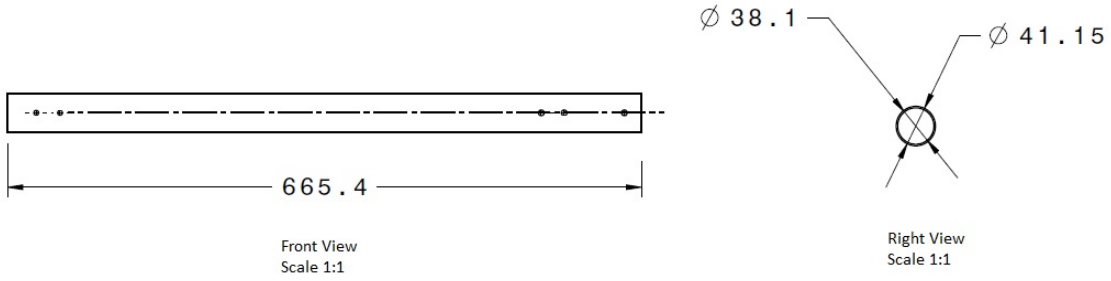


Figure 43 – UAS30-P2 Main Wing Spar.

### 3.1.3 Understanding the need of Spar in UAS-30

The need of spar in UAS30-P2 is based on the following factors:

- The aircraft has a strong skin made up of CFRP, thus contributing well to the stiffness requirement;
- At ground, the spar not only supports the weight of the wing structure; it also supports the fuel tank/batteries housing in the wing which in turn supports the propulsion system. The tail plane is attached directly to the main spar;
- In flight, aerodynamic moments produced due the actions of control surfaces are transmitted within the aircraft, through the spar [72] and [73];
- Sometimes, the aircraft is operated without landing gear, launched by an external catapult system, and is landed in a net recovery system. Thus, impact loads are very crucial in those cases.

### 3.1.4 Loads in spar and spar connector

- **Bending:** Due to the Aerodynamic lift distribution along the wing, weight of the main-plane, tail-plane and fuel tank/batteries during ground operations;
- **Impact:** Due to the aerodynamic gusts during flight and landing in a net recovery system when operated without landing gear;
- **Torsion:** Due to transfer of all the aerodynamic moments produced by the control surfaces and the airfoils;
- **Wear:** Due to the interaction of surfaces of Composite spar with metallic connectors;
- **Fatigue:** To determine the safe life and reliability of the components with the notches for pins to removably fix the spar in place [72], [74] and [75].

### 3.1.5 Work Approach

The path for the work is laid based on the studies in Sections 2.2 and 2.4.2. Firstly, the choice of materials will be reviewed. The material along with suitable shape gives the structure with high efficiency. Thus, after selection of material, appropriate shape will be determined. Figure 44 shows the path for work approach.

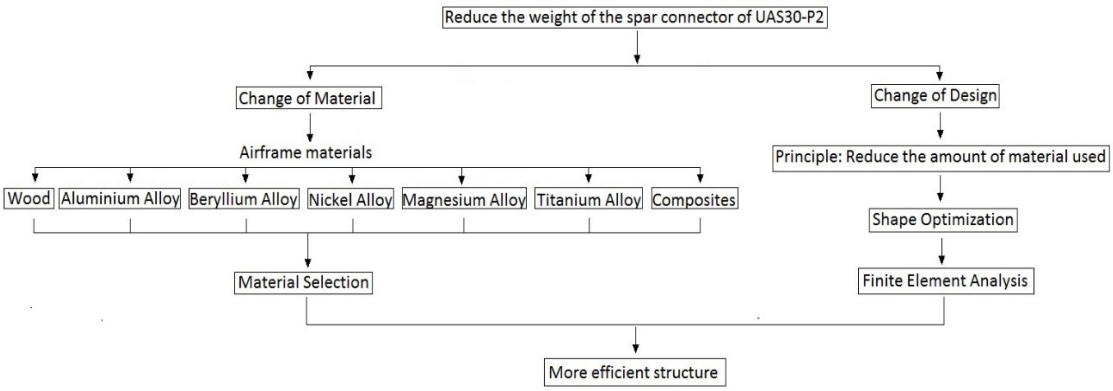


Figure 44: - Work Approach.

## 3.2 Material Selection

There are many ways to select a material for an aircraft component. This is a materials selection of an evolutionary material which involves selecting an existing material for an application where it has been used before. Thus, the process was carried out by direct comparison of engineering and economic factors of materials available for this purpose. These factors are based on the studies in Section 2.4.1. Thus, the materials which are identified based on the studies conducted in Section 2.2, from which most appropriate materials are chosen for selection matrix based on the considerations presented in Table 13, this process is elaborated in Table 15. The appropriate materials are then evaluated in the selection matrix (Section 3.2.4).

### 3.2.1 Functions

The wing spar provides most the weight support and dynamic load integrity of the aircraft UAS30-P2. As discussed in Section 3.1.3, the functions of the spar and spar connector are to support and transmit all the aerodynamic, inertial and structural loads. The aerodynamic distributed load on the wing creates shear force, bending moment and torsional moment at wing spar. Other than that, the auxiliary functions that carried out in the aircraft, results in multiple loads in the wing spar and its connector. These loads are discussed in Section 3.1.4.

### 3.2.2 Materials

Based on various studies performed in Section 2.2, Table 15 gives, the overview about the aerospace materials on the considerations presented in Table 13.

Table 15 - Overview of Airframe Materials.

| Material | Engineering Considerations | Economic Considerations | Comments |
|---|---|---|---|
| Wood | o Unreliability on mechanical properties.<br>✓ Light weight.<br>o Shrinkage of material.<br>o Low working properties.<br>o Poor fatigue resistance. | ✓ High availability.<br>✓ Low cost.<br>o Poor standardization of material. | Wood is a classical material for aircraft structures. Even though they show attractive weight properties, because of its unreliability in mechanical properties and design limitations, as discussed in Section 2.2.1, they are not considered in the selection matrix. |
| Aluminium Alloys | ✓ Good structure efficiency.<br>✓ Light weight.<br>o Good corrosion resistance except to stress corrosion cracking.<br>✓ Good working properties.<br>✓ Good fracture toughness and fatigue resistance. | ✓ Good availability.<br>✓ Moderate cost.<br>✓ Good Standardization of alloys.<br>✓ Reliable supply and usage.<br>✓ Ease of supplement operations. | Aluminium alloys are largely preferred for this type of applications. As it is the current solution in UAS30 P2 and these alloys show a very attractive property thus, the aerospace aluminium alloys which discussed in Section 2.2.2.1, are considered in the selection matrix this. |
| Beryllium Alloys | ✓ Excellent structure factor and good strength.<br>✓ Extremely light weight.<br>✓ Good Corrosion resistance.<br>o Poor Working property, high stiffness.<br>✓ Good fracture toughness and fatigue performance. | o Very low availability.<br>o Very high cost.<br>✓ Good standardization of alloys.<br>o Very limited number of supplies.<br>o Difficult in supplement operations. | Beryllium alloys are outstanding in terms of S.E amongst the materials discussed in Section 2.2.2. These alloys are extremely lighter than the current solution, thus, the beryllium alloys which are discussed in Section 2.2.2.2, are considered in the selection matrix. |
| Nickel Alloy | o Low structure efficiency and Good strength.<br>o Much heavier than aluminium.<br>✓ Good resistance to corrosion.<br>o Poor workability because of high hardness.<br>✓ Good resistance to fatigue and high temperature creep. | o Low availability.<br>o Costs Expensive.<br>✓ Good Standardization of alloys.<br>o Low number of producers.<br>o Difficult of supplement operations. | Nickel alloys are excellent for high temperature applications. But these alloys possess the least SE among the metals discussed in Section 2.2.2.3. Also, considering the fact that it is heavier and expensive than current solution these alloys are not considered in the selection matrix. |

| | | | |
|---|---|---|---|
| Magnesium Alloys | ✓ Decent Structure efficiency and high specific strength.<br>✓ Very Light weight.<br>o Poor corrosion resistance.<br>✓ Good Working ability.<br>o High damping properties but poor fatigue performance. | o Limited number of producers.<br>o No low and stable price.<br>o Only Few optimized alloys.<br>✓ Ease of supplement operations. | Magnesium alloys show poor strength than aluminium. Apart from its poor corrosion and fatigue resistance, considering its attractive weight property which is lower than current solution, thus, the aerospace magnesium alloys which are discussed in Section 2.2.2.4, are considered in the selection matrix. |
| Titanium Alloy | ✓ Good toughness and Structure efficiency.<br>o Twice as Heavier than aluminium.<br>✓ Excellent resistance to corrosion.<br>✓ Good workability but requires special tools and machines.<br>✓ Good fatigue performance. | o Very Expensive.<br>o Need high precision machines and instruments for better tolerance criteria.<br>✓ Good Standardization of alloys.<br>o Difficult to perform supplement operations. | Titanium is a replacement of steel and aluminium when comes to high temperature application. Also, considering the weight factor, cost and machining requirements titanium alloys (Section 2.2.2.5) are not considered in the selection matrix. |
| Steel | ✓ Good toughness and Structure efficiency.<br>o 2.5 times heavier than aluminium.<br>o Very susceptible to Hydrogen embrittlement.<br>✓ Good workability.<br>✓ Good Fatigue resistance. | ✓ High availability.<br>✓ Low to moderate costs.<br>o Reliable supply but not widely used in Airframes.<br>✓ Good standardization of alloys.<br>✓ Ease of supplement operations. | Steel is generally not used in airframes because of its weight penalty (Section 2.2.2.6). Considering it would be heavier than the current solution, steel is not considered in the selection matrix. |
| CFRP | ✓ Very high strength and stiffness.<br>✓ Can save about 10-15% of structural weight.<br>✓ Excellent resistance to corrosion.<br>o Poor workability.<br>o Extremely Poor impact resistance but high fatigue performance. | ✓ Good availability.<br>o Very expensive.<br>✓ Reliable supply.<br>✓ Can be tailored as per requirements.<br>o Hard to fabricate very complex shapes and very slow rates of manufacturing. | The use of properly tailored CFRP can yield a better strength and weight savings of up to 10-15% (Section 2.2.3). However, impact resistance is crucial when it comes to catapult launch and net arrest operations (Section 3.1.4). Also, considering the complexity of the geometry and facilities in CEiiA it is extremely difficult to manufacture. Thus, CFRP is not considered in the selection matrix. |

Note: In Table 15, points marked with bullet type "✓" represents the pros and; points marked with bullet type "o" represents the cons.

### 3.2.3 Weightage of Factors considered in selection matrix

#### *3.2.3.1 Tensile Yield Stress*

All materials have an elastic limit within the plastic deformation is minimal and the material could retain most of its original shape when unloaded. Ductile materials, beyond the elastic limit, permanently deform to great extent owing to a dominant plastic deformation. The point when a material changes from elastic to plastic behavior is called the yield point (also known as the proportional limit). In metallic materials, the yield strength is determined by the amount of stress needed to initiate dislocation slip. Dislocations cannot move when the stress is below the yield point and begin to move when the applied stress exceeds the yield stress. Metals that contain dislocations that can move easily have low yield strength, whereas high-strength metals contain dislocations that are highly resistant to slip. The yield strength of metals is sensitive to the alloy content, type of heat treatment, amount of cold working, grain size and other microstructural features. By appropriate alloying and processing it is possible to greatly increase the yield strength of metals. The strengthening of metals is critical to the design of weight-efficient aircraft structures. Without the ability to increase the yield strength of metals then aircraft structures would be heavy and bulky because of the need to increase their load-bearing section thickness. Thus, the yield strength is an important property in the design of aerospace structures. It is essential that aerospace materials are not subject to stress levels exceeding their yield point, otherwise the structure permanently deforms. The yield strength is used in aerospace design to define the upper stress limit of the material (called the design limit load). Aerospace structures are always designed to operate at stress level well below the design limit load to avoid permanent damage caused by unexpected overloading of the airframe. The failure theories widely used for ductile materials discussed in Section 2.5.2, are based on the tensile yield on which the design limit load of the structure is determined. Considering all this factor the tensile yield is given the highest weightage of 45% among the factors considered in selection matrix.

#### *3.2.3.2 Young's Modulus*

The Young's modulus is the measure of stiffness, and is one of the most important engineering properties for aircraft structural materials. It defines the relationship between stress (force per unit area) and strain (proportional deformation under elastic limit) in a material. Thus, it predicts how much a material deforms under an applied stress. The greater the modulus, the less the material elastically deforms under the application of a given stress. It is a measure of the ability of a material to withstand changes in length when under length wise tension or compression. Thus, for while comparing two closely sized structures with similar cross section made of two different materials, the same stress will produce a strain which depends on the Young modulus of the material. There is a requirement for aircraft structures to have high stiffness to resist excessive deformation under load. Therefore, materials with high elastic

modulus are used in airframes. The elastic modulus of metals is closely related to the binding energy between their atoms. The binding energy between atoms is constant and cannot be changed, and therefore the elastic modulus of a metal is constant. The elastic modulus is not changed significantly by heat treatment, cold working, grain size and other microstructural features that have a large influence on other tensile properties such as strength and ductility. The expression for the Young's modulus is given in Equation 3.1.

$$E = \frac{\sigma}{\epsilon} \tag{3.1}$$

$E$ = Young's modulus; $\sigma$= Applied stress; $\epsilon$=Strain.

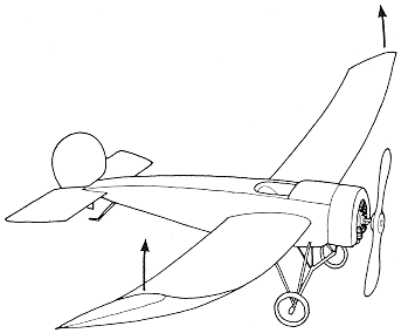

Figure 45 - Deflection of Wings


Figure 46 - Wing stiffness.

Note: In Figure 46, A= High stiffness; B= Low stiffness; C= Low specific stiffness.

Deflection is a function of stiffness of the structure. The aircraft wing is subjected to aerodynamic forces and moments during flight, which result in deflection of the wing, as shown in Figure 45. While at the ground, the wing must support its own weight. UAS30-P2 has high wing span with each wing spanning 2041 mm, and the wing also houses the fuel tanks required to carry fuel for flight. The fuel and structural weight makes each wing as heavy as 5 kg and each tail plane weighs 1.7 kg. Thus, the wing spar must support about 6.7 kg when stationed and must support the weight of the aircraft and gust loads during flight. Thus, for such a long wing it is important that the wing stays stiff to have the least possible deflection during the flight operation. From Section 2.4.2.2, Equation 2.3, has revealed that the Young's modulus has an influence in efficiency of a structure. Considering all this factors, the Young's modulus is given a 35% weightage in the selection matrix.

#### *3.2.3.3 Mass*

An effective way to increase energy efficiency and reduce fuel consumption is reducing the mass of aircraft, as a lower mass requires less lift force and thrust during flight. Lightweight design enables longer flight duration and other improved performance parameters. From in Section 2.4.2.2, the Equation 2.3, has revealed that the density has an influence in the efficiency of a structure. The most effective way to improve

structural efficiency is to opt for a material with lower density which could result to more effective structure compared with increasing stiffness or strength, i.e. using lightweight materials. Thus, considering this factors, the mass is included in the selection matrix and is given a weightage of 20%. Mass is calculated through material density and for a section with length 130 mm and cross section area of 549.49 $mm^2$, which is roughly the section parameters of the critical Section-C of the spar connector, including the thickness of the composite spar mentioned in Section 3.1.

### 3.2.4 Selection Matrix

The materials identified from the study and analysis performed in Section 3.2.2 are ranked based on the weightage factors discussed in section 3.2.3. By this way, the material which is most suitable for the purpose is identified.

Table 16 - Selection matrix.

| Alloys | Tensile Yield (MPa) | Young Modulus (MPa) | Mass (kg) | Score | Ranking |
|---|---|---|---|---|---|
| **Aluminium** | | | | | |
| AA2014 | 415 | 72400 | 200.013 | 57.452 | 4 |
| AA2019 | 290 | 73800 | 202.871 | 46.620 | 7 |
| AA2024 | 325 | 72400 | 197.870 | 49.803 | 5 |
| AA6061 | 216 | 68900 | 192.870 | 40.290 | 11 |
| AA7050 | 505 | 70300 | 202.156 | 64.853 | 3 |
| AA7075 | 520 | 71016 | 200.013 | 66.373 | 2 |
| | | | | | |
| **Beryllium** | | | | | |
| AMS 7902 | 483 | 293027.184 | 132.477 | 96.229 | 1 |
| | | | | | |
| **Magnesium** | | | | | |
| Elektron A8 | 220 | 45000 | 129.294 | 44.355 | 9 |
| AZ91C | 82.737 | 44815.93 | 128.918 | 32.513 | 15 |
| AZ80A | 250 | 45000 | 129.294 | 46.951 | 6 |
| ZM21 | 234 | 44000 | 129.294 | 45.447 | 8 |
| ZK 51A 5Z/ML 12 | 220 | 45000 | 129.294 | 44.355 | 9 |
| ZE41A | 120.658 | 44815.93 | 129.709 | 35.672 | 13 |
| EZ33A | 75.842 | 44815.93 | 130.302 | 31.704 | 14 |
| QE22A | 158.579 | 44815.93 | 129.115 | 39.0458 | 12 |

The material properties are extracted from [23] and [76].

### 3.2.4.1 Beryllium AMS 7902

A versatile material selected when weight and inertia factors exceed those of lower cost aluminium. Beryllium alloys are extremely expensive than the current solution. This alloy was outstanding among other materials in the selection matrix. This is because this alloy has high specific strength and stiffness combined with extremely low weight. Apart from these properties, beryllium alloys are hazardous since, its oxides are toxic. Another fact is that they are allergic and causes lung disorders. This alloys are extremely tuff to be machined in normal conditions. Thus, this alloys requires special high precision machines which are not available in CEiiA. Their cost and availability is also a major concern. Thus, considering this factor this alloy is not chosen for the spar connector.

### 3.2.4.2 Aluminium 7075

This is the current solution used in UAS30-P2. It is a medium to high strength alloy. The attractiveness of this alloy is its tensile strength. Therefore, these alloys are used in fuselage stringers and frames, upper wing stringers, floor beams, seat rails. The temper designation for Aluminium 7075 chosen by CEiiA is T7351. It is a solution heat treated alloy, especially artificially aged for resistance to stress corrosion [77]. Stress-corrosion cracking (SCC) is a term used to describe service failures in engineering materials that occur by slow, environmentally induced crack propagation. The observed crack propagation is the result of the synergistic interaction of mechanical stress and corrosion reactions. The T6 tempered Aluminium 7075 alloys show superior mechanical properties. Considering the highly corrosive conditions in Portugal, the T7351 treated alloy is used by CEiiA to overcome the SCC of most crucial component of UAS30-P2. However, this comes with a penalty of slight reduction in yield strength. Figure 47 shows the relative resistance to SCC for high strength aluminium alloys.

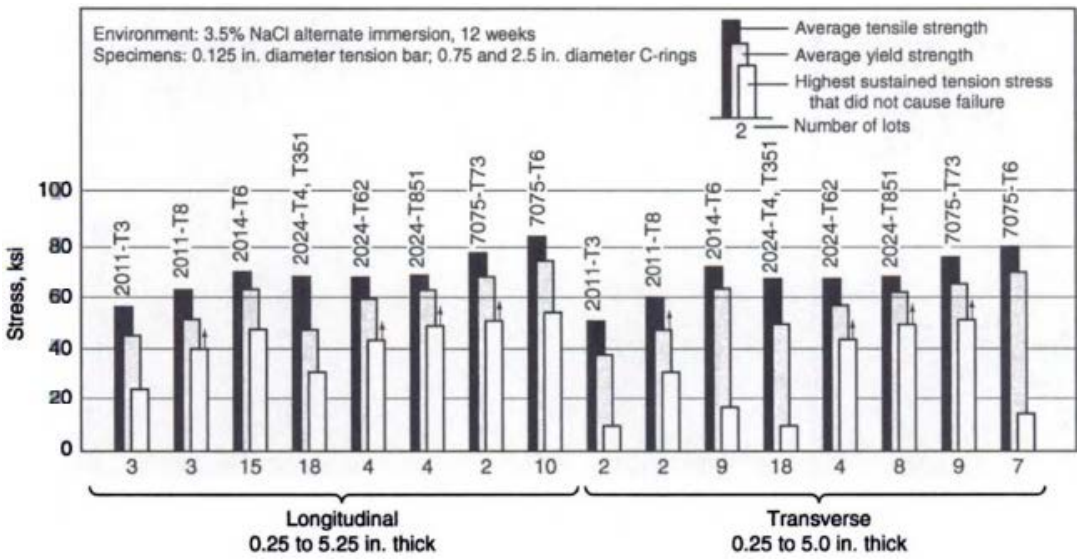


Figure 47 - Relative resistance to SCC of high strength aluminium alloys [77].

Note: The arrows indicate no stress corrosion failures at the highest stress employed.

Thus, considering that the material used in the spar connector was very wisely chosen to serve for the purpose, further work on optimization of the structure shall be carried out with the same material. The following Table 17, gives the properties of the Aluminium 7075 T7351.

Table 17 - Properties of the Aluminium 7075 T7351 [76] and [75].

| Form | **Units** | Bars and Extrusions |
|---|---|---|
| Temper | | T7351 |
| Thickness | (mm) | 50.8-76.2 |
| **Mechanical Properties** | | |
| **$F_{tu}$** | (MPa) | |
| L | | 469 |
| LT | | 448 |
| **$F_{ty}$** | (MPa) | |
| L | | 386 |
| LT | | 359 |
| **$F_{cy}$** | (MPa) | |
| L | | 372 |
| LT | | 379 |
| **$F_{su}$** | (MPa) | 276 |
| **$F_{bru}$** | (MPa) | |
| e/D | 1.5 | 696 |
| e/D | 2 | 903 |
| **$F_{bry}$** | (MPa) | |
| e/D | 1.5 | 558 |
| e/D | 2 | 689 |
| E | (MPa) | 71016 |
| $E_c$ | (MPa) | 72395 |
| G | (MPa) | 26890 |
| μ | | 0.33 |
| **Physical Property** | | |
| $\rho_a$ | ($kg/mm^3$) | $3.649\ e^{-06}$ |

## 3.3 Shape selection

The process of identifying the optimum shape gives a structure with high efficiency. This process is carried out based on the studies performed in Section 2.4.2, from which the suitable shape can be identified based on the iterations of structure analysis of the spar and spar connector for various load conditions. Figure 48 shows the process of shape selection.

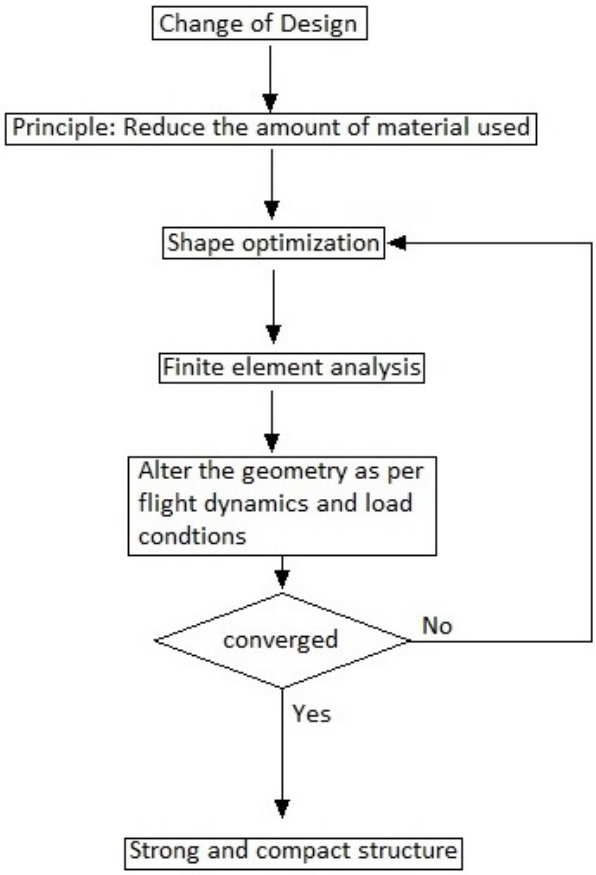


Figure 48: Change of Design.

### 3.3.1 Geometry

As mentioned in Section 3.1.1, the section which is critical among the sections of spar connector is the tubular section which connects the wing spar and the fuselage, marked as “Section-C” in Figure 49. Thus, the calculations are primarily targeted on this section of the spar connector.

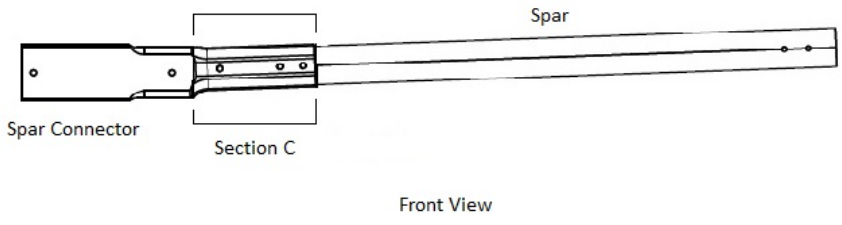


Figure 49: Critical Section (Section-C).

For the ease of calculations, this geometry is approximated as a hollow circular tube of outer diameter, D=23.2 mm; thickness, t=4.1 mm; and length, L=130 mm. This approximation is made based on the moment of inertia of the tubular section, including the thickness of CFRP spar of the existing spar connector shown in Figure 50.

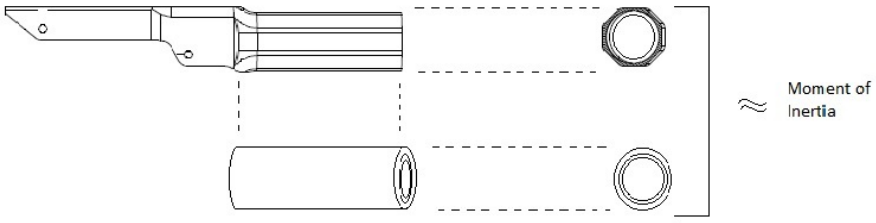


Figure 50 - Geometry approximation.

The use of telescopic pipes as a spar is a predominant solution for the weight reduction as mentioned in Section 2.3.1. However, this solution results in lower stiffness at the wing tips. As shown in Table 18, slight decrease in outer radius of the circular section with constant thickness still gives rise to higher deflection and lower structure factor. For the calculation of deflections, the structure with length and dimensions of approximated Section-C of spar connector is subjected to 100 N of force, as shown in Figure 51, iterations are made for each 0.1 mm reduction in radius and the thickness is kept constant. Wing tips do not contribute to much in aerodynamic lift but in UAS-30 P2 the catapult launch setup is attached at the tips of the spar and net arrest operation causes impact in wing tip Thus, this is not a suitable solution for the UAS30-P2.

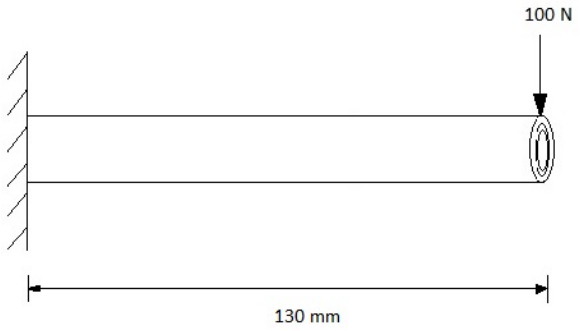


Figure 51 - Deflection load.

Table 18 – Effect of telescope structure.

| Section | Outer Radius (mm) | Thickness (mm) | Area ($mm^2$) | Moment of Inertia ($mm^4$) | Bending Stiffness Factor | Torsional Factor | Deflection (mm) |
|---|---|---|---|---|---|---|---|
| Solid Circular | | | | | | | |
| | 13.180 | - | 545.500 | 23688.160 | 1.000 | 1.000 | 5.890 |
| Hollow Circular | | | | | | | |
| | 23.100 | 4.100 | 541.995 | 122291.200 | 5.630 | 5.110 | 1.130 |
| | 23.000 | 4.100 | 539.420 | 119510 | 5.60 | 5.000 | 1.150 |
| | 22.900 | 4.100 | 536.845 | 117817.500 | 5.580 | 4.970 | 1.170 |
| | 22.800 | 4.100 | 534.271 | 116141.200 | 5.560 | 4.900 | 1.180 |

The mono-spar configuration with a spar profile morphed to wing profile is another efficient solution as it offers a reduction in weight. Nevertheless, it is more suitable to change the spar shape based on the deflection at each load case instead of morphing it with the airfoil section. This can be achieved by the 1-D analysis to check the displacement of spar and its connector at each flight operation.

### 3.3.2 1-Dimensional Analysis

Table 19 presents the analysis tools used for the structure analysis.

Table 19 - Analysis tools.

| Activity | Software used |
|---|---|
| Pre-processing | Altair Hyperworks v17.2<br>Microsoft Excel 2016 |
| Analysis | OptiStruct |
| Post- processing | Altair Hyperworks v17.2<br>Microsoft Excel 2016 |

#### *3.3.2.1 Materials and geometry*

For the 1-Dimensional analysis, the structure is approximated as shown in Figure 52. The sections are split based on the materials and geometry. Each section consists of bar element of size 5 mm. It is the same element size used in the stress report of UAS30-P2 [75]. The 1-D finite element model was constructed by using bar elements as they are simpler to construct and could support flexure and torsion which are more relevant load cases.

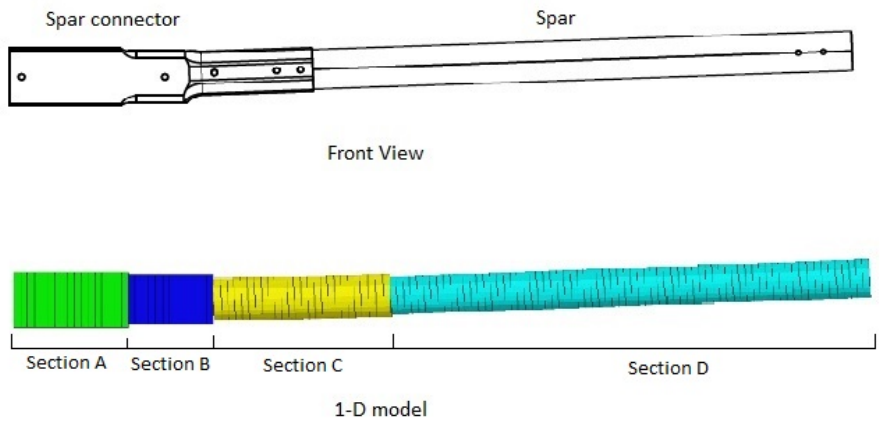


Figure 52 - 1-D Approximation.

##### 3.3.2.1.1 Aluminium 7075

The material used for modelling Section A and B of the spar connector is Aluminium 7075-T7351. The material's properties are presented in Table 17.

#### 3.3.2.1.2 CFRP Tube

The aircraft spar is made up of CFRP tube. The physical and mechanical properties of the CFRP tube are given in Table 20.

Table 20 – CFRP tube properties [75].

| **Mechanical Properties** | **Units** | |
|---|---|---|
| $E_{xx}$ | MPa | 117211 |
| $E_{yy}$ | MPa | 8350 |
| $G_{xy}$ | MPa | 4100 |
| $v_{xy}$ | - | 0.3 |
| $X_t$ | MPa | 1896 |
| $X_c$ | MPa | 2136 |
| $Y_t$ | MPa | 1822 |
| $Y_c$ | MPa | 1787 |
| S | MPa | 81 |
| **Physical Property** | | |
| $\rho_c$ | [kg/mm$^3$] | 1.55 e$^{-6}$ |

#### 3.3.2.1.3 Homogenized Section-C

The section C consists of both aluminium and CFRP tubes. For such cases, the finite element technique has been widely used in implementing the homogenization. However, FEM leads to an overly-stiff model [78]. In our case, since it is going to a comparative method, one still uses finite element technique used by Hypermesh to extract the effective properties of this section, as shown in Table 21.

Table 21 – Effective material properties of homogenized section C.

| **Mechanical Properties** | **Units** | |
|---|---|---|
| $E_{11}$ | MPa | 91476.120 |
| $E_{12}$ | MPa | 45551.160 |
| $G_{12}$ | MPa | 16690.540 |
| $\nu_{12}$ | - | 0.327 |
| **Physical Property** | | |
| $\rho_h$ | [kg/mm$^3$] | 2.881e$^{-6}$ |

The resultant density of the homogenized material is calculated based on the ratios of thickness of materials, as shown in Equation 3.2.

$$\rho_h = \left(\rho_c * \left(\frac{t_c}{t}\right)\right) + \left(\rho_a * \left(\frac{t_a}{t}\right)\right) = 2.881e^{-6} \quad (3.2)$$

$\rho_h$= material density of Section C; $\rho_c$ = density of CRPF tube; $\rho_a$ = density of aluminium 7075; t= total thickness of section C; $t_c$= thickness of CFRP tube; $t_a$= thickness of aluminium 7075-T7351

.

### 3.3.2.2 Section-A

Section-A is modelled with Aluminium 7075-T7351. Thus, the material properties of respective alloy, given in Table 17, are applied to MAT1 data entry for isotropic material and assigned to the bar elements. The section geometry is modelled using Hyperbeam tool as a channel section of dimensions as shown in Figures 53, as per Section 3.1.1.

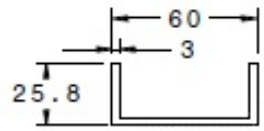


Figure 53A- Cross-section of Section A

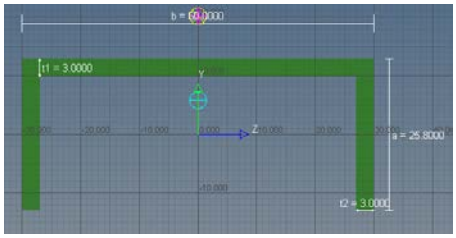

Figure 53B – Hyperbeam model of section A.

Figures 53 – Aspect and dimensions of Section-A. All dimensions are in “mm”.

### 3.3.2.3 Section-B

Section-B is modelled with Aluminium 7075-T7351. Thus, the material property of respective alloy tabulated in Table 17 is applied to MAT1 data entry and assigned to the bar elements. The section geometry is modelled using Hyperbeam tool as a channel section of dimensions as shown in the Figures 54, as per Section 3.1.1.

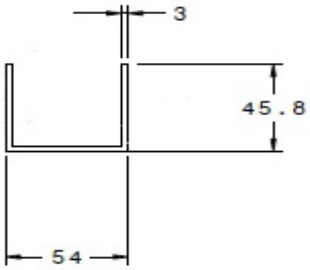


Figure 54A - Cross-section of Section B.

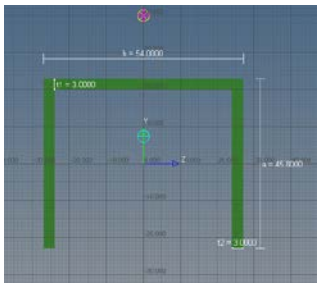

Figure 53B - – Hyperbeam model of section B.

Figures 54 – Aspect and dimensions of Section-B. All dimensions are in “mm”.

### 3.3.2.4 Section-C

As discussed in Section 3.1.1, Section-C is critical in the spar connector as it is the section which connects the wing spar to the fuselage. This section consists of two materials, namely Aluminium and CFRP. Thus, material properties are extracted through Hyperlaminate tool as tabulated in Table 21, and then are assigned to the bar elements with MAT1 data entry for isotropic material, since 1-D elements can support only isotropic materials. The density is approximated based on the thickness of the materials, as shown in Equation 3.2. The geometry approximation of section-C is already discussed in Section 3.3.1. Figures 55 shows the model of section-C being generated in Hyperbeam.

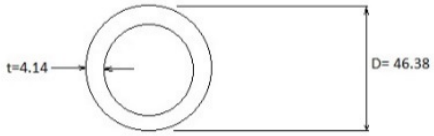


Figure 55A - Cross-section of Section C.

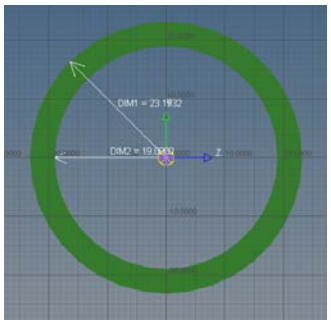

Figure 55B - – Hyperbeam model of section C.

Figures 55 - Aspect and dimensions of Section-C. All dimensions are in “mm”.

### *3.3.2.5 Section-D*

Section D is modelled with the material CFRP. Thus, the properties of respective material in tabulated in Table 20, is assigned to the bar elements with a MAT1 data entry. It is modelled using Hyperbeam tool as a hollow circular section of dimensions as shown in Figures 56, as per the Section 3.1.2.


Figure 56A - Cross-section of Section D

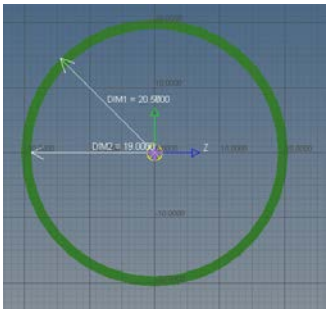

Figure 56B - – Hyperbeam model of section D.

Figures 56 – Section-C of the spar connector generated by Hyperbeam. All dimensions are in “mm”.

As per these section geometries, the moment of inertia of each sections are calculated and are tabulated in Table 22.

Table 22 - MOI of each sections.

| Nodes | Section | Section Moment of Inertia ($I_{xx}$) ($mm^4$) | Section Moment of Inertia ($I_{zz}$) ($mm^4$) |
|---|---|---|---|
| 1001-1016 | Section A | 165218.400 | 18995.771 |
| 1018-1027 | Section B | 206542.800 | 91415.271 |
| 1029-1051 | Section C | 124911.134 | 124911.134 |
| 1053-10 | Section D | 36336.910 | 36336.910 |

The cross-section area of each section is calculated and tabulated in Table 23. Mass is approximately calculated from the section geometry and density of respective materials.

Table 23 - Approximate mass estimation of each sections.

| Section | Area ($mm^2$) | Mass (kg) |
|---|---|---|
| Section A | 316.800 | 0.098 |
| Section B | 418.800 | 0.097 |
| Section C | 359.000 | 0.176 |
| Section D | 186.000 | 0.171 |
| | **Total mass** | **0.542** |

### 3.3.3 Coordinate system.

The model is being analyzed with Global coordinate system. The aircraft axes are shown in Figure 57 and Figure 58. The alignment of spar with the coordinate system is given in Table 24.

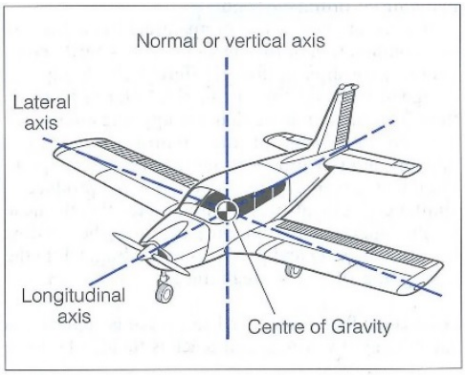


Figure 57 - Aircraft axis.

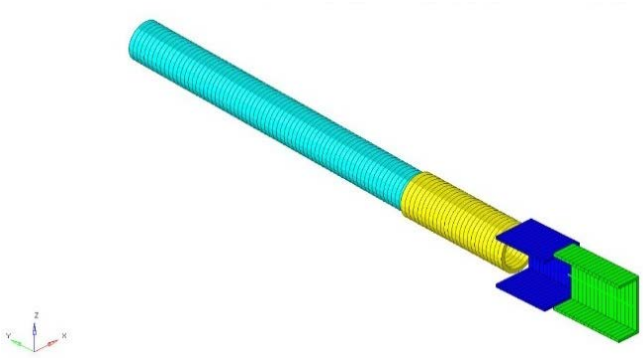

Figure 58 - 1-D Model of spar connector and main spar.

Table 24: Alignment of model with coordinate system.

| Coordinates | Alignment with model |
|---|---|
| X | Longitudinal axis |
| Y | Lateral axis |
| Z | Normal or vertical axis |

### 3.3.4 Boundary Conditions

The boundary conditions are the constraints applied to the model to represent the flight cases. These boundary conditions are applied based the flight dynamics and various operations performed in it the aircraft.

#### *3.3.4.1 Normal Flight Constraints*

For the normal flight case, the lift load generated by the aircraft is equal to the weight of the aircraft. The lift load is generated by the wing, which is transferred to entire aircraft through the spar of the aircraft. Thus, in this case the Section-A and Section-B are constrained representing the pins shown in Figures 59-A and the frame Figures 59-B, which keeps the spar connector attached to the fuselage while the Section C and D are not constrained because they deflect under lift forces and moments. The pins restrict the translation of spar connector in *y*-axis and *z*-axis and restricting rotation around *x*-axis and *y*-axis. The frame keeps the spar connector in place restricting translation in *x*-axis and rotation around *z*-axis, as shown in Figure 60.


Figure 59 A – Constraints for pins.

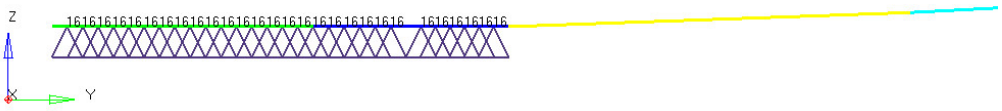


Figure 59 B – Constraints for the attachment frame.

Figures 59 – Constraints for pins and attachment frame in normal flight case.

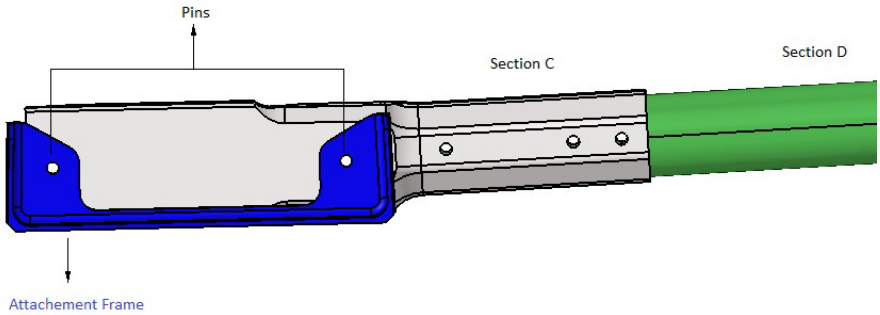


Figure 60 – Attachment frame and pins.

### 3.3.4.2 Catapult Launch Constraints

The catapult is attached in two catapult arms present in each wing. One of these arms is directly connected to the spar, as shown in Figure 61. Even though there are two catapult arms in each wing, all catapult loads are transmitted through the spar since the aircraft has a mono-spar configuration. The aircraft is pulled by the catapult to its $V_{TO}$ through this attachment, shown in Figures 62. Thus, the catapult arm is constrained in all degrees of freedom except in translation in *x*-axis, depicting the catapult pulling in the respective direction. The frames and pins are constrained in *x*-translation, depicting the inertia of the rest of the aircraft during the catapult launch, as shown in Figure 63.

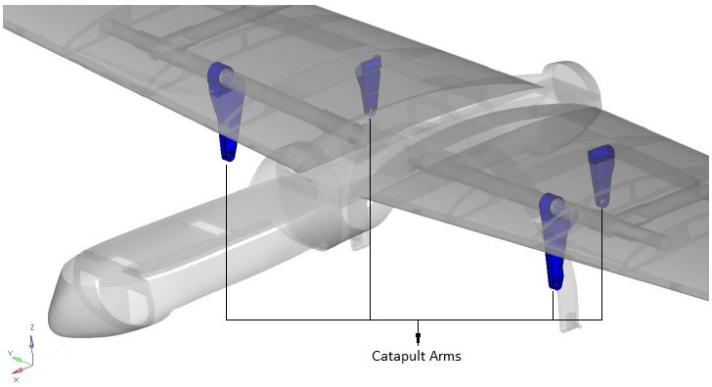


Figure 61 – Catapult arms.

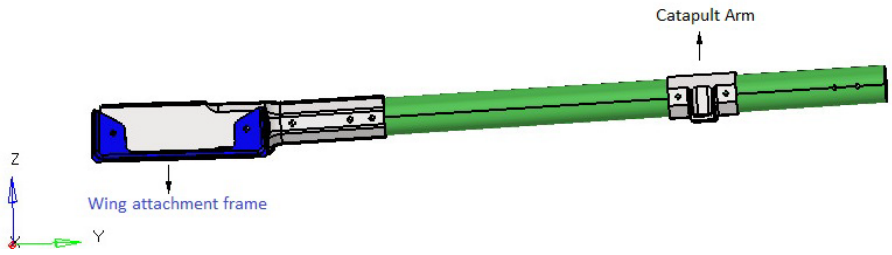


Figure 62 A.- Catapult arm

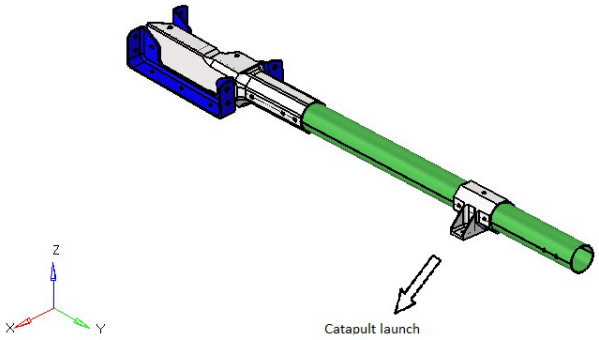


Figure 62 B.- Catapult launch.

Figures 62 – Catapult attachment setup.

Figure 63 – Catapult constraints.

### 3.3.4.3 *Net Arrest Constraints*

When operated without landing gears, the normal landing phase of aircraft is replaced by the net arrest operation. In this case, the aircraft nose of the aircraft is expected to take up all the impact loads. But when subjected to cross wing landing or any instability in yaw, as the aircraft has a high aspect ratio and low body span, the wing tip is very likely to share the impact with the nose. Thus, the net arrest operation is the most critical loading case for the spar. This is shown in Hypercrash model of UAS30-P2 stress report by CEiiA [75].

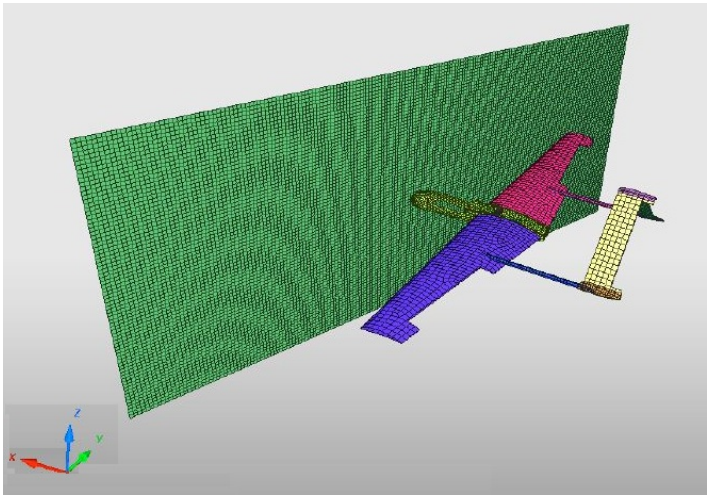

Figure 64 – Hypercrash model of Net Arrest operation [75].

Being conservative, the nose interaction with the net is ignored and the model has been made representing wing tip taking up the impact for the entire mass of the aircraft. However, in actual case the impact is shared between the wing tip and the nose of the aircraft. For this case, the tip of the spar is constrained in the *x*-translation representing the point of impact, as shown in Figures 65A. The attachment frame and pins are constrained in all degrees of freedom except X translation, depicting the inertia of motion of the aircraft, as shown in Figures 65B.

Figure 65 A – Constraints in spar tip and pins for Net arrest operation.

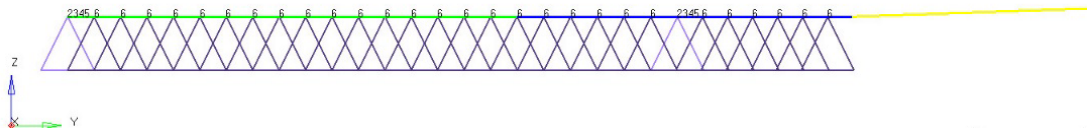

Figure 65 B– Constraints for net arrest operation in attachment frame and pins.

Figures 65 - Constraints for Net Arrest operations.

Table 25 - Boundary Conditions.

| Load Condition | Single Point Constraints (SPC) | Degrees of freedom (DoF) constrained |
|---|---|---|
| Normal Aerodynamic | Pins | 2, 3, 4, 5 |
| | Attachment Frame | 1, 6 |
| Catapult Launch | Attachment Frame and pins | 1 |
| | Catapult attachment | 2, 3, 4, 5, 6 |
| Net Arrest operation | Attachment Frame and pins | 2, 3, 4, 5, 6 |
| | Spar tip | 1 |

Pins and attachment frame is made to check the displacements for normal aerodynamic loads.

### 3.3.5 Loads

The aircraft structures are subjected to structural loads, which are a combination of aerodynamic force and weight of the structure and it varies with the operations performed in the aircraft. Thus, the structural loads are represented in terms of load factors, as shown in the next equation.

$$n = \frac{L}{W} \tag{3.3}$$

n= Load factor; L= Aerodynamic lift; W= Weight.

The forces and moments which are caused by aerodynamic lift from various airfoil, are transferred through the spar connector of the aircraft UAS30-P2. These loads are obtained from the lift force distribution diagram of main plane and tail plane of the aircraft. The aerodynamic lift in main plane and tail plane are extracted by CEiiA using the software XFLR, as shown in Figure 66 and Figure 67.

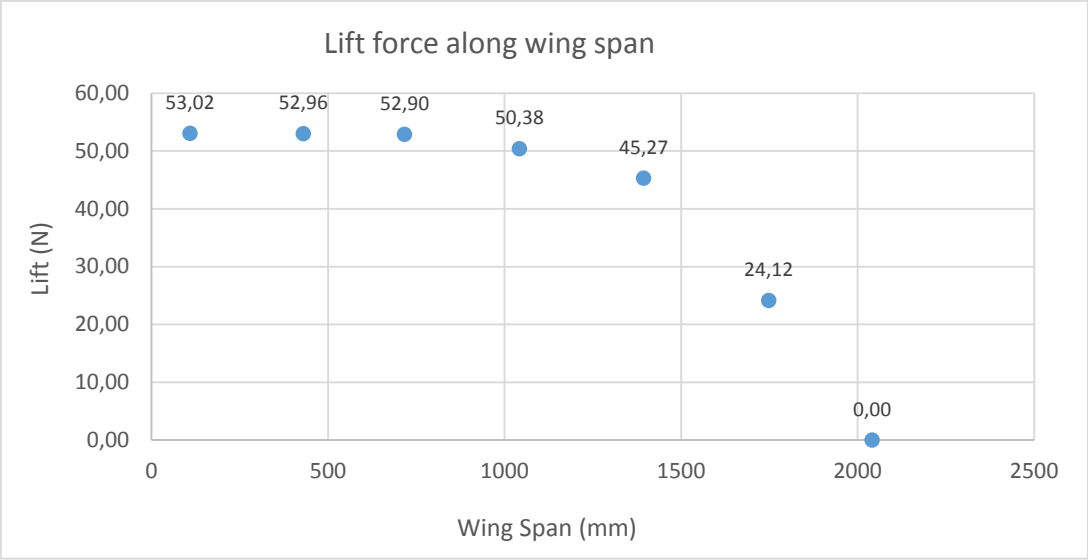


Figure 66 - Wing lift distribution.

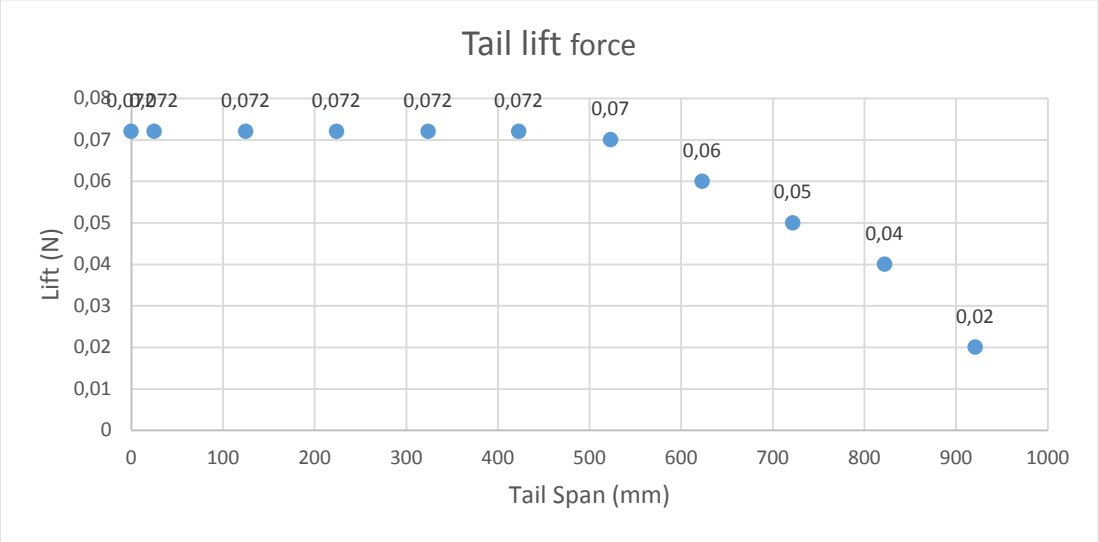


Figure 67 - Tail lift distribution.

The lift forces are series of point loads extracted in each specific points of the wing structure. The lift force in tail contributes to both horizontal and vertical reactions as it is an “inverted V” tail configuration, as shown in Figure 38 and Figure 39, with ruddervators replacing the conventional elevators and rudders of the aircraft. Thus, the aerodynamic forces and moments due to tail are resolved to horizontal and vertical components.

Figure 68 shows the aerodynamic forces and moments of main plane and tail plane resolved to the main spar and its connector.

Table 26 represents calculated forces and moments due to aerodynamic lift of main plane and tail plane of the aircraft. These forces and moments are applied to the nodes at respective locations of the FEM, shown in Figures 69.

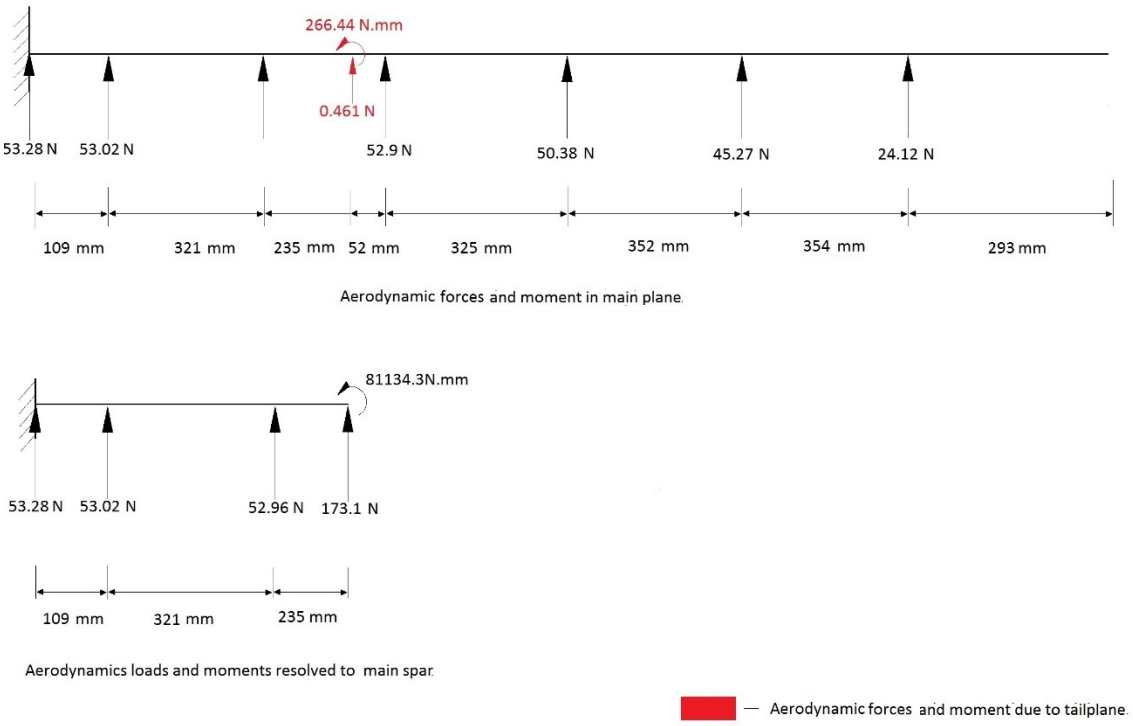


Figure 68 – Resolution of aerodynamic forces and moments from the main and tail plane to main spar and its connector.


Figure 69 A – Aerodynamic forces resolved to aircraft 1-D model.

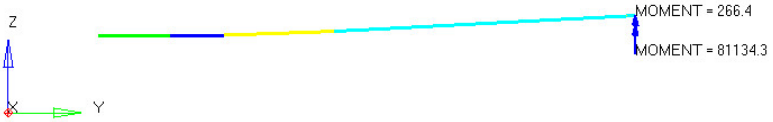


Figure 69 B – Aerodynamic moments resolved to 1-D model.

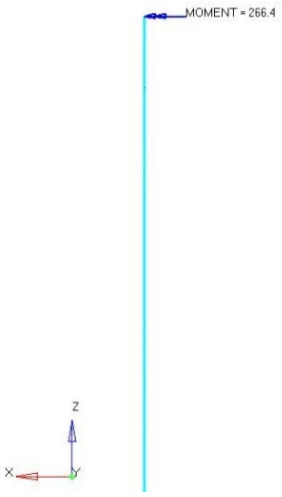


Figure 69 C – Moment due to Yaw created by tail-plane.

Figures 69 - Aerodynamic loads.

Table 26 - 1-D Loads.

| Nodes | Section | Forces (N) | | | Moments (N.mm) | | |
|---|---|---|---|---|---|---|---|
| | | X | Y | Z | X | Y | Z |
| 5 | Section C | - | - | 53.280 | - | - | - |
| 6 | Section C | - | - | 53.020 | - | - | - |
| 8 | Section D | - | - | 53.000 | - | - | - |
| 10 | Section D | 0.430 | - | 173.100 | 266.400 | - | 81134.300 |

From the studies carried out in UAS30-P2, Table 27 represent the mass of each component of the aircraft at its $M_{TOW}$ condition.

Table 27 - Mass data of each component of the aircraft at its $M_{TOW}$ condition.

| Node | Representation | Mass (kg) |
|---|---|---|
| 1016 | Fuselage and Engine | 5.048 |
| 1119 | Wing and fuel | 5.050 |
| 1120 | Tail plane | 1.719 |

The load factors during various operations of the aircraft given in the stress report of UAS30-P2 are represented Table 28.

Table 28 - Gravity loads of the aircraft [75].

| Operations | Load Factors | | |
|---|---|---|---|
| | X | Y | Z |
| Normal Aerodynamic | - | - | -1 |
| Normal Landing | - | - | -3.5 |
| Catapult launch | -2.14 | - | -1 |
| Net Arrest | -2.36 | - | -1 |

### 3.3.6 1-D Results

#### *3.3.6.1 Normal Flight condition*

For Normal flight conditions, the displacement is seen on the tip of the spar depicting the deflection due to aerodynamic lift of the wing, shown in Figure 70. In the actual case, this displacement is far lower than this value since the longeron and the CFRP skin add additional stiffness to the spar.

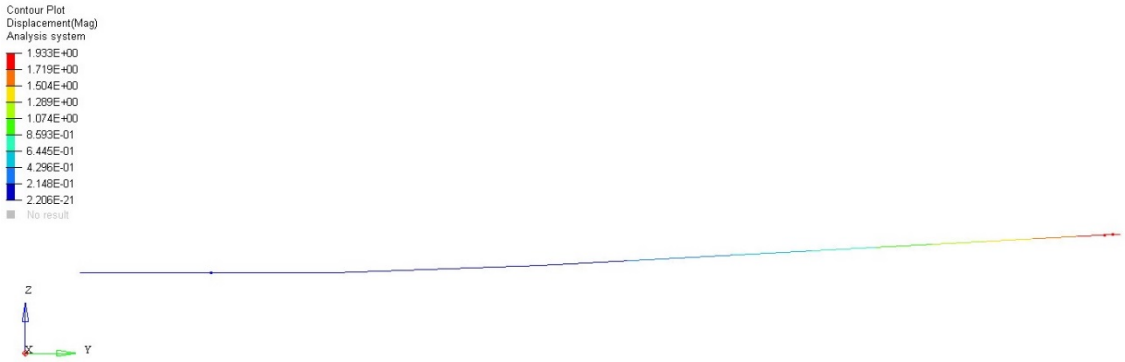


Figure 70 – Displacement due to Normal flight condition.

#### *3.3.6.2 Landing*

The load factor due to landing is in opposite direction to the aerodynamic lift of the aircraft, which means the lift force produced by the wing adds additional support to the spar in this load case, thus, making the tip deflection much lower than in normal flight conditions, shown in Figure 71. In actual case, the $C_l$ of wing is highest in case of landing than in any other phase of flight, which makes the displacement in this load case much lower than the evaluated displacement. This displacement is highest displacement in spar connector (wing root) regarding the *z*-axis load condition.

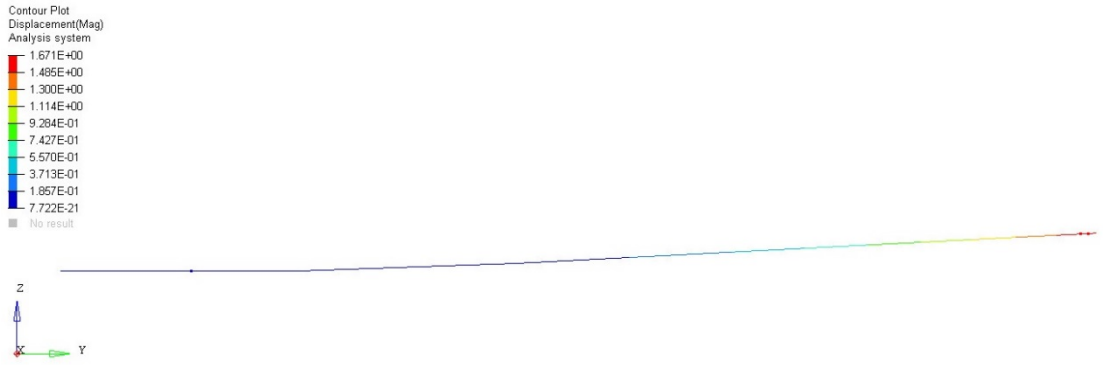


Figure 71 – Displacement due to landing loads.

### 3.3.6.3 Catapult Launch

In this case the aircraft is launched by pulling with a load factor of 2.14 G using the catapult arms attached to the wings. In this load case, since only the port side wing is used, this approximation depicts the entire aircraft being launched with catapult attached in only one wing of the aircraft. However, in actual case there are two catapult arms in each of the wings sharing the launch loads, thus the actual displacements will be much smaller than the displacements obtained from this analysis. Unlike the other two load case results analyzed before, in this load case the displacements are higher in the root section than in the tip.

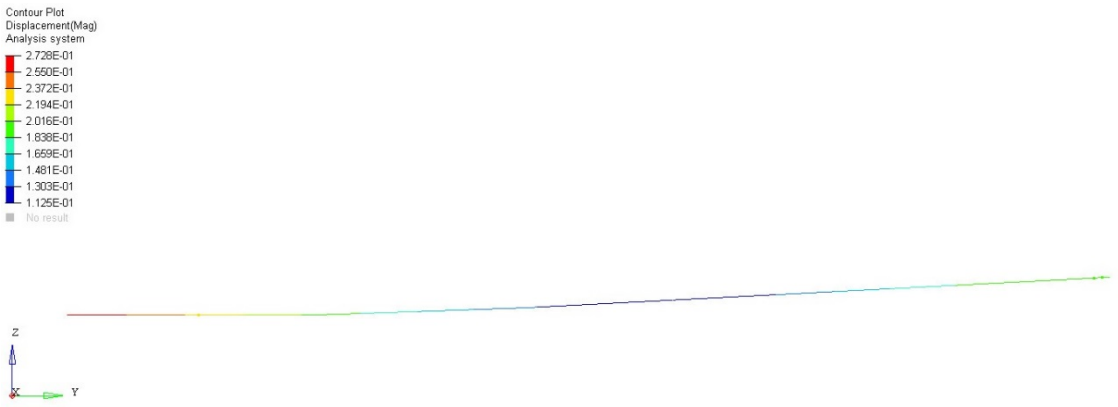


Figure 72 - Displacement due to catapult launch.

### 3.3.6.4 Net arrest

This case is modelled depicting the impact of the aircraft in the wing tip during a cross wind landing or any other rudder instability while performing the net arrest operation. This analysis considers the worst case in which the wing tip taking the impact of entire aircraft. In this case the displacements are highest in the spar connector regarding the x-axis load condition, as shown in Figure 73.

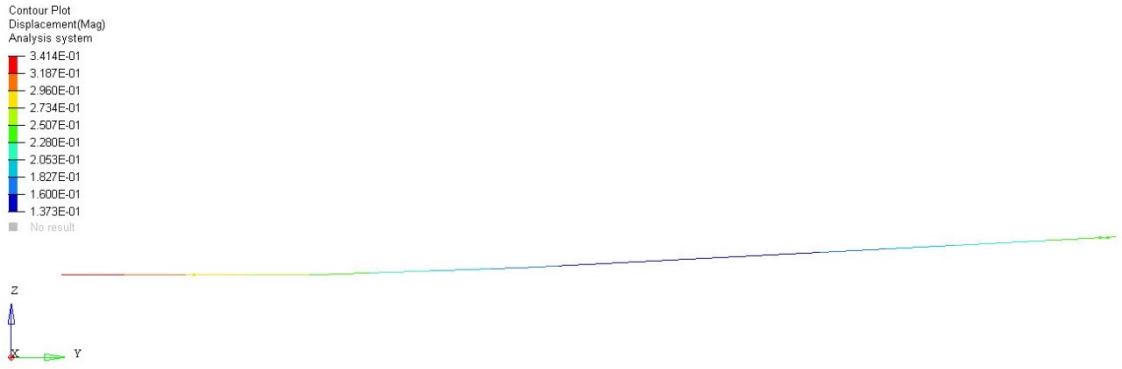


Figure 73 - Displacement due to Net arrest operation loads.

The landing loads were in the direction normal to the flight whereas the impact load due to net arrest operations was in the direction of flight. The average nodal displacements of nodes in the sections of spar connector in these load cases is given in

Table 29. The displacement of spar connector due to net arrest operations was much higher than the displacements due to other operations. This result coincides with the stress report of the UAS30-P2 [75].

Table 29 - Displacement of spar connector at worst cases.

| Nodes | Section | Displacement (Average) | |
|---|---|---|---|
| | | Landing (mm) | Net arrest (mm) |
| 2-6<br>1001-1051 | Section-A<br>Section-B<br>Section-C | 0.01 | 0.26 |

### 3.3.7 Shape optimization

This typical optimization problem focuses on finding the optimal shape of a structure. Standard mathematical optimization techniques are often time consuming due to the high number of internal design variables. Conventional optimization also requires a complete 2-D model as it requires the complete stress profile of the component to provide better material distribution, whereas the 1D analysis could only give the results averaged to the entire cross section. In this case, an attempt was made to choose a geometric profile based on the average nodal displacements of the component, as the 1-D analysis shows that higher displacement in the spar connector structure was noted in the load case for net arrest operations. This coincides with stress report of UAS30-P2 [75]. From the studies performed in Section 2.3.1, the spar profile which is more characterized to airfoil profile has more advantages including slight weight reduction than convention sections. From Section 2.4.2, the elliptical section is the one which could be more characterized to the airfoil profile. Thus, iterations are made in 1-D analysis to extract the optimum dimensions of ellipse which suits the Section-C of the spar connector. The other sections of the spar connector can be modified based on the aspect ratio of the ellipse. The major axis of the ellipse has the higher moment of inertia which could be aligned to the direction of flight, where stiffness requirements are higher. The thickness of the sections remains unchanged. Thus, having this constraint in design variables, the iterations are done with the ellipses with various aspect ratio as per the differences in moment of inertia along *x*-axis and *z*-axis.

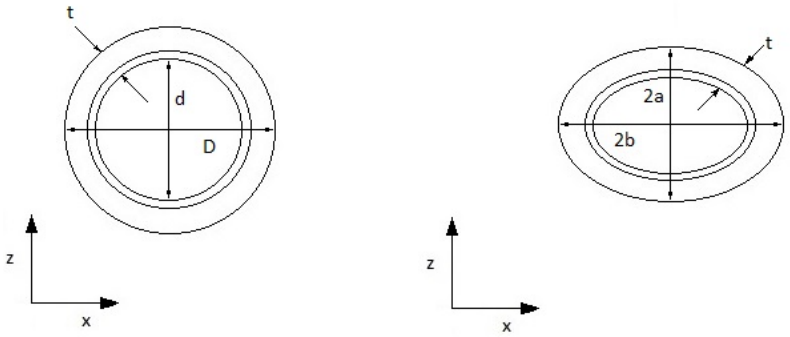


Figure 74 – Circular to elliptical transformation.

Table 30 - Optimization of major axis of elliptical section with respect of section C.

| | Section-C | | | Aspect ratio | ($I_{xx}$) ($mm^4$) | ($I_{zz}$) ($mm^4$) | Difference in Inertia (% ) | Area ($mm^2$) |
|---|---|---|---|---|---|---|---|---|
| | D (mm) | d (mm) | t (mm) | | | | | |
| | 46.38 | 38.2 | 4.1 | - | 122943.5 | 122943.5 | 0 | 545 |
| Iteration | 2b (mm) | 2a (mm) | t (mm) | | | | | |
| 1 | 44.18 | 40.8 | 4.1 | 0.93 | 130827 | 116137.5 | 10 | 547.1 |
| 2 | 44.18 | 39.4 | 4.1 | 0.93 | 127511 | 107382.3 | 15 | 538 |
| 3 | 44.18 | 37.9 | 4.1 | 0.85 | 125355.9 | 99709.11 | 20 | 534.1 |
| 4 | 44.18 | 36.4 | 4.1 | 0.82 | 120443.6 | 90053.12 | 25 | 518.7 |

Table 31 - Change in section dimensions with respect to elliptical ration of Section C.

| Analysis | Section-C | | | Aspect ratio | Section-A | | | Section-B | | | Section-D | | |
|---|---|---|---|---|---|---|---|---|---|---|---|---|---|
| | D (mm) | d (mm) | t (mm) | | b (mm) | h (mm) | t (mm) | b (mm) | h (mm) | t (mm) | D (mm) | d (mm) | t (mm) |
| **Original sections** | 46.38 | 46.38 | 4.1 | - | 25.8 | 60 | 3 | 45.8 | 54 | 3 | 41.15 | 38.1 | 1.5 |
| **Iteration** | 2b (mm) | 2a (mm) | t (mm) | | b (mm) | h (mm) | t (mm) | b (mm) | h (mm) | t (mm) | 2b (mm) | 2a (mm) | t (mm) |
| **1** | 44.18 | 40.8 | 4.1 | 0.93 | 25.8 | 55.40 | 3 | 45.8 | 48.15 | 3 | 38.98 | 35.6 | 1.5 |
| **2** | 44.18 | 39.4 | 4.1 | 0.93 | 25.8 | 53.50 | 3 | 45.8 | 48.15 | 3 | 38.98 | 34.2 | 1.5 |
| **3** | 44.18 | 37.9 | 4.1 | 0.85 | 25.8 | 50.42 | 3 | 45.8 | 45.3 | 3 | 38.98 | 32.7 | 1.5 |
| **4** | 44.18 | 36.4 | 4.1 | 0.82 | 25.8 | 49.434 | 3 | 45.8 | 44.49 | 3 | 38.98 | 31.2 | 1.5 |

As studied in Section 2.5.1, FEM computes nodal displacement using the material properties from which other parameters such as stress, strain, etc. are derived from the elements. Thus, nodal displacements are the backbone in FEM. In this analysis, the 1-D model is subjected to point loads and single point constraints (SPCs) which results in higher nodal displacement but this is not the same in actual cases. Thus, the average nodal displacements in each section of the spar connector are considered as a platform of comparison in the iterations. The change in dimensions of the other sections with respect to the aspect ratio of ellipse are given in Table 31. Based on these dimensions, some iterations were carried out to check for a solution which gives a similar nodal displacement of that of the original solution and yields better weight savings.

#### *3.3.7.1 Iteration – 1*

For the first iteration, the aspect ratio of Section C is chosen in such way that it gives a 10% reduction in moment of inertia in the direction of landing loads whereas keeping the MOI in the direction of net arrest operation similar to that of original section. Figure 75 and Figure 76 show the displacement in landing and net arrest load case, respectively. The average nodal displacement in spar connector is tabulated in Table 32.

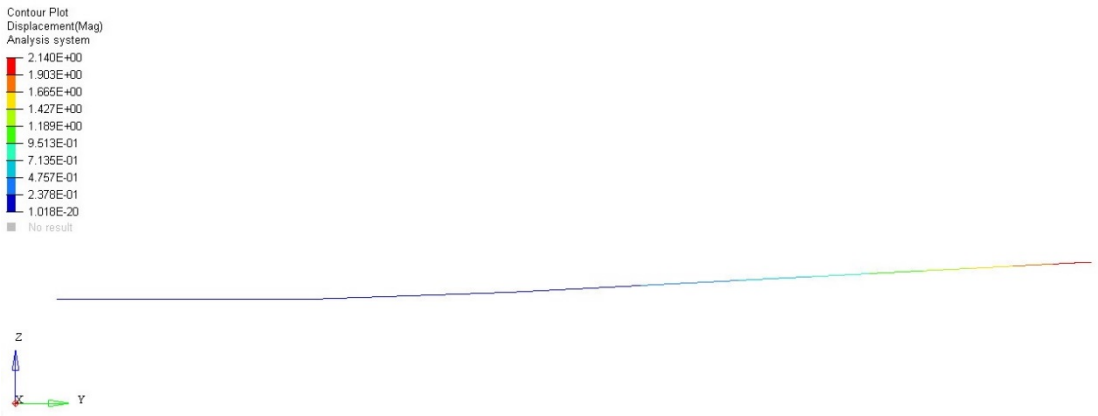


Figure 75 - Displacement in landing load case (Iteration – 1).

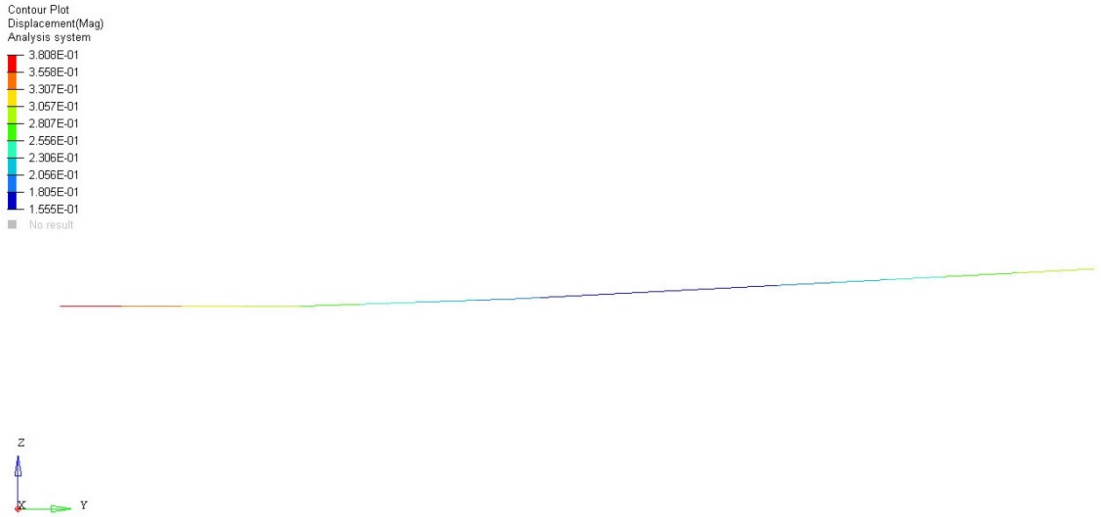


Figure 76 - Displacement in net arrest operation (Iteration – 1).

Table 32 – Average nodal displacement in spar connector (Iteration – 1).

| **Iteration** | **Average nodal displacement in spar connector sections.** (mm) | |
|---|---|---|
| | Landing | Net Arrest |
| 1 | 0.011 | 0.280 |

### *3.3.7.2 Iteration – 2*

For this iteration, the aspect ratio of Section-C is chosen in such way that it gives a 15% reduction in moment of inertia in the direction of landing loads, whereas keeping the MOI in the direction of net arrest operation similar to that of original section. Figure 77 and Figure 78 show the displacement in landing and net arrest load case, respectively. The average nodal displacement in spar connector is tabulated in Table 33.

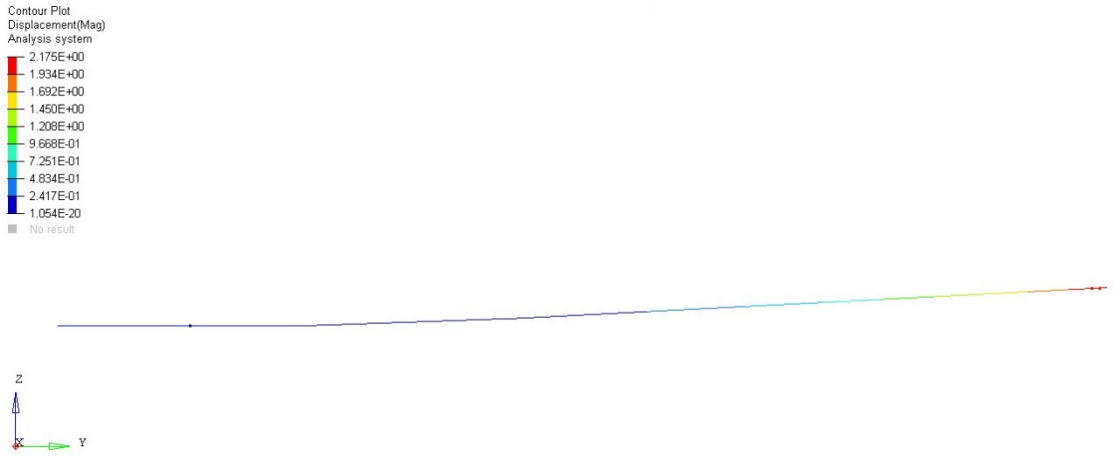


Figure 77 - Displacement in landing load case (Iteration – 2).

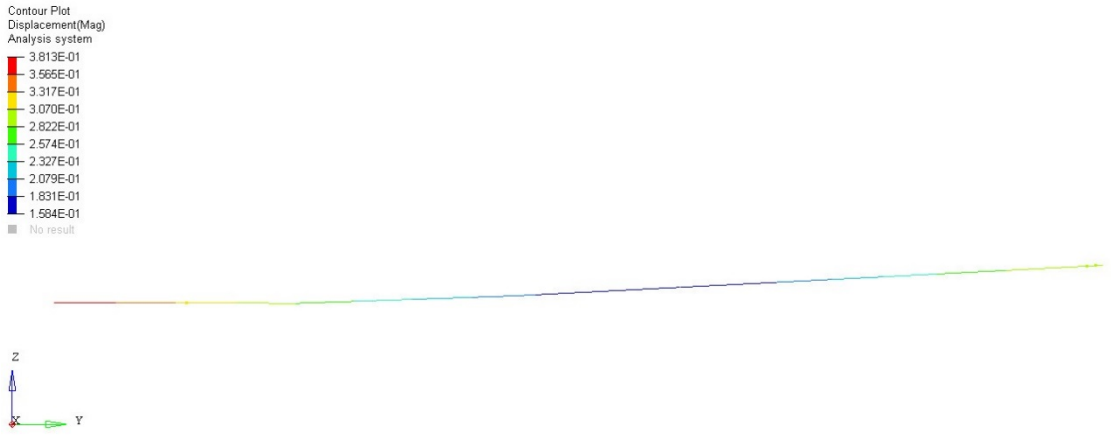


Figure 78 - Displacement in net arrest operation (Iteration – 2).

Table 33 - Average nodal displacement in spar connector (Iteration – 2).

| Iteration | Average nodal displacement in spar connector sections. (mm) | |
|---|---|---|
| | Landing | Net Arrest |
| 2 | 0.019 | 0.280 |

### *3.3.7.3 Iteration – 3*

For this iteration, the aspect ratio of Section-C is chosen in such way that it gives a 20% reduction in moment of inertia in the direction of landing loads, whereas keeping the MOI in the direction of net arrest operation similar to that of original section. Figure 79 and Figure 80 show the displacement in landing and net arrest load case, respectively. The average nodal displacement in spar connector is tabulated in Table 34.

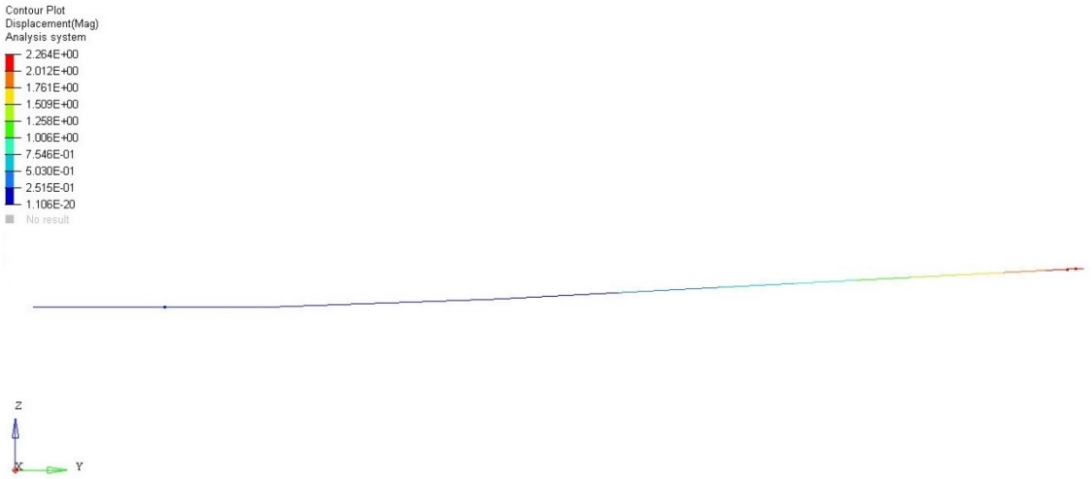


Figure 79 - Displacement in landing load case (Iteration – 3).

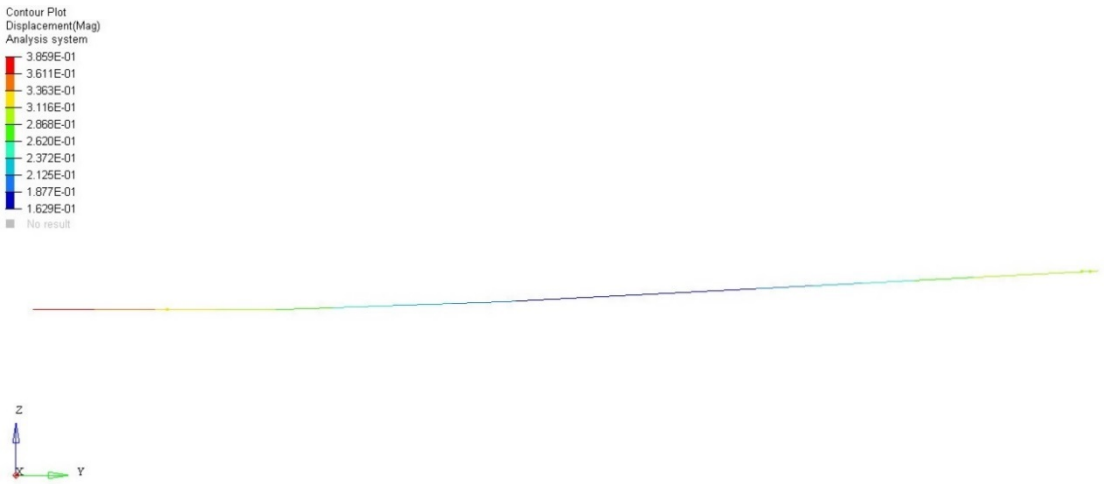


Figure 80 - Displacement in net arrest operation (Iteration – 3).

Table 34 - Average nodal displacement in spar connector (Iteration – 3).

| **Iteration** | **Average nodal displacement in spar connector sections.** (mm) | |
|---|---|---|
| | Landing | Net Arrest |
| 3 | 0.012 | 0.280 |

### *3.3.7.4 Iteration – 4*

For this iteration, the aspect ratio of Section-C is chosen in such way that it gives a 25% reduction in moment of inertia in the direction of landing loads, whereas keeping the MOI in the direction of net arrest operation similar to that of original section. Figure 81 and Figure 82 show the displacement in landing and net arrest load case, respectively. The average nodal displacement in spar connector is tabulated in Table 35.

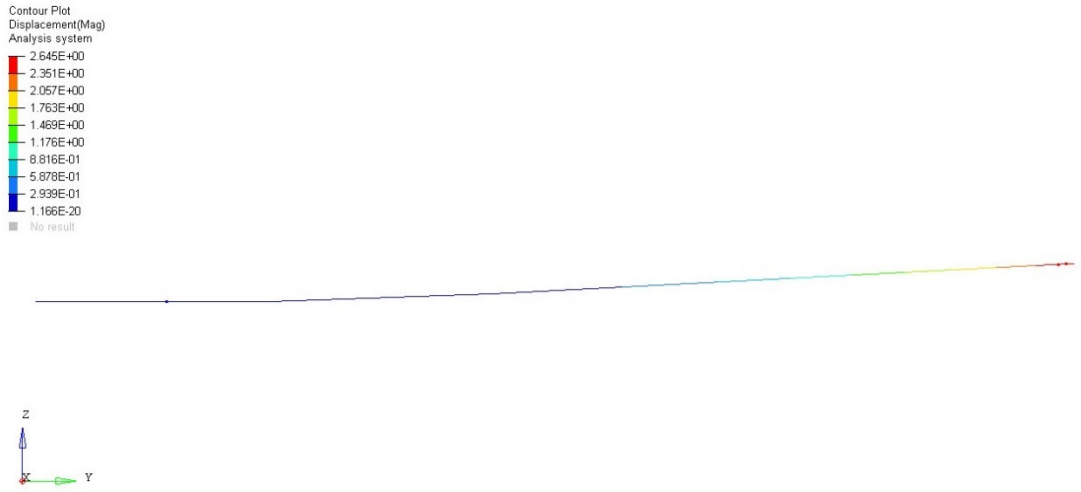


Figure 81 - Displacement in landing load case (Iteration – 4).

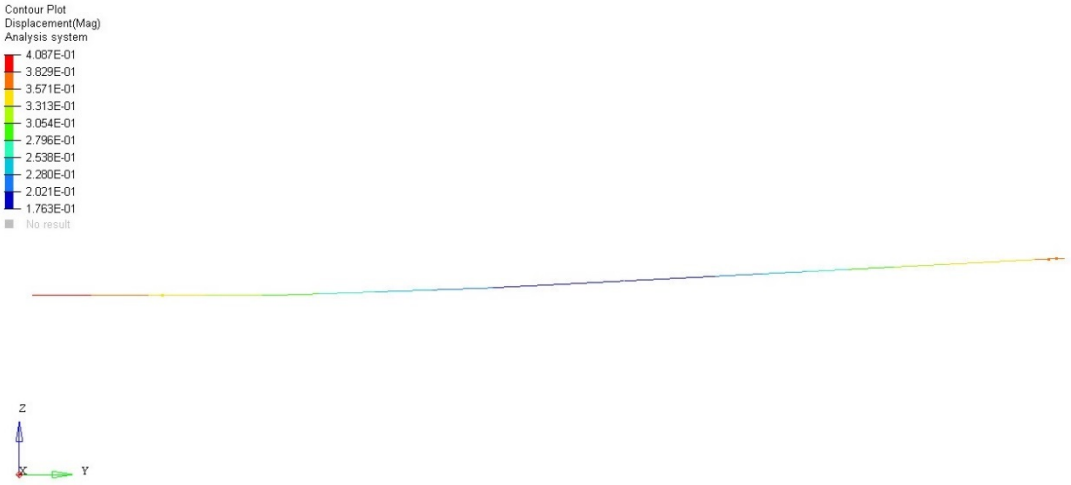


Figure 82 - Displacement in net arrest operation (Iteration – 4).

Table 35 - Average nodal displacement in spar connector (Iteration – 4).

| **Iteration** | **Average nodal displacement in spar connector sections. (mm)** | |
|---|---|---|
| | Landing | Net Arrest |
| 4 | 0.013 | 0.300 |

The average nodal displacements of the spar sections are presented in Table 36. At the beginning of the iteration, the displacement in landing load case raised higher as noted in iterations 1 and 2. Then for the third iteration the displacement in landing was much lower and significantly converged to that of original displacement, while producing decent weight savings. On further iteration, the displacement starts increasing in both the load conditions.

Table 36 - Worst case displacement of spar connector sections in each iteration.

| **Iteration** | **Average nodal displacement in spar connector sections. (mm)** | |
|---|---|---|
| | Landing | Net Arrest |
| 1 | 0.011 | 0.280 |
| 2 | 0.019 | 0.280 |
| 3 | 0.012 | 0.280 |
| 4 | 0.013 | 0.300 |

Figure 83 shows the 1-D model used for the iteration-3, which had a better convergence effect regarding the original result. The approximate sectional masses of each section are estimated in Table 37.

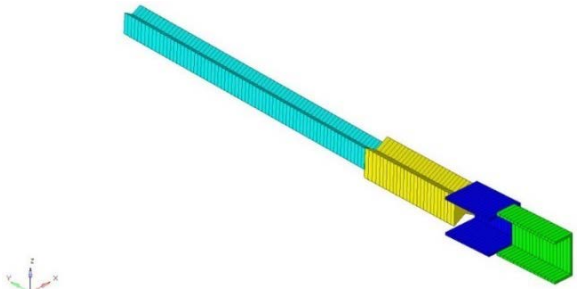

Figure 83: 1-D analysis for iteration-3.

Table 37 - Approximate mass estimation of optimized sections.

| Node | Section | Area ($mm^2$) | Mass (kg) |
|---|---|---|---|
| 1001-1017 | Section-A | 288 | 0.089 |
| 1017-1028 | Section-B | 392 | 0.091 |
| 1028-1052 | Section-C | 335.1 | 0.165 |
| 1052-10 | Section-D | 168.8 | 0.156 |
| | | **Total mass** | **0.501** |

Mass is approximately calculated from the section geometry and density of respective materials.

It is estimated that an overall weight saving of about 8.2% can be attained in the optimized structure, with almost the same performance characteristics of the non-optimized structure spar connector. To understand the complete stress profile of the structure, it is necessary to conduct a 2-D analysis and perform a comparison between both.

## 3.4 CAD Model

Based on the dimensions discussed in Table 31, a CAD model was performed using Catia V5, as shown in Figures 84. Figure 85 shows the sectional view of the spar connector.

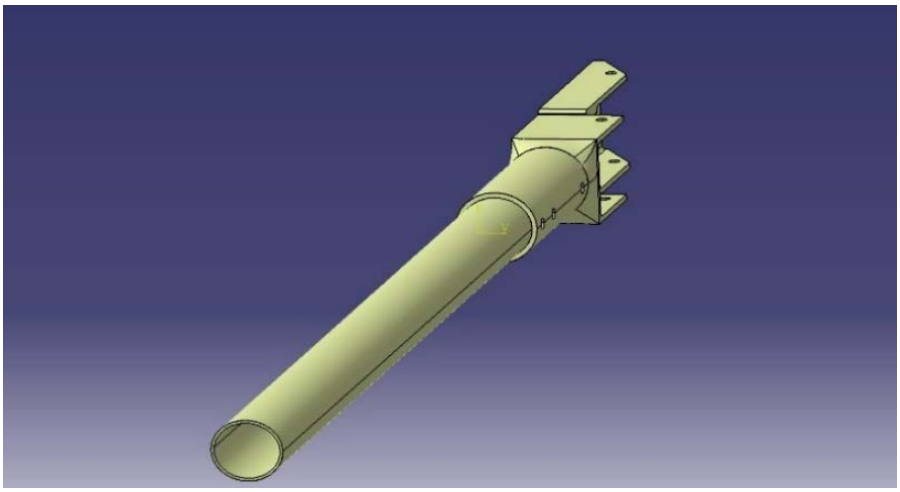

Figure 84-A.

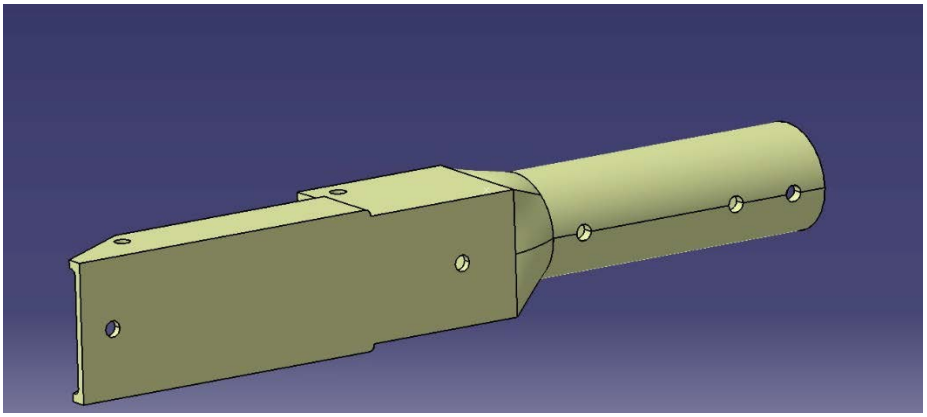

Figure 84-B.

Figures 84 – CAD model of optimized spar and its spar connector.

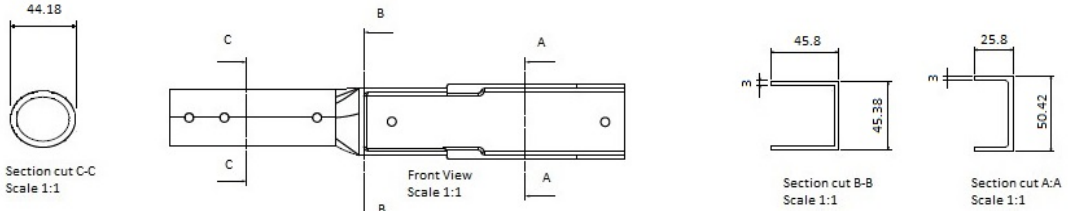


Figure 85 – Sections of optimized spar connector (Dimensions in mm).

## 3.5 2-D Analysis

### 3.5.1 Finite Element Modelling

Figure 86 shows the 2-D finite element model of the component. The element types and loads used in the model are tabulated in Table 38.

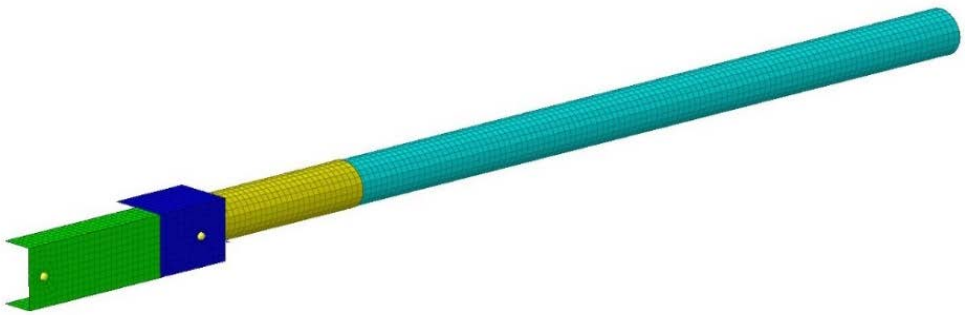

Figure 86- Finite Element Model for 2-D analysis.

Table 38 – Finite elements.

| Component/Parameter | Element/Load assigned |
|---|---|
| Structure | CQUAD/CTRIA |
| Joints and fasteners | RBE2 |
| Masses | CONM2 |
| Constraints | SPC |
| Aerodynamic Loads | FORCE/MOMENT |
| Inertial Loads | GRAV |
| Load distribution elements | RBE2/RBE3 |

### 3.5.2 Materials

The metallic spar connector is made of Aluminium 7075 T7351 and the spar is a composite structure with a CFRP Tube. The metallic structure is assigned with the property card PSHELL and the composite structure is assigned with the property card PCOMP. The material properties are presented in Table 17 and Table 20 respectively. The structure is meshed predominantly using 2-D quadrilateral (CQUAD) elements, as triangular (CTRIA) elements possess high stiffness resulting in high local stress concentration [79]. Thus, TRIA elements was used only in the places where regular size QUAD elements will give a poor mesh quality due to the complexity of geometry in those regions. The element size of 5 mm is maintained in the structure. This is the same size chosen in the stress report of UAS30-P2 [75]. Table 39 gives the material card for the elements used to construct the finite element model. The material properties of the structure are assigned through these material cards.

Table 39 – Material card.

| Element Type | Property card | Geometric Properties | Material Card | Material Properties |
|---|---|---|---|---|
| Shell | PCOMP | t | MAT8 | $E_1$, $E_2$, $\nu_{12}$, $G_{12}$, $\rho$, $X_t$, $X_c$, $Y_t$, $Y_c$, S |
| Shell | PSHELL | t | MAT1 | E, G, $\nu$, $\rho$, $S_T$, $S_C$, $S_S$ |

### 3.5.3 Coordinate System

A local coordinate system, shown in Figure 87, was created so that the structure is oriented in the way as can be seen in Section 3.5.3. The loads and constraints are oriented based on this local coordinate system.

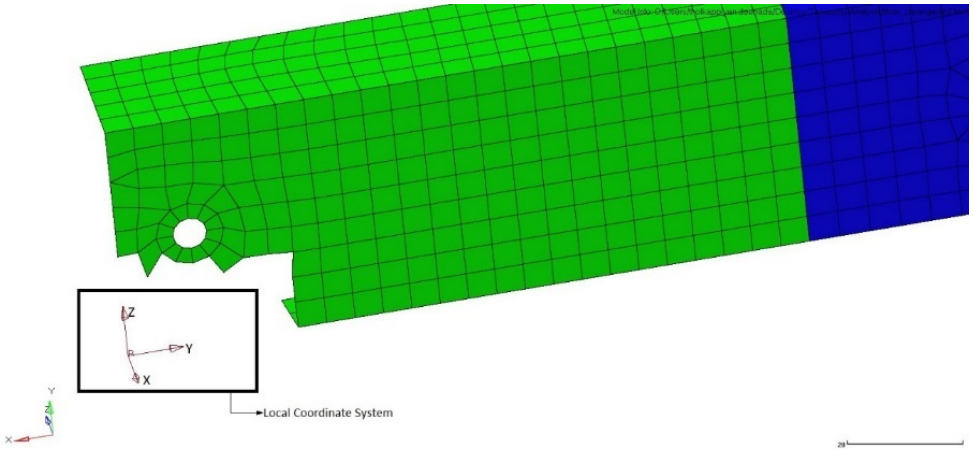


Figure 87 – Local Coordinate system.

Note: Elements were masked for the better visibility of local coordinate system.

### 3.5.4 Load Conditions

The loads discussed in Section 3.5.4 are applied to the structure, discussed in the following sub-chapters.

#### *3.5.4.1 Aerodynamic Loads*

The aerodynamic forces and moments resolved to the spar and its connector sections discussed in Section 3.5.4.1, are applied to the 2-D model. Applying forces to single nodes may impose high stress gradients due to the singularity which occurs in applying force to an infinitesimally small area. Thus, the point loads are applied by splitting it equally to all nodes in the respective zone, as shown in Figures 88. These forces are tabulated in Table 40. By this way, excessive stress gradients which could occur due to point loads are eliminated.

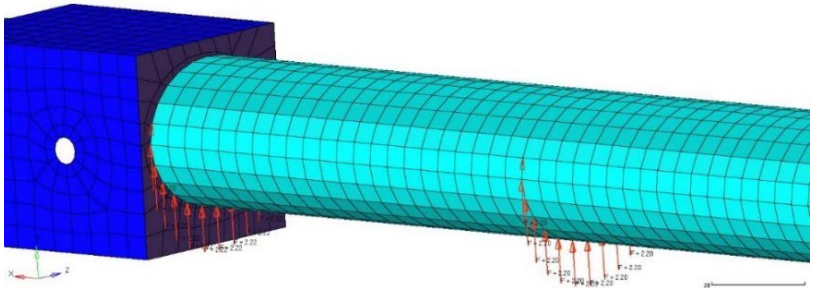

Figure 88 A - Application of aerodynamic forces to nodes

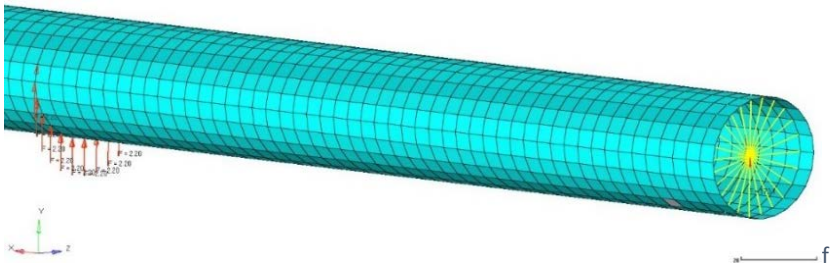


Figure 88 B – Application of aerodynamic moments.

Figures 88 – Application of aerodynamic forces and moments.

In case of the resolved moments, applying them to each node creates undesired stress levels, as shown in Figure 89. To overcome this problem, a rigid body element is created in that zone as a load distributing element. However, rigid imposes stiffness in the zone resulting in high stresses in the elements in vicinity. Thus, a load distributing rigid body element (RBE2) is created only in the case of application of moments where it is more needed, as shown in Figure 90.

Table 40 shows the magnitude and direction of the applied forces and moments.

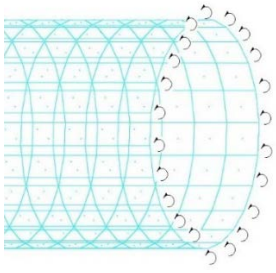

Figure 89 – Effect of applying moments directly to nodes.

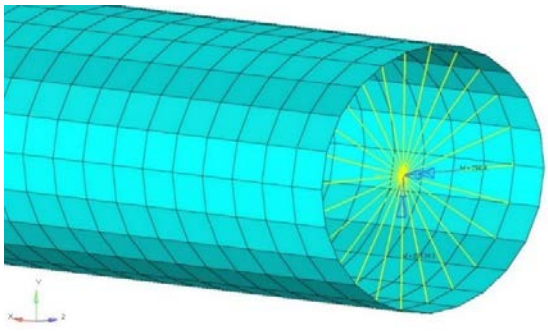

Figure 90 – Application of resolved moments through RBE2 load distributing elements.

Table 40 – Application of forces and moments.

| Nodes | Section | Forces (N) | | | | | Moments (N.mm) | | |
|---|---|---|---|---|---|---|---|---|---|
| | | X | Y | Z | Number of nodes in the cross section | Force applied to each node (N) | X | Y | Z |
| 5 | Section D | - | - | 53.28 | 28 | 1.90 | - | - | - |
| 6 | Section D | - | - | 53.02 | 28 | 1.892 | - | - | - |
| 8 | Section D | - | - | 53.0 | 28 | 1.892 | - | - | - |
| 10 | Section D | 0.43 | - | 173.1 | Forces and moments were applied to load distributing RBE2. | | 266.4 | - | 81134.3 |

### 3.5.4.2 *Inertial Loads*

The inertial loads are applied with the gravity card as mentioned in Table 28.

### 3.5.4.3 *Masses*

The structural mass of each component of the aircraft is applied through 1-D mass elements. The centre of mass of each component is extracted from the CATIA shown in Figures 91.

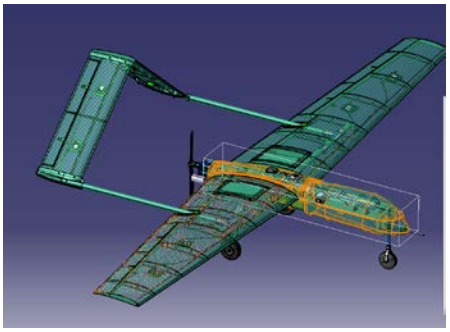

Figure 91 A- $C_G$ of Fuselage.

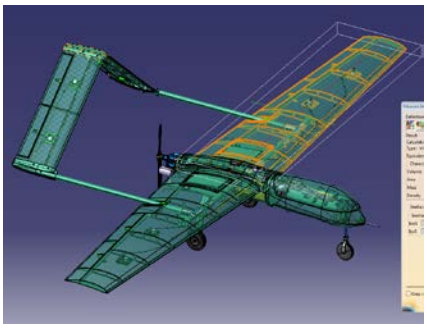

Figure 91 B- $C_G$ of wing.

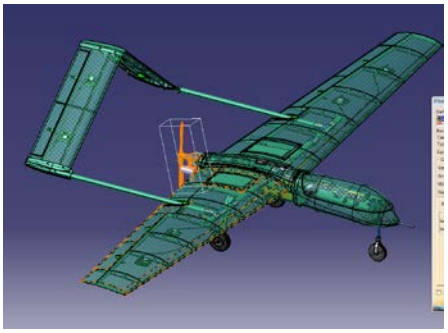

Figure 91 C- $C_G$ of Engine.

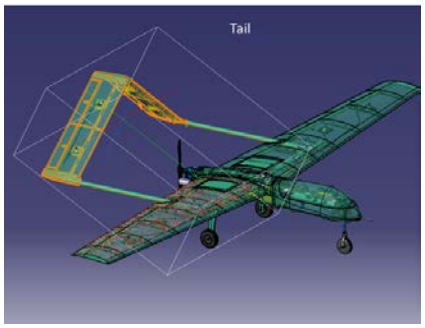


Figure 91 D- $C_G$ of Tail.

Figures 91 - Position of the centres of mass of aircraft components.

The software mentioned above computes the mass and centre of mass of each selected components, considering the geometric features and the material inputs of

the component and all its child parts including the non-structural mass. The mass of the fuselage and engine is distributed in Section-A and Section-B as they are inside the fuselage, as shown in Figure 92. The mass of the wing at its $M_{ToW}$ condition, which includes the weight of the wing structure and fuel, is distributed to all nodes in Section D, which is the composite spar of the aircraft. The mass of the tail section is distributed in the nodes of tail connection, as shown in Figures 93A and Figures 93B. This method of distribution of mass could not be achieved in 1-D analysis, because the nodes of an element could possess translational degrees of freedom only (DoF 123), thus the rigid body element (RBE) which are used to distribute the mass from the positions of its respective $C_{G,}$ could possess infinite rotation if applied to 1-D elements. Thus, for the 1D analysis the mass was directly applied to the structural nodes regardless of their $C_G$ positions.

Table 41 – Mass and position of $C_G$ of UAS30-P2 components.

| Component | Mass (kg) | X (mm) | Y (mm) | Z (mm) |
|---|---|---|---|---|
| Fuselage | 4.45 | 343.43 | 74.3 | 562.23 |
| Wing | 5.05 | -7.58 | 996.67 | 628.91 |
| Tail | 1.71 | -1130.4 | 406.79 | 445.18 |
| Engine | 0.60 | -519.52 | 77.36 | 292.86 |

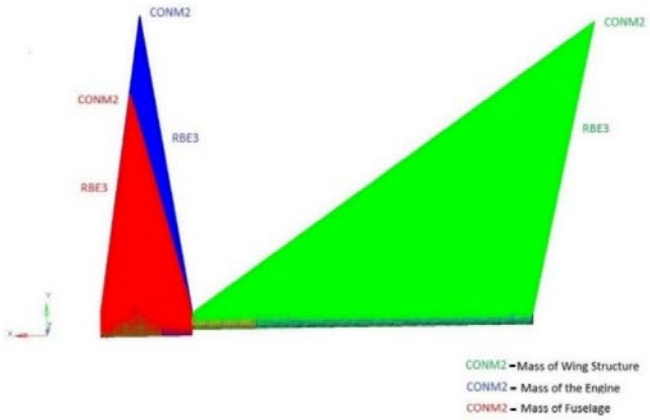


Figure 92 – Application of wing, fuselage and engine masses.

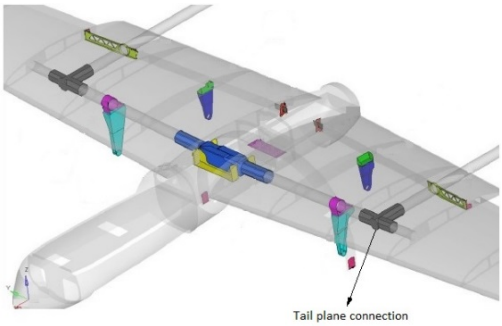


Figure 93 A- Tail-plane connection.

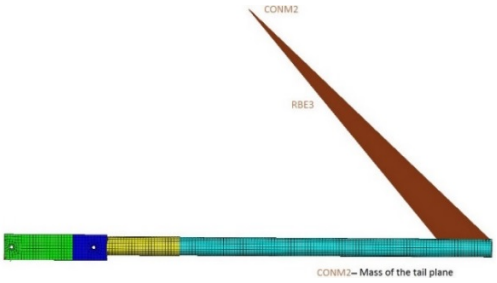


Figure 93 B- Application of tail-plane masses.

Figures 93 – Application of aircraft component masses.

### 3.5.5 Connections

The pins used to connect the spar connector with the aircraft are replaced by rigids body elements (RBE2), as a load distributing element, as shown in Figures 94 A. This element will allow extract interface loads which could be applied to the aircraft during its structural analysis. The connection between the metallic spar connector and the composite spar is firm and has a very low tolerance. Thus, for this connection, rigid elements connecting each node in the Section C of both surfaces are created to ensure a firm connection, shown in Figures 94B.

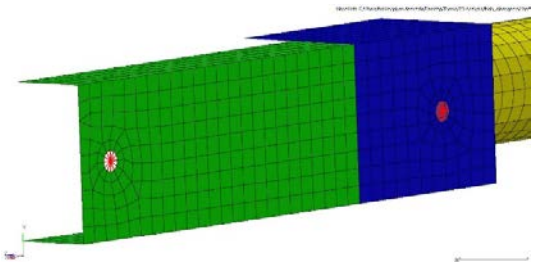

Figure 94 A- Pins

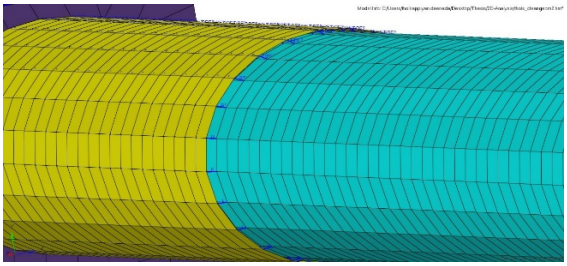

Figure 94 B- Spar and spar connector interface.

Figures 94 – Joints and fasteners.

### 3.5.6 Boundary Conditions

The boundary conditions for the 2-dimensional finite element model are applied in the same way as discussed in the Section 3.3.4 for 1-D modelling except for the fact that the single point constraints (SPCs) are now distributed to larger number of nodes resembling the actual connection. The DoF for this SPCs are tabulated in Table 25.

#### *3.5.6.1 Normal Flight Constraints*

The constraints for the pins are created in the independent nodes of the rigid element mentioned in Section 3.5.5. The constraints for the connection frame are made in such a way that it resembles the actual frame setup, as shown in Figures 95A and Figures 95B. Since all six degrees of freedom are constrained in the spar connector itself, the application of masses of fuselage and engine has less significance in this case. However, for normal flight conditions, the weight of the aircraft is equal to the lift force generated. Since the applied forces and moments are due to lift generated in normal flight condition, the model could still represent the actual flight case regardless of the constraints.

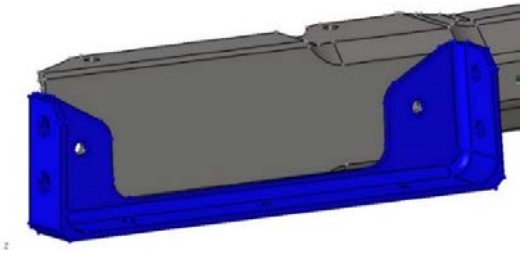

Figure 95 A- Spar connector and attachment frame interface.

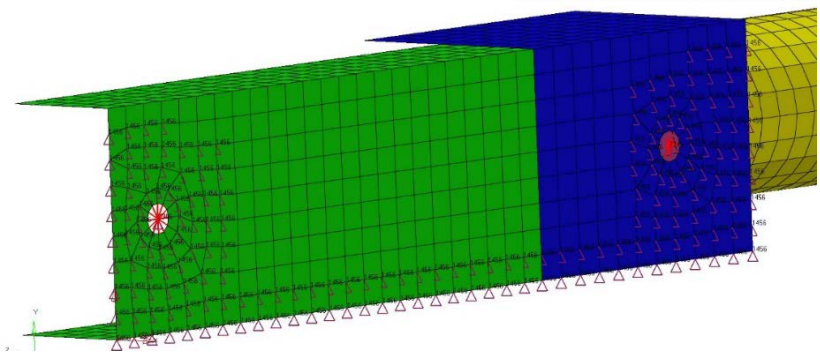

Figure 95 B- F.E model of spar connector and attachment frame interface.

Figures 95 – Normal flight case constraints.

### *3.5.6.2 Catapult Launch Constraints*

Similarly, the SPCs for the catapult arm are distributed to large number of nodes in such a way that it resembles the connection of catapult arm and the frame more precisely than in the 1D model as shown in Figures 97A and Figures 97B. Along with this, the application of masses at its respective $C_G$ positions could yield better results than in the 1D cases. The DoF assigned to the constraints for this load case are discussed in the Section 3.3.4.2.

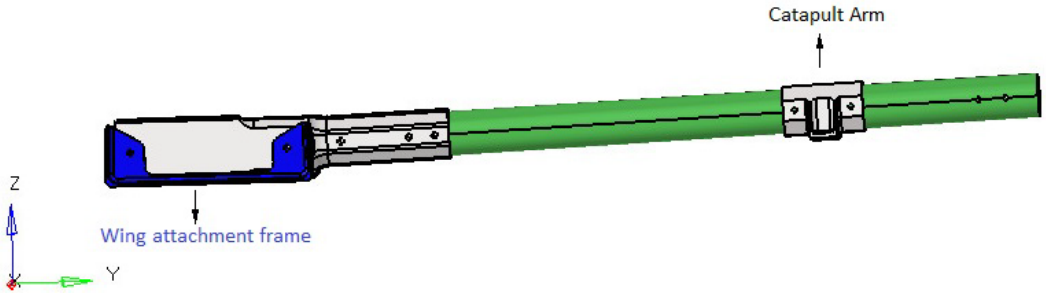


Figure 96 - Catapult arm in spar.

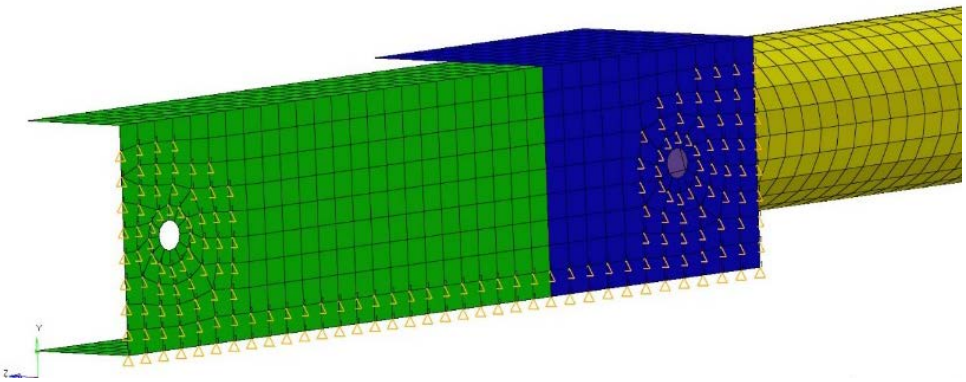

Figure 97 A- Constraints for spar connector in catapult launch case.

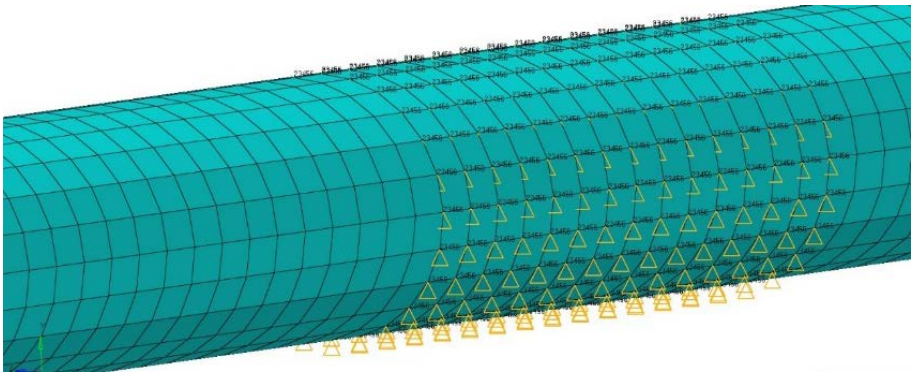

Figure 97 B – Constraints for catapult arm.

Figures 97 – Catapult constraints.

### *3.5.6.3 Net Arrest Constraints*

For this load cases the DoF of the constraints are defined as discussed in the Section 3.3.4.3. The constraints for the attachment frame combined with the masses will act as the inertia of motion, and it is distributed to a large number of nodes resembling the actual connection setup. All the nodes in the tip of the spar are constrained in *x*-axis to resemble the impact of net arrest operation, shown in Figures 98A and Figures 98B.

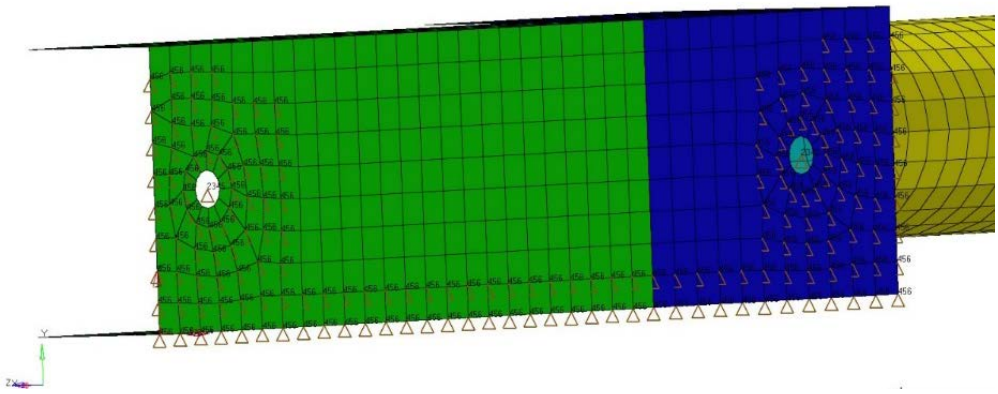

Figure 98 A- Constraints for spar connector in net arrest case.

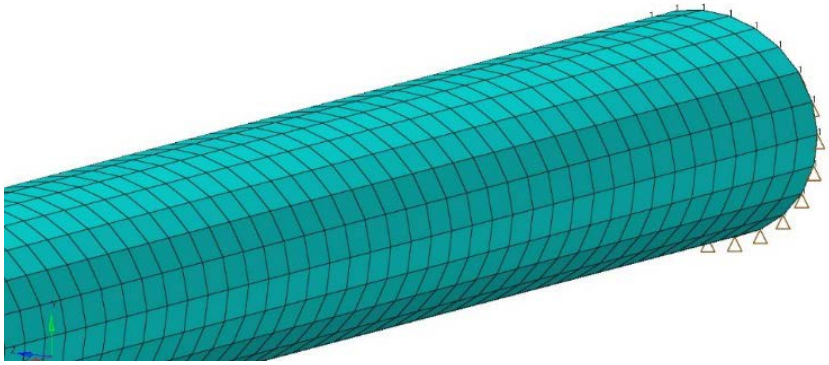

Figure 98 B- Constraints for spar tip in net arrest case.

Figures 98 – Constraints for Net arrest case.

### 3.5.7 2-D Analysis Results

The finite element model of the original structure and the shape optimized structure are solved using the solver Optistruct. The results are given in the following sub-chapters.

#### *3.5.7.1 Displacement*

The displacement of the original and shape optimized structure are given in the following sub-chapters.

##### 3.5.7.1.1 Original structure

Figure 99, and Figure 100 show the displacements for each load cases in the original structure which is currently in use as wing attachment setup of the UAS30-P2. The values of displacement, which are tabulated in Table 42, did not converge with the displacement values UAS30-P2's stress report [75]. This is because, in this work, the additional support provided by the ribs and longeron of the wings are not considered. This provides a very conservative result in the analysis carried out.

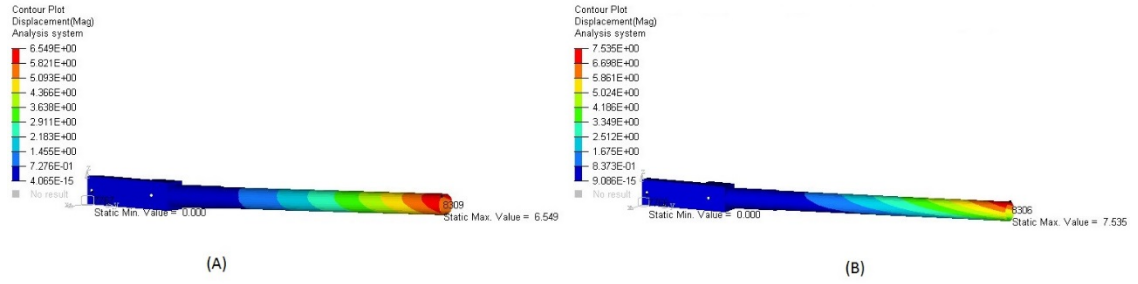


Figure 99 – Displacement due to normal flight (A) and landing loads (B), respectively.

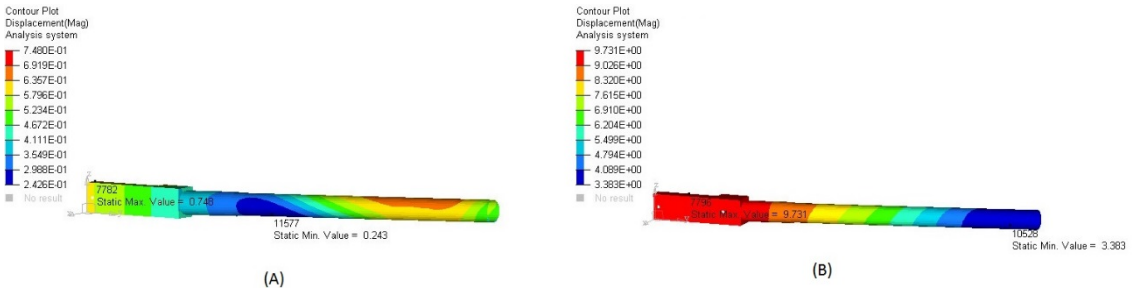


Figure 100 – Displacement due to catapult launch (A); and net arrest loads (B), respectively.

Table 42 – Displacements due to various load cases original structure.

| Load Case | Max. Displacement (mm) | Min. Displacement (mm) |
|---|---|---|
| Normal Flight | 6.549 | 0 |
| Landing | 7.535 | 0 |
| Catapult Launch | 0.748 | 0.243 |

| | | |
|---|---|---|
| Net Arrest | 9.731 | 3.383 |

### 3.5.7.1.2 Optimized structure

Figure 101 and Figure 102 show the displacements for each load cases in the shape optimized wing attachment structure. The values of displacement of shape optimized structure are tabulated in Table 43.

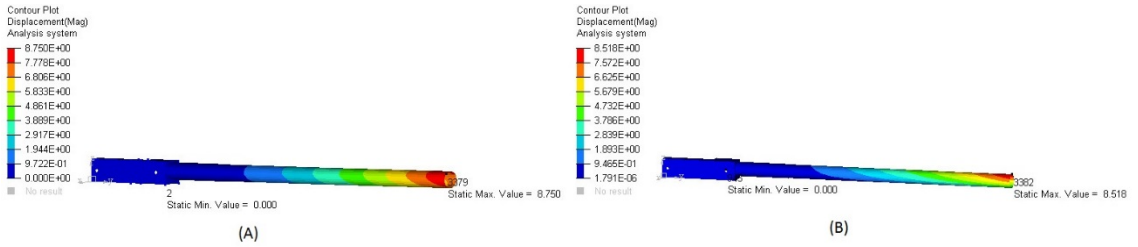


Figure 101 - Displacement due to normal flight (A) and landing loads (B), respectively for optimized structure.

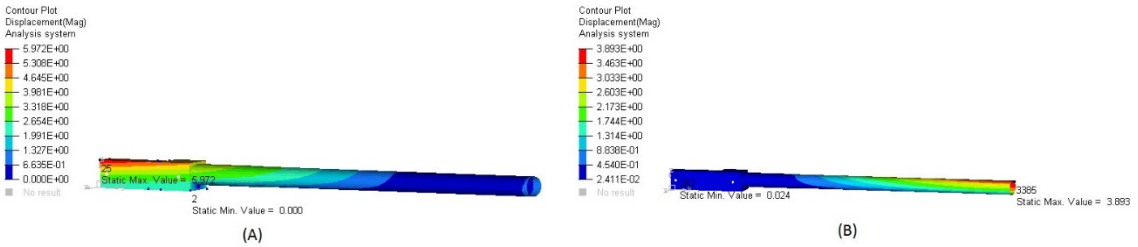


Figure 102 – Displacement due to catapult launch (A) and net arrest loads (B), respectively for optimized structure.

Table 43 – Displacements due to various load cases in shape optimized structure.

| Load Case | Max. Displacement (mm) | Min. Displacement (mm) |
|---|---|---|
| Normal Flight | 8.750 | 0 |
| Landing | 8.518 | 0 |
| Catapult Launch | 5.972 | 0 |
| Net Arrest | 3.893 | 0.024 |

The value of displacements did not converge with the displacements values in 1-D analysis. This is because the 1D solution provides the averaged results of the cross section. For example, the constrain made in a node of a 1D model means that the entire cross section is constrained in that region. This factor is more refined in the 2D models, as loads and constraints could be applied in more realistic way, as discussed in Sections 3.5.6 and 3.5.4. Further, the homogenized properties of “Section-C” in 1D model provides excess stiffness to the structure, as discussed in Section 3.3.2.4.

### 3.5.7.2 *Metallic spar connector*

The following sub-chapters present the von Mises stress in the metallic parts of original and the shape optimized structure.

#### 3.5.7.2.1 Original Structure

Figure 103 and Figure 104 show, the von Mises stress equivalence for each load cases in the original structure, which is currently in use as wing attachment setup of the UAS30-P2. The values of von Mises stress in the original spar connector are tabulated in Table 44.

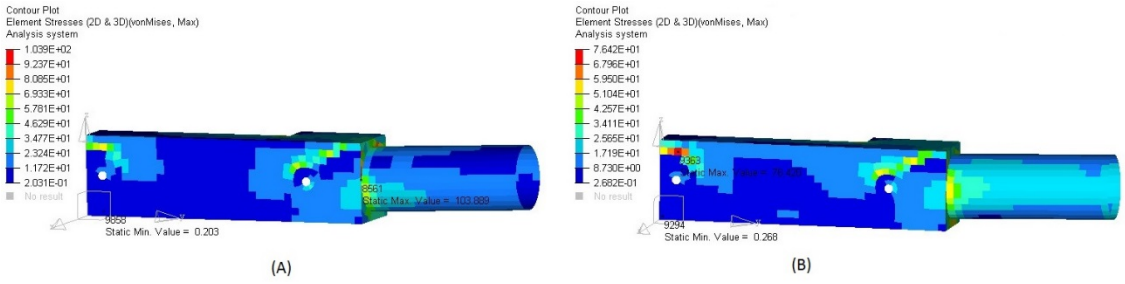


Figure 103 –von Mises stress on metallic components for normal flight (A) and landing load cases (B), respectively.

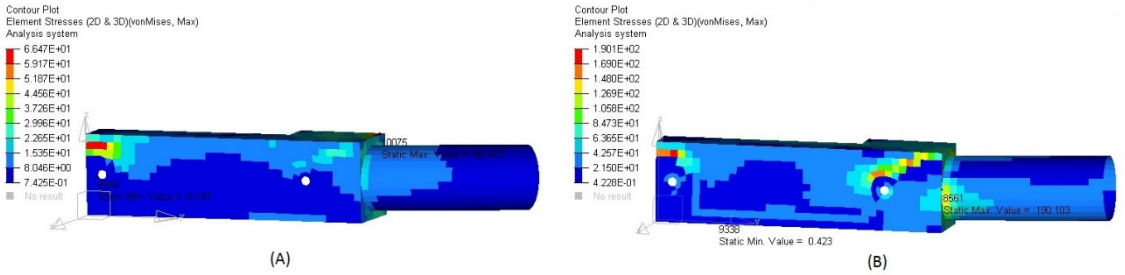


Figure 104 – von Mises stress on metallic components for catapult (A) and net arrest load cases (B), respectively.

Table 44 – von Mises stress for various load cases in original structure.

| Load Case | Max. von Mises stress (MPa) | Min. von Mises stress (MPa) |
|---|---|---|
| Normal Flight | 103.889 | 0.203 |
| Landing | 76.428 | 0.268 |
| Catapult Launch | 66.473 | 0.743 |
| Net Arrest | 190.103 | 0.423 |

### 3.5.7.2.2 Optimized structure

Figure 105 and Figure 106 show the von Mises stress equivalence for each load cases in the shape optimized wing attachment structure. The values of von Mises stress in shape optimized spar connector are tabulated in Table 45.

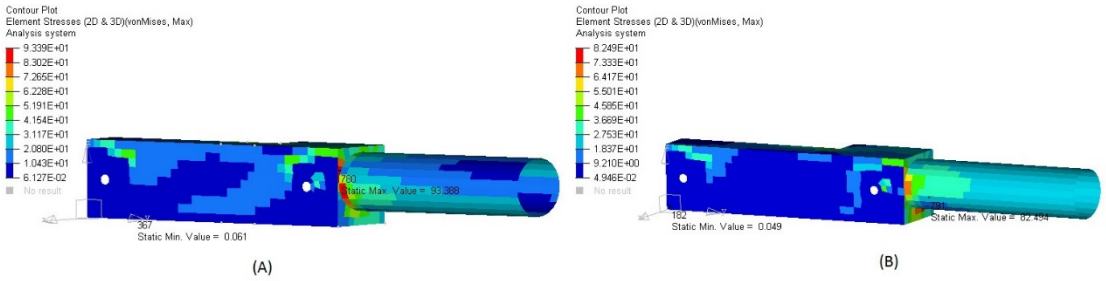


Figure 105 – von Mises stress on metallic components for normal flight (A) and landing load cases (B), respectively for the optimized structure.

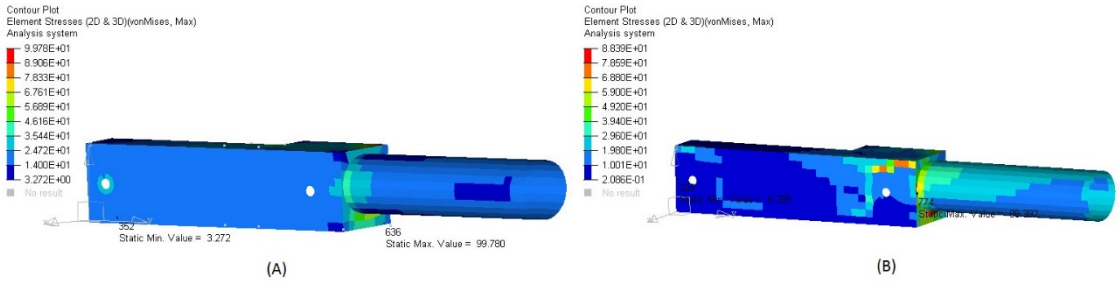


Figure 106 – von Mises stress on metallic components for catapult (A) and net arrest load cases (B), respectively for the optimized structure.

Table 45 – von Mises stress for various load cases in shape optimized structure.

| Load Case | Max. von Mises stress (MPa) | Min. von Mises stress (MPa) |
|---|---|---|
| Normal Flight | 93.39 | 0.061 |
| Landing | 82.494 | 0.049 |
| Catapult Launch | 99.780 | 3.272 |
| Net Arrest | 88.392 | 0.209 |

### 3.5.7.3 *Margin of Safety of metallic part*

The margin of safety of the original and shape optimized spar connector obtained using the von Mises stress, as discussed in Section 2.5.2, are presented in the following sub-chapters.

#### 3.5.7.3.1 Original Structure

Figure 107 gives the von Mises stresses in the original spar connector.

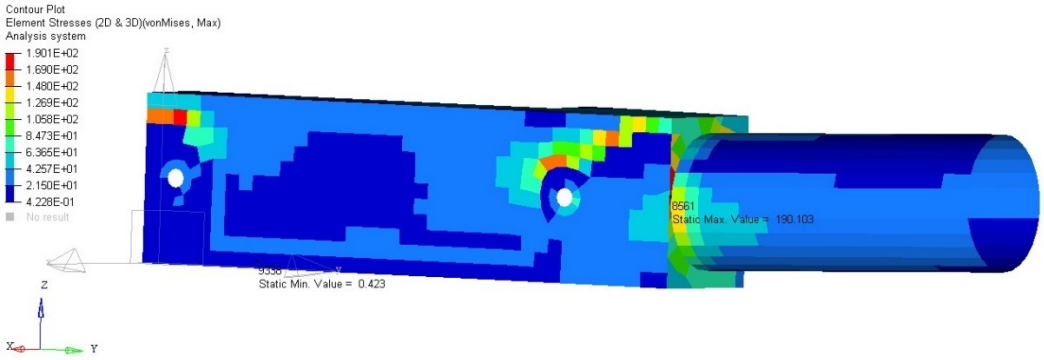


Figure 107 – von Mises stress in worst case for the original structure.

The minimum margin of safety for von Mises stress at ultimate load condition is:

$$MS_{vm} = \frac{469}{190.1 * 1.5} - 1 = 0.64 \tag{3.4}$$

The maximum von Mises was noted during Net arrest operation ( Table 44).

#### 3.5.7.3.2 Optimized Structure

Figure 108 gives the von Mises stresses in shape optimized spar connector.

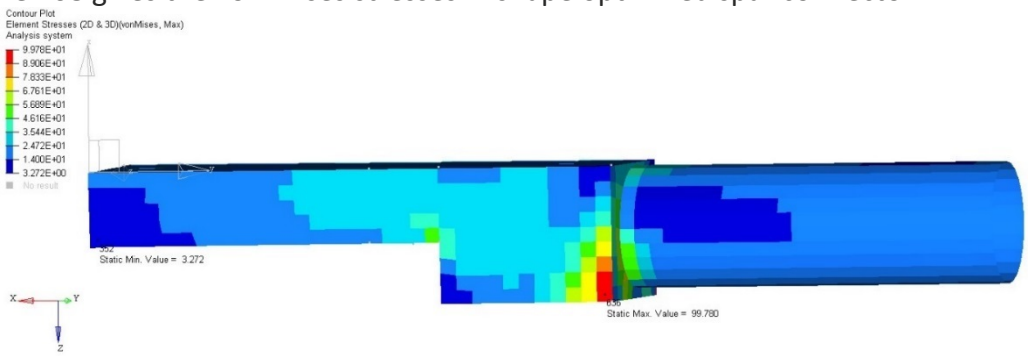


Figure 108 - von Mises stress in worst case for the shape optimized structure.

The minimum margin of safety for von Mises stress at ultimate load Condition is:

$$MS_{vm} = \frac{469}{99.78 * 1.5} - 1 = 2.31 \tag{3.5}$$

The maximum von Mises was noted during catapult launch (Table 45).

### *3.5.7.4 Composite Spar*

The results of original and shape optimized CFRP spar of UAS30-P2 are presented in the following sub-chapters.

#### 3.5.7.4.1 Original Structure

The results of original CFRP spar are presented in the following sub-chapter.

##### 3.5.7.4.1.1 Maximum Principal Strain

The maximum principal strain of the composite spar for all load cases are shown in Figure 109.

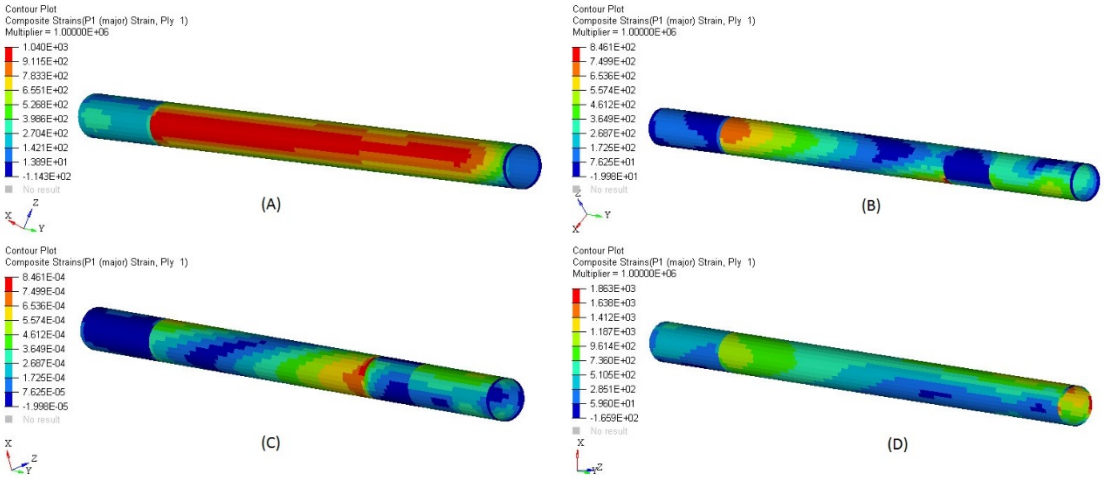


Figure 109 – Maximum principal strain for original composite spar. Clockwise from top left; (A) -Normal flight; (B) – Landing; (C) - Catapult launch, (D) - Net arrest operation.

##### 3.5.7.4.1.2 Minimum Principal Strain

The minimum principal strain of the composite spar for all load cases are shown in Figure 110.

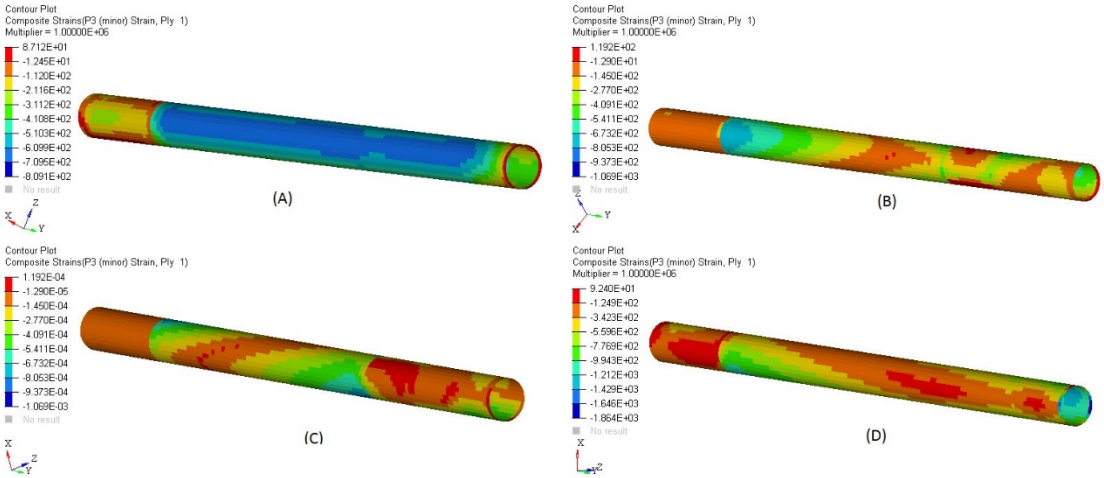


Figure 110 – Minimum principal strain for original composite spar. Clockwise from top left; (A) -Normal flight; (B) – Landing; (C) - Catapult launch, (D) - Net arrest operation.

#### 3.5.7.4.1.3 Maximum Shear Strain

The maximum principal strain of the composite spar for all load cases are shown in Figure 111.

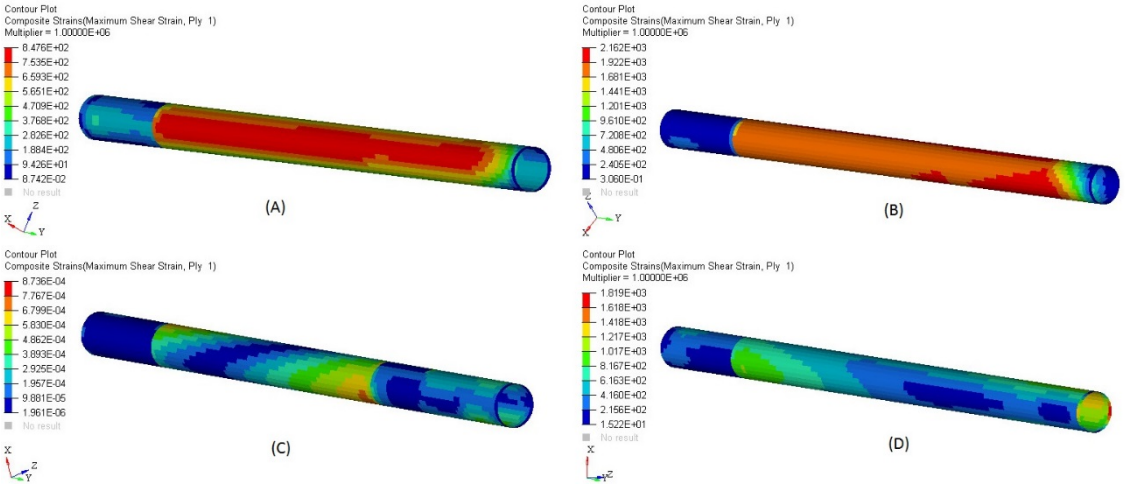


Figure 111 - Maximum shear strain for original composite spar. Clockwise from top left; (A) -Normal flight; (B) – Landing; (C) - Catapult launch, (D) - Net arrest operation.

#### 3.5.7.4.1.4 Failure Index

The failure indices for each load case, evaluated from the material allowable, shown in Table 20, are calculated by the solver using Equation 2.12. The Figure 112, shows the failure indices for all load cases.

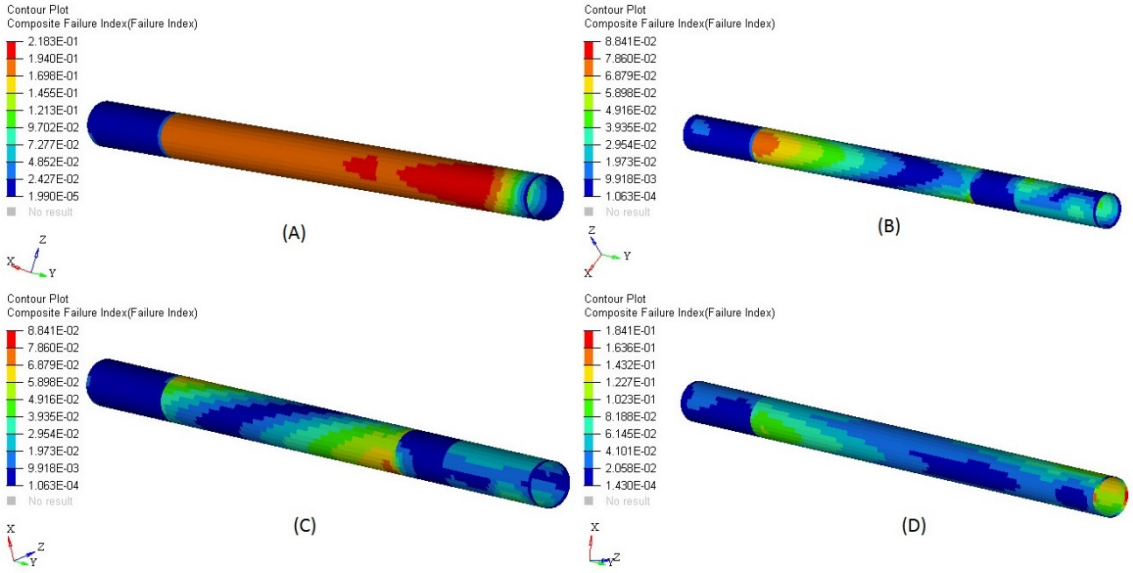


Figure 112 – Failure Indices for original composite spar. Clockwise from top left; (A) -Normal flight; (B) – Landing; (C) - Catapult launch, (D) - Net arrest operation.

The maximum shear strain, failure indices, maximum and minimum principal strain of the original spar are tabulated in Table 46.

Table 46 – Strain and failure indices for original structure.

| Load Case | Maximum Principal Strain | Minimum Principal Strain | Maximum Shear Strain | Failure Index |
|---|---|---|---|---|
| **Normal Flight** | 1220 | -809.1 | 847.6 | 0.21 |
| **Landing** | **2310** | **-2352** | **2162** | 0.08 |
| **Catapult Launch** | 846.1 | -1069 | 873.6 | 0.08 |
| **Net-arrest Operation** | 1863 | -1864 | 1819 | 0.18 |

Note: Failure indices less than 1 signifies that the composite spar doesn't fail under the load cases.

#### 3.5.7.4.1.5 Worst cases

From Table 46, the worst strain cases in tension, compression and shear are identified, shown in Figure 113, Figure 114 and Figure 115, respectively. From these cases, the spar is evaluated whether it complies with the requirements specified in Section 2.5.4.

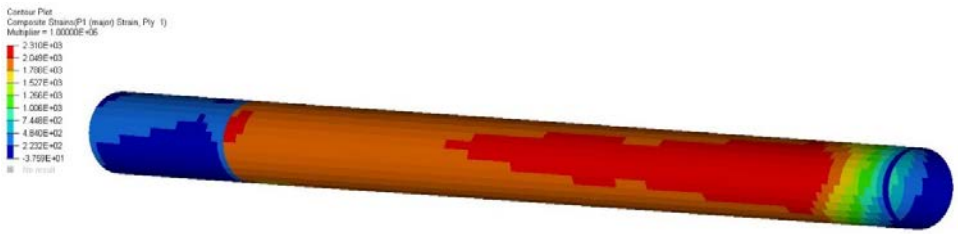

Figure 113 – Maximum strain in tension of original structure.

The maximum strain in tension was due to landing loads (Table 46). The safety factor for tension as per Section 2.5.4, is given by:

$$\left|\frac{\epsilon_1}{e_T}\right| = 0.46 \tag{3.6}$$

The value of safety factor less than 1 signifies that the composite structure meets the requirement.

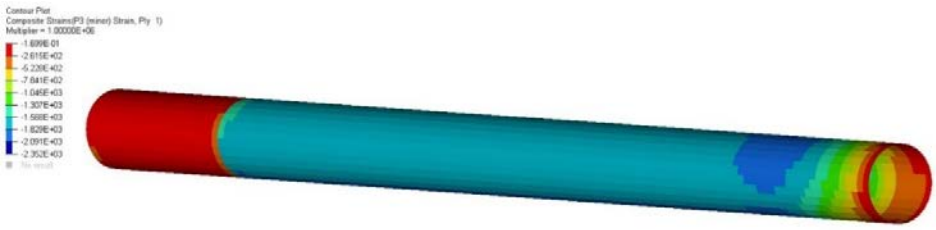

Figure 114 – Maximum strain in compression original structure.

The maximum strain in compression was due to landing loads (Table 46). The safety factor for compression as per Section 2.5.4, is given by:

$$\left|\frac{\epsilon_2}{e_C}\right| = 0.90 \tag{3.7}$$

The value of safety factor less than 1 signifies that the composite structure meets the requirement.

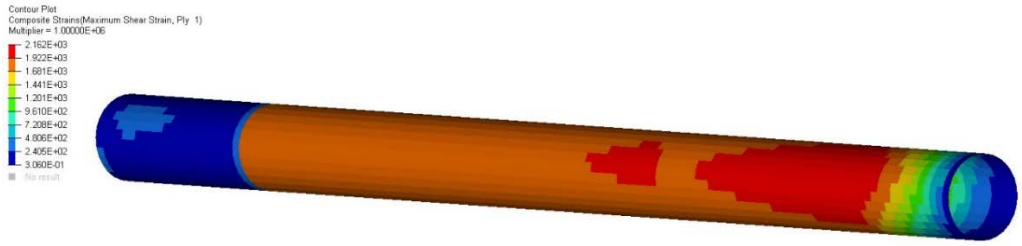


Figure 115 – Maximum shear strain in original structure.

The maximum shear strain was due to landing loads (Table 46). The safety factor for shear as per Section 2.5.4, is given by:

$$\left|\frac{\gamma_{12}}{e_{LT}}\right| = 0.41 \tag{3.8}$$

The value of safety factor less than 1 signifies that the composite structure meets the requirement.

#### 3.5.7.4.2 Shape Optimized Structure

The results of analysis on the shape optimized CFRP spar are presented in the following sub-chapters.

##### 3.5.7.4.2.1 Maximum principal Strain

The maximum principal strain of the optimized composite spar for all load cases is shown in Figure 116.

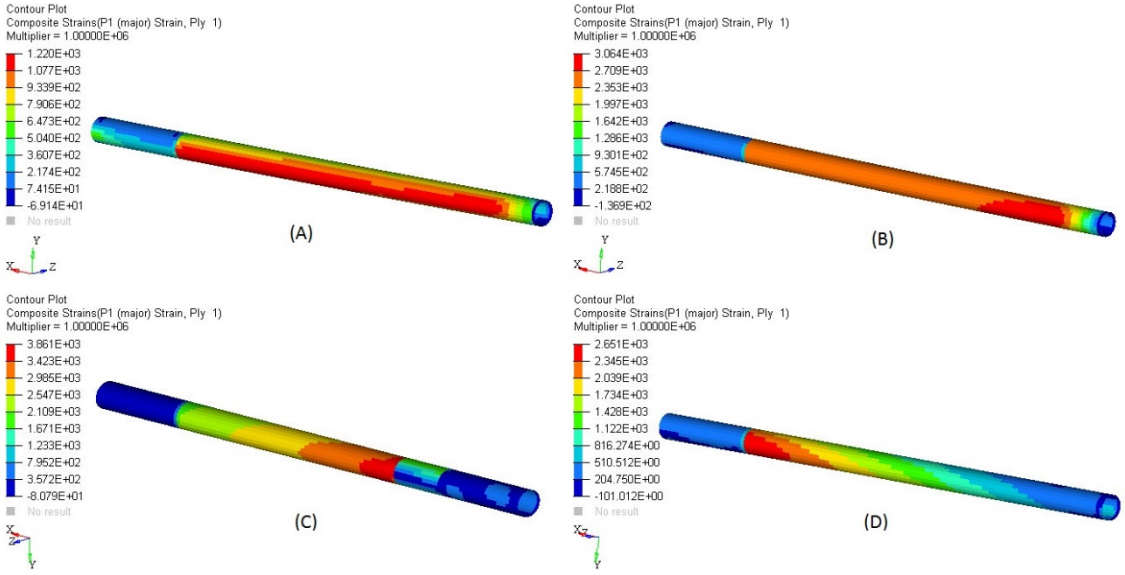


Figure 116 – Maximum principal strain of the optimized composite spar. Clockwise from top left; (A) -Normal flight; (B) – Landing; (C) - Catapult launch, (D) - Net arrest operation.

### 3.5.7.4.2.2 Minimum principal strain

The minimum principal strain of the optimized composite spar for all load cases is shown in Figure 117.

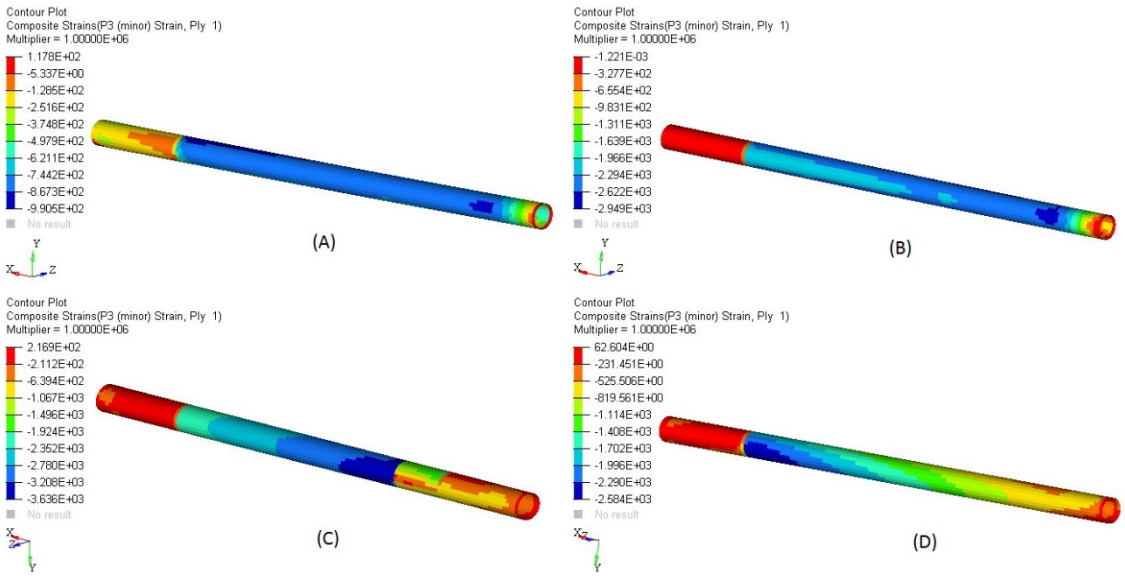


Figure 117 – Minimum principal strain of the optimized composite spar. Clockwise from top left; (A) -Normal flight; (B) – Landing; (C) - Catapult launch, (D) - Net arrest operation.

### 3.5.7.4.2.3 Maximum shear strain

The maximum shear strain of the optimized composite spar for all load cases is shown in Figure 118.

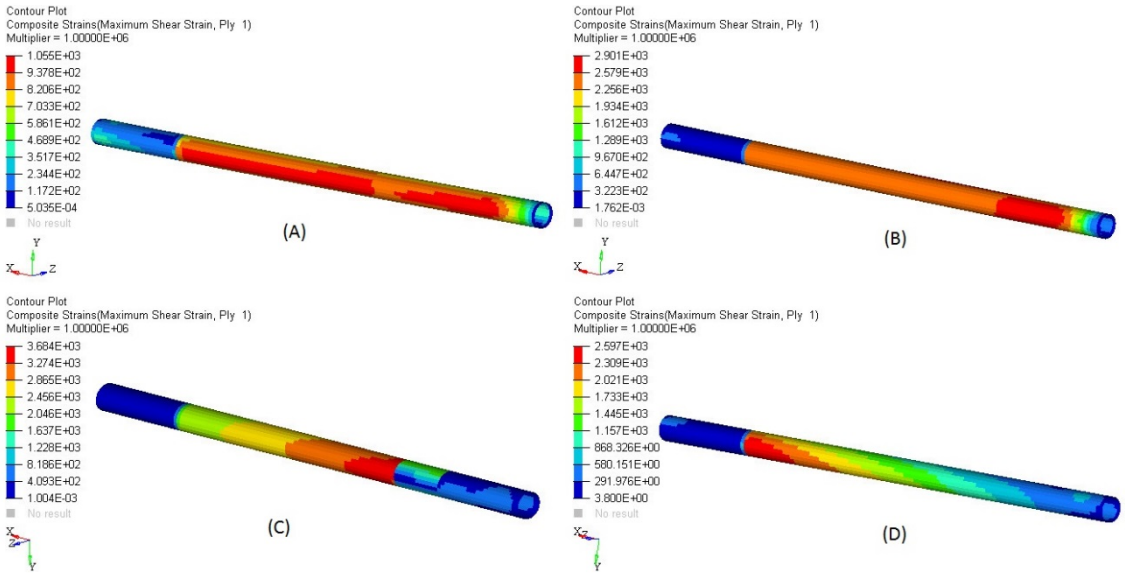


Figure 118 – Maximum shear strain of the optimized composite spar. Clockwise from top left; (A) -Normal flight; (B) – Landing; (C) - Catapult launch, (D) - Net arrest operation.

#### 3.5.7.4.2.4 Failure Index

The failure indices for each load case, evaluated from the material allowable, shown in Table 20, are calculated by the solver using Equation 2.12 The Figure 119, shows the failure indices of the optimized composite spar for all load cases.

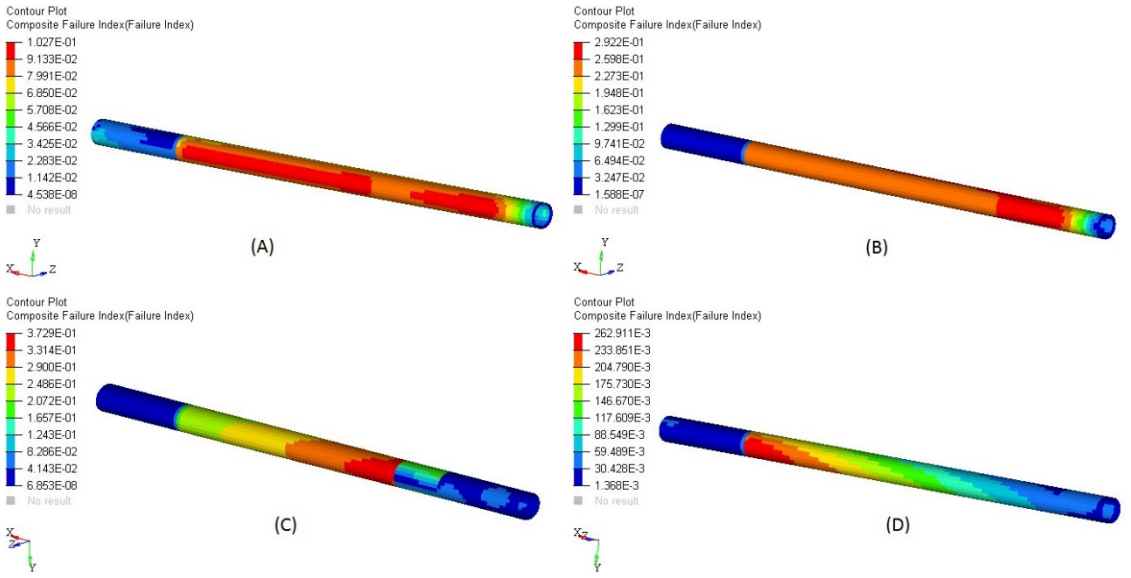


Figure 119 – Failure Indices of the of the optimized composite spar. Clockwise from top left; (A) -Normal flight; (B) – Landing; (C) - Catapult launch, (D) - Net arrest operation.

The maximum shear strain, failure indices, maximum and minimum principal strain of the shape optimized composite spar is tabulated in Table 47.

Table 47 – Strain and failure indices for shape optimized composite spar.

| Load Case | Maximum Principal Strain | Minimum Principal Strain | Maximum Shear Strain | Failure Index |
|---|---|---|---|---|
| **Normal Flight** | 1220 | -990.5 | 1055 | 0.102 |
| **Landing** | **3064** | -2949 | 2901 | 0.292 |
| **Catapult Launch** | 3861 | **-3636** | **3684** | 0.37 |
| **Net-arrest Operation** | 2651 | -2584 | 2597 | 0.262 |

Note: Failure indices less than 1 signifies that the composite spar doesn't fail under the load cases.

#### 3.5.7.4.2.5 Worst cases

From the Table 47, the worst strain cases in tension, compression and shear are identified, shown in Figure 120, Figure 121 and Figure 122. From these cases, the optimized spar is evaluated whether it complies with the requirements specified in Section 2.5.4.

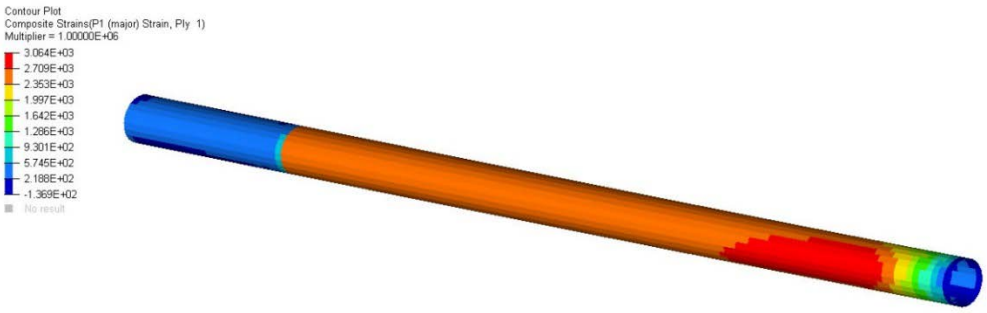


Figure 120 – Maximum strain in tension for optimized composite spar.

The maximum strain in tension was due to landing loads (Table 47). The safety factor for tension, as per Section 2.5.4, is given by:

$$\frac{\epsilon_1}{e_T} = 0.61 \tag{3.9}$$

The value of safety factor less than 1 signifies that the composite structure meet the requirement.

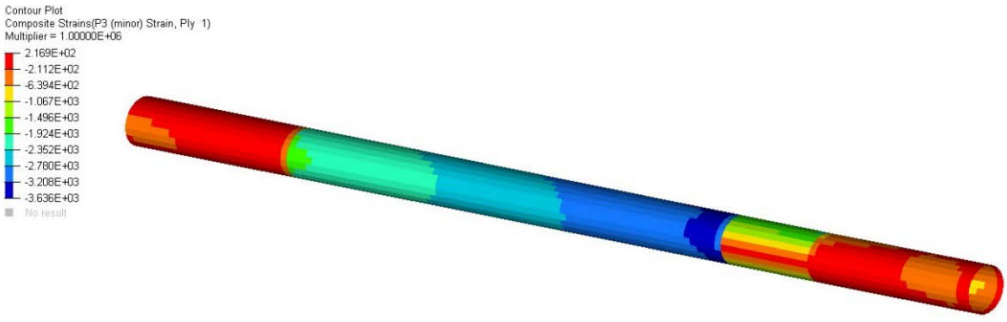


Figure 121 – Maximum strain in compression for optimized composite spar.

The maximum strain in compression was due to catapult launch loads (Table 47). The safety factor for compression, as per Section 2.5.4, is given by:

$$\frac{\epsilon_2}{e_C} = 1.39 \tag{3.10}$$

The value of safety factor greater than 1 signifies that the composite structure fails to meet the requirement.

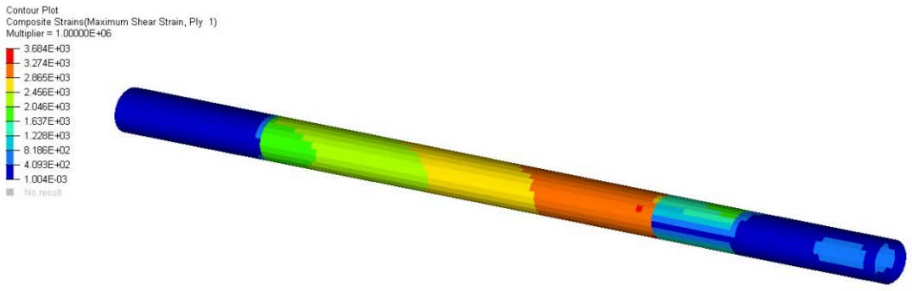


Figure 122 – Maximum shear strain for optimized composite spar.

The maximum strain in shear was due catapult launch loads (Table 47). The safety factor for shear, as per Section 2.5.4, is given by:

$$\frac{\gamma_{12}}{e_{LT}} = 0.70 \tag{3.11}$$

The value of safety factor less than 1 signifies that the composite structure meets the requirement.

# CONCLUSIONS

# 4 CONCLUSIONS AND PROPOSALS OF FUTURE WORKS

## 4.1 Conclusions

The selection of materials review that the material used in the spar connector is as per the regulations and best suited to meet the design requirements among the materials available for the same purpose. Further studies on it, ensured the durability of the material in the aviation environment (such as heat, rain, humidity and erosive conditions).

The shape optimization of the structure was carried out by using the approximated 1-D analysis and its displacement results in the structure. The optimized geometry was identified based on the results and the design constraints were defined based on the studies performed earlier in the thesis.

A comparative study of the structural mass is was performed after the optimization has been done. The difference in initial and final mass after the introduction of shape optimization:

Initial mass = 0.547 kg

Final mass = 0.501 kg

An appreciable difference was observed in the mass of the structure. There is an 8.24% decrement in the weight of the structure, and hence in the wing. Further, on conducting the 2-D analysis of the optimized and non-optimized structure it is noted that the optimized metallic structure possesses lower stress in all loads cases than the non-optimized structure. Thus, the reduction of weight accompanied by the improvement in the performance characteristics is of the metallic spar connector, which is the most significant advantage which is achieved in this thesis work. The significance is that the optimized structure is comparatively lighter and more reliable because of its higher factor of safety. The 2-D analysis on the optimized composite spar revealed that the optimized composite spar meets the requirement in almost all cases except for the catapult launch load cases, in which the CFRP spar doesn't fail structurally but the compressive strain was higher than the allowable compressive strain. The main objectives achieved in this thesis are tabulated in Table 48.

Table 48 - Summary of the achievements obtained through this work.

| Objectives | Achievements | State |
|---|---|---|
| The possibility for change of material for the spar connector of the Unmanned aerial vehicle UAS30-P2. | The choice of materials is reviewed based on the detailed studies and has been identified that the choice of material used in the spar connector was wisely made. |  |
| Optimize the aluminium spar connector of the unmanned aerial vehicle UAS30-P2. | The aluminium spar connector has been shape optimized to possess higher structure efficiency. |  |

This work also allowed the author to extend his personal skills regarding the knowledge about aircraft materials and aircraft structures. The most important knowledge gained in this work is the knowledge about the FEM, for solving structural problem and its respective software skills. The internship in CEiiA allowed to gain practical experience in actual structural engineering problems. The direct and frequent interactions with many experienced engineers and trained professionals in the company provided perfect guidelines to grow as a good engineer. The resources provided by the company helped to acquire continuous practical knowledge and self-confidence. Further, the author has been contracted as a stress engineer in the same company, which shall provide a platform for continuous practice and learning.

## 4.2 Proposals of future works

Many different adaptations and experiments have been left for the future due to lack of time. Future work concerns deeper analysis of mechanism used to fix the wings in place, through the spar connector. As the UAV has a larger wing span and the wings are comparatively heavier. Thus, the assembly of the aircraft is during every mission is tedious time consuming and requires the hands of more than two persons. New proposals to try different methods of attachments which would insert an ease in assembly of the aircraft was always my thought. The following are the proposals for future work:

- The optimized composite spar although it doesn't structurally fail, but fails to meet the requirement in maximum compressive strain specified for BVID criteria. Thus, in future works the composite spar will be improved.
- Making the spar connector as a one single piece, instead of two halves for each wing. By this way the number of fasteners used in the structures will reduce, thus decreasing the complexity in assembly.
- Try making other optimization techniques such as the topology optimization of the component to enhance further weight savings.

# REFERENCES AND OTHER SOURCES OF INFORMATION

## 5.1 Papers in International Journals

# 5 REFERENCES AND OTHER SOURCES OF INFORMATION

## 5.1 Papers in International Journals

### 5.1.1 Bibliography

[1] R. Austin, Unmanned Aircraft Systems, Wiley and Sons, Ldt., 2010.

[2] The UAV, "The UAV," [Online]. Available: https://www.theuav.com/. [Accessed 23 March 2018].

[3] P. G. Fahlsrom and T. J. Gleason, Introduction to UAV Systems, Forth Edition ed., John Wiley & Sons, Ltd.,, 2012.

[4] General Atomics, "Unmanned Systems and Sensor," 2018. [Online]. Available: http://www.ga.com/unmanned-aircraft-systems-and-sensors. [Accessed 15 March 2018].

[5] The Defence Post, "Boeing Insitu ScanEagle drone systems," The Globe Post network, 29 March 2018. [Online]. Available: https://thedefensepost.com/2018/03/29/us-orders-8-scaneagle-uas-afghan-security-forces/. [Accessed 29 March 2018].

[6] Army Technology, "LUNA Aerial Reconnaissance and Surveillance UAV," 2017. [Online]. Available: https://www.army-technology.com/projects/luna/. [Accessed 08 March 2018].

[7] S. Camm, Aeroplane Construction, London: Crosby Lockwood and Son, 1919.

[8] UAV Factory, "EPSILON 135," UAVFACTORY LTD., 03 March 2018. [Online]. Available: http://www.uavfactory.com/product/80. [Accessed 20 March 2018].

[9] G. Natarajan, "Ground Control Stations for Unmanned Air Vehicles," *Defence Science Journal,* Vols. 51, No. 3, no. Special Issue Papers, pp. 229-237, 2001.

[10] Federal Aviation Administration, AMT Airframe Handbook, vol. I, Oklahoma: United States Department of Transportation, 2012.

[11] SoliForum 3D Printing Community, "SoliForum 3D Printing Community," [Online]. Available: http://www.soliforum.com/topic/3470/3d-printing-and-home-aircraft-building/. [Accessed 03 March 2018].

[12] K. Hanns.Patent US2123429A, 1936.

[13] S. J. Kim, J. W. Shin, H.-G. Kim, T.-U. Kim and S. Kim, "The modified Brazier approach to predict the collapse load of a stiffened circular composite spar under bending load," *Aerospace Science and Technology,* vol. 55, pp. 474-481,

August 2016.

[14] P. L. Jakab, "Wood to Metal: The Structural Origins of the Modern Airplane," *Journal of Aircraft,* pp. 914-918, 1999.

[15] A. P. Mouritz, Introduction to Aerospace materials, Cambridge: Woodhead Publishing Limited, 2012.

[16] T. Dursun and C. Soutis, "Recent developments in advanced aircraft aluminium alloys," *Material and Design,* vol. 56, pp. 862-871, 2014.

[17] M. C.-Y. Niu, Airframe Stress Analysis and Sizing, 2nd ed., Hong Kong: Hong Kong Conmilit Press Ltd., 1999.

[18] ASM International, ASM Specialty Handbook: Aluminum and Aluminum Alloys, J. Davis, Ed., Materials Park, OH: ASM International, 1993.

[19] F. Campbell, Manufacturing technology for aerospace structural materials, 1st ed., New York: Butterworth-Heinemann Publication, 2006.

[20] Indian Institute of Metals Series, Aerospace Materials and Material Technologies, vol. 1, N. E. Prasad and R. J. H. Wanhill, Eds., 2017.

[21] ASM International, Alloying Understanding the Basics, J. D. &. Associates, Ed., Materials Park, Ohio: ASM International, 2001, pp. 351-416.

[22] P. Rambabu, N. E. Prasad, V. Kutumbarao and R. Wanhill, "Aluminium Alloys for Aerospace Applications," *Aerospace Material and Technologies,* pp. 29-52, 2017.

[23] P. N Eswara, A. A Gokhale and W. RJH, Aluminum–Lithium alloys: processing, properties and applications, S. Merken and J. Freeland, Eds., Waltham, MA 02451: Elsevier Inc., 2014.

[24] Materion Corporation, "Beryllium-The miracle metal," Materion Corporation, [Online]. Available: https://materion.com/-/media/files/corporate/ehs/beryllium-the-miracle-metal.pdf. [Accessed 10 June 2018].

[25] B. Hussey and J. Wilson, Light Alloys directory and Databook, 1998.

[26] ASM International, Lightweight materials: Understanding the basics, F. Campbell, Ed., Ohio: ASM International, 2012.

[27] G. F. Titterton, Aircraft Materials and Processes, New Delhi: Himalayan Books, 2013.

[28] D. Koshal, Manufacturing Engineer's Reference Book, London: Butterworth-Heinemann Ltd., 1993.

[29] V. Sadkov, Y. Laponov, V. Ageev and N. Korovina, "Perspectives and conditions for Mg alloys application in “Tupolev” airplanes," in *Materials of the second international conference and exhibition, magnesium—broad horizons*, Las Vegas, 2013.

[30] M. S. Bhuiyan, Y. Mutoh, T. Murai and S. Iwakam, "Corrosion fatigue behavior of extruded magnesium alloy AZ61 under three different corrosive environments," *International Journal of Fatigue,* p. 1756–1765, 2008.

[31] I. Ostrovsky and Y. Henn, "Present State and future of Magnesium in Aerospace Industry," in *New Channenges in Aeronautics, ASTEC'07*, Mascow, 2007.

[32] German society for material science, Magnesium alloys and technology, K. U. Kainer, Ed., Weinheim: Wiley-VCH Verlag GmbH, 2003.

[33] K. Tokaji, M. Nakajima and Y. Uematsu, "Fatigue crack propagation and fracture mechanisms of wrought magnesium alloys in different environments," *International Journal of Fatigue,* pp. 1137-1143, 2009.

[34] F. Yang, S. Yin, S. Li and Z. Zhang, "Crack initiation mechanism of extruded AZ31 magnesium alloy in the very high cycle fatigue regime," *Materials Science and Engineering A,* p. 131–136, 2008.

[35] K. W. Guo, "A Review of Magnesium/Magnesium Alloys Corrosion and its Protection," *Recent Patents on Corrosion Science,* pp. 13-21, 2010.

[36] A. Kiełbus, "Corrosion resistance of Elektron 21 magnesium alloy," *Journal of Achievements in Materials and Manufacturing Engineering,* vol. 22, pp. 29-32, May 2007.

[37] L. Gerd and W. James C, Titanium: engineering materials and processes, 2nd ed., Berlin: Springer, 2007.

[38] ASM International, Handbook of workability and process design, G. E. Dieter and S. L. S. Howard A. Kuhn, Eds., Materials Park, OH 44043-0002: ASM International, 2003.

[39] A. Sathyapalan, M. Free and Z. Fang, "Exploring alternative methods for titanium production," in *Proceedings of the 13th World Conference on Titanium*, San Diego, California, 2016.

[40] A. Baker, S. Dutton and D. Kelly, Composite materials for aerospace structures, Reston, VA 20191: American Institute of Aeronautics and Astronautics Inc., 2004, p. 371.

[41] F. Campbell, Structural composite materials, Ohio 44073-0002: ASM International.

[42] L.Zhu, N.Li and P.R.N.Childs, "Light-weighting in aerospace component and system design," *Propulsion and Power Research,* vol. 7, pp. 103-119, 2018.

[43] R. J. Basso, "Wind turbine blade construction". United States of America Patent US4728263A, 1986.

[44] N. D. P., P. Brion and B. Petallaz, "Propeller blade with modified spar stiffness". European Patent office, United States of America Patent EP2660144A1, 06 November 2013.

[45] H. M. McCoy.United States of America Patent US2542042A, 1944.

[46] H. Neuhierl.United States of America Patent US3935664A, 1974.

[47] R. N. Pham.United States of America Patent US5836541A, 1997.

[48] A. V. Levy and I. Palyka.United States Of America Patent US6425794B1, 1999.

[49] A. Lai.United States of America Patent US7182666B2, 1999.

[50] M. A. F. Castaner.United States of America Patent US7182666B2, 2007.

[51] M. A. F. Castaner and K.-B. Sheng.United States of America Patent US20110117806A1, 2009.

[52] R. Boyer, J. Cotton, M. Mohaghegh and R. Schafrik, " Materials considerations for aerospace applications," *Material Research Society,* vol. 40, pp. 1055-1065, 21 December 2015.

[53] D. S. Ebnesajjad, "New Materials & Applications," Boeing, 7 March 2017. [Online]. Available: https://chemical-materials.elsevier.com/new-materials-applications/air-force-one-technology-materials-meatloaf/. [Accessed 28 March 2018].

[54] Springer-Science+Business media, B.V, High Performance Materials in Aerospace, H. M. Flower, Ed., London: Springer Science & Business Media, 2012.

[55] E. Ordoukhanian and A. M. Madni, "Blended Wing Body Architecting and Design: Blended Wing Body Architecting and Design:," in *Conference on Systems Engineering Research, Procedia Computer Science 28*, California, 2014.

[56] M. F. Ashby, Materials selection in mechanical design, Woburn, MA 01801-2041, 1999.

[57] J. P. Leiva, "Structural Optimization Methods and Techniques to Design Efficient Car Bodies," in *Proceedings of International Automotive Body Congress*, Michigan, 2011.

[58] P. Christensen and A. Klarbring, An Introduction to Structural Optimization, vol. 153, Linköping: Springer Science & Business Media, 2008.

[59] J. Reddy, An Introduction to the Finite Element Method, Texas: McGraw-Hill, Inc., 1993.

[60] O. Zienkiewicz, The Finite Element Method: Its Basis and Fundamentals, 6th ed., Burlington, Massachusetts: Butterworth-Heinemann, 2005.

[61] K.-J. Bathe, Finite Element Procedures, 2nd ed., Watertown, Massachusetts: Prentice Hall, Pearson Education, Inc. , 2014.

[62] R. G. Sexsmith and T. M. Cigic, The Engineering Handbook, R. C. Dorf, Ed., New York: CRC Press LLC, 2000.

[63] V. B. Bhandari, Design of Machine elements, 3rd ed., New Delhi: Tata McGraw-Hill, 2010.

[64] R. M. Christensen, The Theory of Materials Failure, Oxford: Oxford University Press, 2013.

[65] M. Rajanish, D. N. NV, D. R. S.Sharma and D. B. Pal, "A Review Of Failure Of Composite Materials," *Journal of Engineering Research and Applications (IJERA),* vol. III, no. 2, pp. 122-124, April 2013.

[66] R. F. Gibson, Principles of Composite materials mechanics., New York: McGraw-Hill, Inc., 1994.

[67] Altair, "OptiStruct Help," Altair Hyperworks, 2017. [Online]. Available:

https://altairhyperworks.com/hwhelp/Altair/2017/help/os/topics/solvers/elements_composite_interpretation_of_results_r.htm?hl=failure. [Accessed 06 June 2018].

[68] G. N. Mangurian, "The Aircraft Structural Factor of Safety," NATO Advisory group for aeronautical research and development, 1957.

[69] E.F. Bruhn, Analysis and Design of Flight Vehicle Structures, 1973.

[70] North Atlantic Treaty Organization, Light Unmanned Aircraft Systems airworthiness requirements, NATO standardization agency, 2014.

[71] A. E. Lovejoy and d. Przekop, "Imparting Barely Visible Impact Damage to a Stitched Composite Large-Scale Pressure Box," Reston, VA, United States, 2016.

[72] J. John D. Anderson, Introduction to Flight, 3rd ed., New York: McGraw-Hill Book Company, 1989.

[73] J. John D. Anderson, Fundamentals of Aerodynamics, 2nd ed., New York: McGraw-Hill, Inc., 1991.

[74] D. J. Peery and J. J. Azar, Aircraft Structures, 2nd ed., New York: McGraw-Hill Book Company, 1982.

[75] CEiiA, "UAS30 P2 Stress Report," CEiiA, Porto, 2016.

[76] R. C. Rice, J. L. Jackson, J. Bakuckas and S. Thompson, Metallic Materials Properties Development and Standardization (MMPDS), Virginia 22161: Federal Aviation Administration, 2003.

[77] ASM International, Corrosion of Aluminium and alloys, Materials Park, OH 44073-0002: ASM International, 1999.

[78] E. Li, Z. Zhang, C. Chang, G. Liu and Q. Li, "Homogenization for composite material properties using smoothed finite element," 2006. [Online]. Available: https://pdfs.semanticscholar.org/38dd/b53cef17daceb30753473cc5310ee48caebf.pdf. [Accessed 06 June 2018].

[79] M. Jadhav, P. D. Darade and S. S. Deshpande, "On The Accuracy of Finite Element Method for static and Dynamic Problem," in *International Conference on Global Trends in Engineering, Technology and Management* , Jalgaon, 2016.